NASA
Technical
Paper
2549
C.2
April 1986

Static Internal Performance of a Thrust Vectoring and Reversing Two-Dimensional Convergent-Divergent Nozzle With an Aft Flap

Richard J. Re and
Laurence D. Leavitt

NASA

NASA Technical Paper 2549

1986

Static Internal Performance of a Thrust Vectoring and Reversing Two-Dimensional Convergent-Divergent Nozzle With an Aft Flap

Richard J. Re and
Laurence D. Leavitt

Langley Research Center
Hampton, Virginia

NASA
National Aeronautics
and Space Administration

Scientific and Technical Information Branch

SUMMARY

The static internal performance of a multifunction nozzle having some of the geometric characteristics of both two-dimensional convergent-divergent and single expansion ramp nozzles has been investigated in the static-test facility of the Langley 16-Foot Transonic Tunnel. The internal expansion portion of the nozzle consisted of two symmetrical flat surfaces of equal length, and the external expansion portion of the nozzle consisted of a single aft flap. The aft flap could be varied in angle independently of the upper internal expansion surface to which it was attached. The effects of internal expansion ratio, nozzle thrust-vector angle (-30° to 30°), aft flap shape, aft flap angle, and sidewall containment were determined for dry and afterburning power settings. In addition, a partial afterburning power setting nozzle, a fully deployed thrust reverser, and four vertical takeoff or landing nozzle configurations were investigated. Nozzle pressure ratio was varied up to 10 for the dry power nozzles and 7 for the afterburning power nozzles.

Results of the investigation indicate that this nozzle concept provided relatively high performance levels throughout the vector angle range. Nozzle discharge coefficient was dependent upon the thrust-vector angle but independent of flow direction (either up or down). The thrust-reverser configuration provided levels of reverse thrust performance well in excess of 50 percent.

INTRODUCTION

Development of turbine engines for aircraft propulsion systems has been accompanied by the evolution of the axisymmetric (circular cross sections) nozzle because of its logical integration advantages. Extensive experience with axisymmetric nozzles has produced the capability to design structurally and thermally efficient exhaust systems with high internal performance for many applications. However, experimental investigations (refs. 1 through 4) have shown that airplane performance penalties can occur when the exhaust system is integrated into the airframe on some twin-engine fighter aircraft. The most significant installation penalties (increased drag) occur on twin-engine configurations where the engines are mounted side by side in the fuselage and the nozzles are blended into the afterbody along with other airplane components such as vertical and horizontal stabilizers. The installation of engines and other components at the rear of twin-engine fighter configurations tends to result in an afterbody that is more nearly rectangular in shape than round. This installation results in external fuselage lines (nearly rectangular at the inlet station) which must transition to two distinct circular shapes at the nozzles. This transition often results in complex afterbody shapes and can produce large boattail angles, bases, and gutters that contribute to the installation drag penalty.

Many studies have been made of the application of nonaxisymmetric nozzles to fighter airplane configurations having missions requiring extensive maneuver capability (refs. 5 and 6). The nonaxisymmetric nozzle offers internal performance comparable with that of axisymmetric nozzles and is more amenable to the incorporation of thrust vectoring and thrust reversing for additional airplane maneuver and control capability. The inherent structural weight advantage of the axisymmetric nozzle is lost when deflection of the thrust vector for powered lift or control is required.

In addition, the nonaxisymmetric nozzle presents the opportunity to avoid airplane performance losses by improving aft-end integration.

Two types of nonaxisymmetric nozzles on which significant experimental internal performance data are available are the two-dimensional convergent-divergent nozzle (refs. 7 through 10) and the single expansion ramp nozzle (refs. 7 and 11 through 13). The two-dimensional convergent-divergent nozzle incorporates identical upper and lower expansion surfaces of equal length so that the flow expansion process (nozzle unvectored) over the diverging surfaces is symmetric in the vertical plane. The single expansion ramp nozzle is nonsymmetric and expands the flow both internally and externally. One expansion surface of the single expansion ramp nozzle is much longer than the other. Internal expansion occurs between the throat and trailing edge of the short expansion surface (flow bounded by two expansion surfaces) and external expansion occurs over the external portion of the longer surface (flow bounded by external portion of long surface and free-air boundary). These nozzles usually incorporate extensive surface curvature on the long expansion surface and therefore do not have symmetric internal or external expansion processes.

The present paper contains the static internal performance of a multifunction nozzle having some of the geometric characteristics of both two-dimensional convergent-divergent and single expansion ramp nozzles. This nozzle expands the flow internally as a two-dimensional convergent-divergent nozzle (symmetric expansion) and externally over an aft flap as a single expansion ramp nozzle. The internal expansion portion of the nozzle geometry consisted of two identical flat surfaces of equal length. The external portion of the nozzle (or aft flap) could be varied in angle independently of the internal expansion surface to which it was attached. The effects of internal expansion ratio, nozzle-thrust-vector angle (-30° to 30°), aft flap shape, aft flap angle, and sidewall containment were determined for dry and afterburning power settings. A partial afterburning power setting nozzle was investigated by using components from the dry and afterburning nozzle configurations. A fully deployed thrust reverser and four vertical takeoff or landing nozzle configurations were also investigated. This investigation was conducted in the static-test facility of the Langley 16-Foot Transonic Tunnel at nozzle pressure ratios up to 10 for unvectored dry power nozzles and up to 7 for afterburning power nozzles.

SYMBOLS

All the forces (with the exception of resultant gross thrust) and angles are referred to the model centerline (body axis). A detailed discussion of the data-reduction and calibration procedures as well as definitions of forces, angles, and propulsion relationships used herein can be found in reference 7.

A_e nozzle-exit area, in^2 (A_e measured in the vertical plane at end of nozzle upper and lower flaps)

A_t nozzle geometric throat area (measured), in^2

F measured thrust along body axis, lbf

F_i ideal isentropic gross thrust, $w_p\sqrt{\frac{RT_{t,j}}{g^2}\left(\frac{2\gamma}{\gamma - 1}\right)\left[1 - \left(\frac{p_a}{p_{t,j}}\right)^{(\gamma-1)/\gamma}\right]}$, lbf

F_r resultant gross thrust, $\sqrt{F^2 + N^2}$, lbf

g	gravitational constant, 32.17 ft/sec^2
$h_{t,n}$	nominal nozzle-throat height for dry power nozzles, 0.92 in.
$l_{f,nom}$	nominal length of the flat aft flap, in. (see fig. 10(b))
M	measured pitching moment (about point on model centerline at station 29.39), in-lb (see fig. 1(b))
N	measured normal force, lbf (see fig. 1(b))
NPR	nozzle pressure ratio, $p_{t,j}/p_a$
p	local static pressure, psi
p_a	ambient pressure, psi
$p_{t,j}$	jet total pressure, psi
R	gas constant, 1716 $ft^2/sec^2-°R$
Sta.	model station, in.
$T_{t,j}$	jet total temperature, °R
w_i	ideal weight-flow rate, lb/sec
w_p	measured weight-flow rate, lb/sec
x	axial coordinate measured from nozzle connect station (Sta. 41.13), in.
x'	axial component of orifice coordinate system with origin at the termination of upper and lower nozzle divergent flap surfaces, in. (see fig. 10)
y	vertical coordinate measured from horizontal model centerline (positive upwards), in.
α	aft flap initial angle, deg (see fig. 2)
γ	ratio of specific heats, 1.3997 for air
Δ	incremental value
δ	resultant thrust-vector angle, $\tan^{-1}(N/F)$, deg
δ_l	lower flap angle, deg (see fig. 2)
δ_u	upper flap angle, deg (see fig. 2)
δ_v	geometric thrust-vector angle measured from horizontal reference line, $\frac{\delta_l - \delta_u}{2}$, deg

ρ divergence angle of nozzle divergent flap surface, deg

σ aft flap terminal angle, $\sigma = \alpha$ for flat aft flap (see fig. 2)

Nozzle and nozzle component designations:

First two characters in nozzle configuration designation:

A1 afterburning power setting with $\rho = 2.7°$

A2 afterburning power setting with $\rho = 11.0°$

A3 afterburning power setting with $\rho = 6.85°$ and $\delta_v = \pm 4.15°$

D1 dry power setting with $\rho = 1.5°$

P1 partial afterburning power setting with $\rho = 2.1°$

P2 partial afterburning power setting with $\rho = 6.25°$

V1 vertical takeoff or landing configuration 1

V2 vertical takeoff or landing configuration 2

V3 vertical takeoff or landing configuration 3

V4 vertical takeoff or landing configuration 4

Third character in nozzle configuration designation:

F flat aft flap surface

C curved aft flap surface

Fourth character in nozzle configuration designation:

L long sidewalls

S short sidewalls

APPARATUS AND METHODS

Static-Test Facility

This investigation was conducted in the static-test facility (ref. 14) of the Langley 16-Foot Transonic Tunnel. All tests were conducted with the jet exhausting to the atmosphere. This facility utilizes the same clean, dry-air supply as that used in the 16-Foot Transonic Tunnel and a similar air-control system, including valving, filters, and a heat exchanger (to operate the jet flow at constant stagnation temperature).

Single-Engine Propulsion-Simulation System

A sketch of the single-engine air-powered nacelle model (ref. 14) on which various nozzles were mounted is presented in figure 1(a) with a typical nozzle configuration attached. An external high-pressure air system provided a continuous flow of clean, dry air at a controlled temperature of about 530°R (at the instrumentation section). This high-pressure air was varied up to approximately 10 atm (1 atm = 14.7 psia) and was brought through a dolly-mounted support strut by six tubes which connect to a high-pressure plenum chamber. As shown in figure 1(b), the air was then discharged perpendicularly into the model low-pressure plenum through eight multiholed sonic nozzles equally spaced around the high-pressure plenum. This method was designed to minimize any forces imposed by the transfer of axial momentum as the air is passed from the nonmetric high-pressure plenum to the metric (mounted to the force balance) low-pressure plenum. Two flexible metal bellows are used as seals and serve to compensate for axial forces caused by pressurization.

The air was then passed from the model low-pressure plenum (circular in cross section) through a transition section, choke plate, and instrumentation section which were common for all nonaxisymmetric nozzles investigated. The transition section provided a smooth flow path for the airflow from the round low-pressure plenum to the rectangular choke plate and instrumentation section. The instrumentation section had a flow-path width-to-height ratio of 1.437 and was identical in geometry to the nozzle airflow entrance. All nozzle configurations were attached to the instrumentation section at model station 41.13.

Nozzle Design and Models

Nozzle concepts.- The two-dimensional convergent-divergent (2-D C-D) nozzle is a nonaxisymmetric exhaust system in which a symmetric internal contraction and expansion process takes place in the vertical plane. Basic nozzle components consist of upper and lower flaps to regulate the contraction and expansion process and flat nozzle sidewalls to contain the flow laterally. The flap inner surface geometry can be varied or altered by actuators so that (1) engine power setting can be changed by varying the throat height, and (2) expansion surface angle (surface downstream of the throat) can be varied for optimum expansion of the exhaust flow. The two-dimensional nature of the flaps and sidewalls of the 2-D C-D nozzle facilitates the incorporation of performance capabilities not readily amenable to axisymmetric designs. The 2-D C-D nozzle can be designed to (1) vector the exhaust flow up or down by varying the geometry of the upper and lower flaps and (2) reverse or spoil the thrust by opening ports upstream of the throat while deploying internal blockers from the flaps to divert the flow to the thrust-reverser ports.

The single expansion ramp nozzle (SERN) concept incorporates nonsymmetric internal/external flow expansion. Basic SERN components consist of (1) a two-dimensional variable-geometry convergent-divergent upper-flap assembly used to vary nozzle power setting (throat area), (2) a two-dimensional lower flap used to vary internal expansion ratio, and (3) a two-dimensional portion of the upper flap serving as an external expansion surface. The throat of a SERN is forward of the variable portion of the lower flap so that power setting (throat area) is independent of lower flap angle (internal expansion ratio). Variations in the geometry of the SERN upper flap assembly generally affect internal and external expansion ratio as well as power setting. Moderate amounts of vectoring (up to about 20°) can be obtained from a SERN by incorporating independent actuation of a portion of the external expansion surface into the design (refs. 4, 9, 11, and 12).

The nozzle concept of the present investigation combines features of the 2-D C-D and SERN concepts into a single nozzle design with multifunction capability. That is, the forward portion of the present nozzle concept is a 2-D C-D nozzle with the aforementioned power setting, expansion ratio, and vectoring capabilities of a 2-D C-D nozzle. The addition of a flap at the downstream end of the upper flap of the 2-D C-D nozzle produces a nozzle similar in appearance to a SERN. However, this independently actuated aft flap is primarily used for external expansion or as an airplane trim or control device. Thrust vectoring would be accomplished with the 2-D C-D portion of the nozzle with the aft flap following as a portion of the upper flap. Thrust reversing would occur in the convergent section of the nozzle by deploying portions of the upper and lower flaps to form a blocker.

Unvectored- and vectored-thrust nozzle models.- The nozzle models of the present investigation were attached to the propulsion simulation system (fig. 1(a)) at station 41.13 and had a constant flow path width of 4.00 in. Nozzle geometry was varied by combining interchangeable upper, lower, and aft flaps and sidewalls. The parameters for unvectored- and vectored-thrust nozzles were power setting (throat area), internal expansion ratio, aft flap angle, aft flap shape, and sidewall length. The values of unvectored- and vectored-thrust nozzle parameters selected for this investigation are presented in table I, and a sketch showing component angular sign conventions is presented in figure 2. Sketches giving geometric details of some of the unvectored- and vectored-thrust nozzle configurations are presented in figures 3 through 5, and details of the long and short sidewalls are shown in figure 6. The nozzles with 6.85° divergence angle were made up from one flap from each of the 2.7° and 11.0° unvectored nozzles (fig. 3(a)).

Thrust-reverser nozzle model.- The thrust-reverser nozzle resulting from the deployed 2-D C-D components is shown in figure 7. It can be seen that the upper and lower port passages are not identical (formed through differing structures). The geometric throats are the same size and occur at the same orientation in each port between point C on the flap and the blocker surface. The reverse-thrust angle designed into the port was 135° (blocker angle) measured forward from a horizontal reference line. Geometrically, a 135° reverse-thrust angle can provide a 70.7-percent component of thrust in the reverse direction.

Vertical takeoff or landing nozzle model.- Four nozzle configurations designed to deflect the thrust vector downward 90° for vertical takeoff or landing are shown in figure 8. These configurations are not directly related to the present multifunction nozzle but could result from a derivative version of this nozzle concept. The geometric details of the blocker and lower flap components are shown in figure 9.

Instrumentation

A three-component (normal force, axial force, and pitching moment) strain-gage balance was used to measure the forces and moments on the model downstream of station 20.50 in. (See fig. 1(a).) Jet total pressure was measured at a fixed station in the instrumentation section (fig. 1(a)) by means of a four-probe rake through the upper surface, a three-probe rake through the side, and a three-probe rake through the corner. A shielded thermocouple probe, also located in the instrumentation section, was used to measure jet total temperature. Weight-flow rate of the high-pressure air supplied to the nozzle was determined by calibration of pressure and temperature measurements in the high-pressure plenum against the known performance of standard axisymmetric Stratford choke nozzles (ref. 14). Internal static-pressure orifices were located on the planview centerlines of the unvectored (fig. 10) and vectored nozzle

upper, lower, and aft flaps. The thrust-reverser model had static-pressure orifices only on the blocker centerline as shown in figure 11. The vertical takeoff or landing nozzles had pressure orifices on the blocker and lower flap centerlines as shown in figure 12.

Data Reduction

All data were recorded on magnetic tape with 50 frames of data averaged at each data point for use in computations. With the exception of resultant gross thrust F_r, all force data in this report are referenced to the model centerline.

The basic performance parameters used for the presentation of results are F/F_i, F_r/F_i, δ, $M/F_i h_{t,n}$, and w_p/w_i. The internal thrust ratio F/F_i is the ratio of actual nozzle thrust (along the body axis) to ideal nozzle thrust where ideal nozzle thrust is based on measured weight-flow rate and total-temperature and total-pressure conditions in the nozzle instrumentation section. The balance axial-force measurement, from which actual nozzle thrust is subsequently obtained, is initially corrected for model weight tares and balance interactions. Although the bellows arrangement was designed to eliminate pressure and momentum interactions with the balance, small bellows tares on all balance components still exist. These tares result from a small pressure difference between the ends of the bellows when internal velocities are high and also small differences in the forward and aft bellows spring constants when the bellows are pressurized. As discussed in reference 9, these bellows tares were determined by running calibration nozzles with known performance over a range of expected normal forces and pitching moments. The balance data were then corrected in a manner similar to that discussed in reference 9 to obtain actual nozzle thrust, normal force, and pitching moment. The resultant gross thrust F_r, used in resultant thrust ratio F_r/F_i, and the resultant thrust-vector angle δ are then determined from these corrected balance data. Resultant thrust ratio F_r/F_i is equal to internal thrust ratio F/F_i as long as the jet-exhaust flow remains unvectored ($\delta = 0°$). Significant differences between F_r/F_i and F/F_i occur when jet-exhaust flow is turned from the axial direction. The parameter $M/F_i h_{t,n}$ is the ratio of pitching moment resulting from vectoring and flow expansion over the aft flap to the product of ideal thrust and nominal dry power throat height $h_{t,n}$. Nominal dry power throat height was selected arbitrarily as a nondimensionalizing length because isolated nozzle tests do not have a set of airplane nondimensionalizing constants associated with them. Nozzle discharge coefficient w_p/w_i is the ratio of measured weight-flow rate to ideal weight-flow rate where ideal weight-flow rate is based on jet total pressure $p_{t,j}$, jet total temperature $T_{t,j}$, and measured nozzle (or port) throat area. Nozzle discharge coefficient is, then, a measure of the ability of a nozzle to pass mass flow.

PRESENTATION OF RESULTS

The basic nozzle internal performance data obtained in this investigation are presented in figures 13 through 24, which will not be discussed individually. However, reference will be made to the performance of those nozzles directly relevant to the discussion as the need arises. Local static pressures were measured on the nozzle internal surfaces for various nozzle total pressure ratio settings and are presented in ratio form in tables II through V. Table I, which contains a summary of the nozzle (unvectored and vectored) geometric parameters, also contains the figure and table numbers in which the basic internal performance and local pressure ratio data can be found for each combination of parameters.

Nozzle internal thrust ratio F/F_i, resultant thrust ratio F_r/F_i, thrust-vector angle δ, pitching moment ratio $M/F_i h_{t,n}$, and discharge coefficient w_p/w_i are presented graphically as a function of nozzle pressure ratio (NPR) in figures 13 through 22 for the unvectored and vectored nozzle configurations. Figure 23 presents internal performance data for the thrust-reverser configuration. A negative value of thrust ratio indicates thrust in the reverse direction. The data obtained on the vertical takeoff or landing configurations are presented in figure 24. Normal force ratio N/F_i is presented as an additional parameter for the thrust reverser and vertical takeoff or landing configurations.

RESULTS AND DISCUSSION

Basic Data

The internal performance data shown in figures 13 through 22 exhibit characteristics of both 2-D C-D and SERN nozzles. In general, nozzle thrust ratio performance was similar to that measured for 2-D C-D nozzles (refs. 7 and 10) and is characterized by one performance peak occurring at or near the NPR required for fully expanded nozzle flow (design NPR). An exception to the previous observation occurred when $\delta_v < 0°$. For these cases (fig. 15 for example), internal performance data were typical of single-expansion-ramp nozzle data (refs. 7, 12, and 13) and were often characterized by a tendency to have two nozzle thrust ratio performance peaks. These two peaks occur as a result of two separate exhaust-flow expansion processes. The first (internal expansion) occurs as the exhaust flow expands in the region between the nozzle throat and nozzle exit formed by the downstream edge of the upper and lower flaps. The second expansion process (external expansion) occurs between the upper aft flap (located downstream of the exit) and the lower jet free boundary.

The resultant thrust-vector angle data presented in figures 13 through 22 illustrate another characteristic of SERN nozzles: significant resultant thrust-vector angles δ (hence differences in resultant thrust ratio F_r/F_i and internal thrust ratio F/F_i) can occur on unvectored ($\delta_v = 0°$) configurations. The nonlinear variation of resultant thrust-vector angle δ with NPR at all values of δ_v is also characteristic of SERN nozzles and is caused by changing compression-expansion wave patterns impinging on the external expansion surface (aft flap) as NPR is varied. The aft flap has a large, unopposed, normal projected area, hence normal force can change significantly with varying NPR. An axial-force performance penalty results for any nonzero value of resultant thrust-vector angle because the thrust is being turned away from the axial direction. The magnitude of this penalty can be assessed by comparing the difference between resultant and internal thrust ratio at a given NPR.

Measured values of nozzle discharge coefficient w_p/w_i for all nozzles were between 0.94 and 0.98 and were essentially unaffected by changes in NPR.

Performance Comparisons

The design pressure ratios for the internal portions of the unvectored nozzles varied from 3.05 to 5.43 as indicated in table I. However, for purposes of summary data, a nominal NPR of 4.0 has been selected for all nozzles.

Effect of geometric thrust-vector angle.- The effects of geometric thrust-vector angle on nozzle performance parameters are presented in figures 25 and 26. Typical

internal static pressure distributions (configuration A1FS) for a range of δ_v are shown in figure 27.

The variation in discharge coefficient with geometric vector angle (fig. 25) was nearly symmetrical about $\delta_v = 0°$ for afterburning and dry power nozzle configurations. This symmetry was expected since the nozzle geometry in the convergent section and the throat was identical for $\delta_v = 30°$ and $-30°$ and for $\delta_v = 15°$ and $-15°$. Examination of internal static pressure distributions (fig. 27) indicates nearly identical flow characteristics for upward (δ_v negative) and downward (δ_v positive) vectoring cases. Nozzle discharge coefficient peaks at $\delta_v = 0°$ (fig. 25) and falls off at nonzero values of δ_v indicating throat shape and/or convergence altered relative to the unvectored case. Thrust-vectoring schemes which use both upper and lower flaps generally alter the nozzle surface shape at and ahead of the throat since the vectoring actuation modifies a portion of the convergent section. (Compare upper and lower flap surface shapes in figures 3(a), (b), and (c), for example.) As seen in figure 27, the throat location (location at which the ratio of static pressure to jet total pressure is 0.528, hence local Mach number is 1.0) moves downstream on the upper flap as geometric thrust-vector angle is increased from $\delta_v = 0°$ (positive δ_v) and moves downstream on the lower flap as geometric thrust-vector angle is decreased from $\delta_v = 0°$ (negative δ_v). Since the entire static pressure distribution for the unvectored case $\delta_v = 0°$ is below $p/p_{t,j} = 0.528$, it is obvious (by extrapolation) that the throat occurs somewhere upstream of the most forward orifice location; hence it can be stated that, in general, actual throat location moves downstream on the upper flap for $\delta_v > 0$ and downstream on the lower flap for $\delta_v < 0$. This reorientation of the throat for ±30° of vectoring decreased discharge coefficient by 0.03 for the afterburning power nozzles and 0.02 for the dry power nozzles (fig. 25).

The effect of geometric thrust-vector angle on resultant thrust ratio is presented in figure 26 for afterburning and dry power nozzle configurations. As seen F_r/F_i was relatively independent of δ_v, varying no more than 1 percent over the entire range of vector angle investigated. For these configurations in which $\delta_u - \alpha = 0°$, the lowest values of resultant thrust ratio occurred for $\delta_v = -30°$, probably because of exhaust flow separation on the aft flap. Static pressure distributions for configuration A1FS (fig. 27) indicate that exhaust flow over the last 40-percent of the aft flap could be separated. Exhaust flow separation on the external expansion surface is typical for single expansion ramp nozzles at negative vector angles (ref. 12).

Values of thrust ratio F/F_i peak near $\delta_v = 0°$ (fig. 26(a)) since the exhaust flow is directed away from the axial direction when vectoring. Characteristic shapes of these F/F_i curves appear to be nearly identical, but some curves are slightly offset relative to others. These offsets are a function of aft flap shape and the magnitude of $\delta_u - \alpha$ and can be related directly to changes in effective aft flap angle. These results indicate that an aircraft utilizing this nozzle concept could cruise at a nonzero value of geometric thrust-vector angle ($\delta_v \approx 2.5°$ for flat aft flap configurations or $\delta_v \approx -2.5°$ for curved aft flap configurations) to optimize internal nozzle performance.

As can be seen in figure 26(b), aft flap curvature or negative rotation of the aft flap provide nearly constant increases in resultant turning angle δ over the geometric thrust-vector angle δ_v range tested. All configurations presented in figure 26(b) indicate that the exhaust flow was being turned effectively as $\Delta\delta/\Delta\delta_v \approx 1.0$. Whether or not resultant thrust-vector angle was equal to the geometric thrust-vector angle depended entirely upon the resultant thrust-vector angle

intercept at $\delta_v = 0°$. Recall that δ is dependent upon NPR for external expansion surface nozzles and that figure 26 is for a nominal NPR of 4.0.

The effects of geometric thrust-vector angle on pitching moment ratio are presented in figure 26(c). These data are essentially a mirror image of the resultant thrust-vector angle results and because of the similarities will not be discussed herein. Remember that an increase in δ results in a decrease in pitching moment, hence the slope change in $M/F_i h_{t,n}$ relative to δ_v.

Effect of aft flap initial angle.- The effect of aft flap initial angle on internal performance at NPR = 4.0 for several nozzle configurations is presented in figures 28 through 30. An example of typical internal static pressure distributions (configuration A1FS, $\delta_v = 0°$) over a range of aft flap initial angles is shown in figure 31 at a nominal NPR of 4.

For all configurations, downward rotation (from positive to negative α) of the aft flap resulted in increased resultant thrust-vector angle. (See figs. 28 through 30.) This was, of course, accompanied by a decrease in pitching moment ratio resulting from the increased normal force on the aft flap as the aft flap was rotated downward. Static pressure distribution data (fig. 31) show increased pressure on the aft flap as it is rotated downward and hence, increased positive (upward) normal force. The $\alpha = -8.3°$ case appears to have a shock located near the nozzle upper flap/aft flap juncture.

The effects of aft flap initial angle on resultant and internal thrust ratios (figs. 28 through 30) were dependent upon configuration variables such as geometric thrust-vector angle, aft flap shape, and nozzle internal area ratio; however, several general trends can be noted. Highest resultant thrust ratio values generally occurred when the aft flap was oriented such that the resultant thrust-vector angle δ was approximately equal to the geometric vector angle. In reality, however, the peak F_r/F_i probably occurred when the aft flap initial angle α had minimal impact on the supersonic flow exiting the upper and lower 2-D C-D divergent flap segments. It has long been recognized that deflecting supersonic exhaust flow generally results in some performance losses (ref. 9). Highest internal performance F/F_i generally occurred at the aft flap initial angle which resulted in values of resultant thrust-vector angle δ near zero. For dry power nozzle configuration D1FS (fig. 30) with $\delta_v = \pm 15°$ and $\pm 30°$, highest performance for each δ_v occurred at the aft flap initial angle which generated turning angles nearest zero. For example, consider $\delta_v = 30°$, highest measured thrust performance occurred at $\alpha = -28.5°$. The measured turning angle δ at this aft flap initial angle was 27.5° and was the lowest turning angle measured for the $\delta_v = 30°$ configuration. Configuration A3FS (with $\delta_v = 4.15°$, fig. 28) was the exception with the highest resultant thrust ratio F_r/F_i occurring at $\alpha = -8.3°$ and the highest thrust ratio F/F_i occurring at $\alpha = -4.5°$. Based on the general trends discussed previously, highest F_r/F_i and F/F_i values would be expected to occur for aft flap initial angles α of -2.8° and 2.7°, where resultant turning angles of approximately 3.8° and 1° were measured, respectively. Reasons for the departure of this configuration from general trends are unknown.

Effect of aft flap shape.- The effect of aft flap shape on internal performance parameters at an NPR of 4.0 can be found in figures 26, 28, and 29. Recall that the third digit in the configuration code represents aft flap shape (C for curved and F for flat). An example of typical internal static pressure distributions for a change in aft flap shape is presented in figure 32 at a nominal nozzle pressure ratio of 4.

Changing aft flap shape from flat to curved resulted in a downward rotation in the aft flap trailing edge (terminal angle) by 11° as indicated in the nozzle geometry sketches shown in figures 3 through 5. This 11° change in aft flap terminal angle resulted in increases in measured resultant thrust-vector angle δ ranging from approximately 3.5° to 8° above those measured for the flat aft flap shape. Actual levels of these increases were dependent upon other variables such as nozzle power setting, expansion ratio, geometric thrust-vector angle, and aft flap initial angle α. For example, the effects of aft flap shape on resultant turning angle were larger for the dry power configuration than for afterburning configurations. (See fig. 26.) This result would be expected, since the aspect ratio of the jet as it leaves the upper flap is greater for the dry power nozzles than the afterburning power nozzles and the thinner jet (more like a jet sheet) can be turned more effectively by a single surface (the aft flap). Static pressure distributions for a typical configuration (fig. 32) show that with the curved aft flap the pressure was higher along the entire flap than with the flat aft flap. This higher pressure results in an increase in the positive normal-force component on the aft flap; thereby, resultant thrust-vector angle is increased and larger nose down (negative) pitching moments are produced. The effects of aft flap shape on resultant and internal thrust ratios are similar to those noted previously for variation of aft flap angle α.

Effect of sidewall length.- The effect of sidewall length on performance increments as a function of NPR is presented for typical afterburning and dry power nozzle configurations in figures 33(a) and (b), respectively. Typical static pressure distributions for the afterburning nozzle configuration with long and short sidewalls ($\delta_v = 0°$) are provided at three values of NPR in figure 34. The performance increments $\Delta(F_r/F_i)$, $\Delta(F/F_i)$, $\Delta\delta$, and $\Delta(M/F_i h_{t,n})$ are defined as the performance for the configuration with long sidewalls minus the performance for the configuration with short sidewalls. A negative performance increment would therefore indicate short sidewall configuration performance greater than long sidewall configuration performance.

Performance increments $\Delta(F_r/F_i)$ and $\Delta\delta$ (fig. 33) were generally negative at low NPR's indicating that the long sidewall provided lower resultant thrust ratios and lower (or more negative) resultant thrust-vector angles than the short sidewall configurations. However, with the exception of A3FL and A3FS at higher NPR's, the long sidewall produced higher resultant thrust ratios and higher (or less negative) resultant thrust-vector angles. This probably occurs because, at high NPR, especially above design NPR (table I), the exhaust flow would tend to expand or spread more in the lateral direction when the short sidewall is installed. Expansion of exhaust flow through the open sides would result in decreases in both resultant thrust and resultant thrust-vector angle. The long sidewall prevents these losses at high NPR; but at low NPR, where there is less tendency for the flow to expand laterally, the long sidewall results in a thrust loss probably caused by increased friction drag.

Static pressure distributions (on the flap centerline) for afterburning nozzle configurations A1FL and A1FS are presented in figure 34. At low NPR's (NPR = 2), static pressures on the forward portion of the aft flap were lower for the long sidewall configuration than for the short sidewall. The result, as discussed previously, is lower (or more negative) resultant thrust-vector angles for the long sidewall. Increased static pressures on the aft portion of the aft flap at higher NPR's (4.0 and 6.0) would similarly explain the higher resultant thrust-vector angles measured for the long sidewall configuration relative to the short sidewall configuration.

Actual magnitudes of the increment in resultant thrust ratio for variations in sidewall length were generally within 0.5 percent for nozzle pressure ratios near design values ($3.0 \leq NPR \leq 5.0$) and were consistent with sidewall length effects noted for previous investigations of 2-D C-D and SERN nozzle configurations (refs. 7, 10, and 11). As noted in reference 11, increasing sidewall containment (or length) generally results in an increase in the effective expansion ratio of a configuration. Comparison of figures 15(a) and (c) indicates a definite shift in the NPR at which peak resultant thrust ratio occurs for change in sidewall length. Resultant thrust ratio for the long sidewall configurations (fig. 15(c)) tended to peak at $NPR \geq 6.0$; and for the short sidewall configurations resultant thrust ratio peaked at $3.0 < NPR < 4.0$. When the performance increments between the two configurations are computed at a constant NPR, these differences in effective expansion ratio appear. Comparing peak performance levels for a given nozzle flap geometry indicates there is little effect of sidewall length on peak performance as reported in references 5 and 8 to 10.

THRUST-REVERSER NOZZLE

To reverse thrust in, or ahead of, the convergent portion of a forward flight nozzle it is desirable to move the throat (minimum area) to the reverser ports (or passages) to avoid the losses that would be incurred by turning a supersonic flow. If nozzle back pressure on the engine is to be maintained within acceptable limits to avoid stall or overspeed, the effective areas (or mass flow) of both the unvectored and reverser nozzles must remain nearly the same. In practice, actuation (or structural) considerations and reverser passage length constraints necessitate the utilization of less than ideal reverser ports and can result in low efficiency. Therefore, when thrust is reversed under such conditions the reverser ports should have an enlarged throat area based on the expected ratio of discharge coefficients (based on the throat area of each) of the forward flight and thrust-reverser nozzles.

The thrust-reverser nozzle of the present investigation represents the dry power condition for the engine and is therefore related to the "D1-type" forward flight nozzles (see table I and fig. 5). The thrust-reverser-nozzle geometric throat area (sum of top and bottom port minimum areas) was sized approximately 20 percent greater than the "D1-type" nozzles to compensate for an expected decrease in discharge coefficient.

The discharge coefficients (based on reverser port area) measured in this investigation are shown in figure 23 for nozzle pressure ratios from 1.5 to 7.0. The variation in discharge coefficient with nozzle pressure ratio at low NPR's is large and is typical for ports of this type (refs. 10, 15, and 16). Comparison of measured values of nozzle discharge coefficient at NPR = 3.0 for the reverser (0.760 from fig. 23) with that of the unvectored nozzle (0.977 from figs. 21 and 22) indicates that the reverser port area should be $\frac{0.977}{0.760} = 1.286$ times unvectored nozzle throat area to prevent undesirable back pressure characteristics on the engine at this condition. As noted previously, the reverser port area was sized to be only 20 percent larger than the unvectored nozzle area; hence, an increase in port area would be desirable.

Static pressures measured on the surface of the blocker (fig. 35) indicate that sonic (choked) flow did not occur in the plane of minimum reverser port area (top port). The sonic line ($p/p_{t,j} = 0.528$) intersects the surface of the blocker at a point near the 90° break in the blocker surface. This sonic point location is

similar to that shown in the reverser of reference 15 which had a large number of pressure orifices installed in the port passage surfaces. Isobars derived from sidewall static pressures (ref. 15) at a nozzle pressure ratio of 5.0 indicate that one end of the sonic line was at the sharp port corner and the other end at the blocker near the port exit. The sharpness of the port corner of the present configuration and pressures measured on the blocker surface suggest that the orientation of the sonic line is similar to that of reference 15.

The thrust ratio (F/F_i) data of figure 23 show that as would be expected with a 135° blocker angle, well over 50 percent of the thrust was reversed over the NPR range. However, the difference in geometry between the top and bottom ports results in a vertical force component as shown in the normal force and pitching moment ratios of figure 23. This effect is caused by the geometry differences downstream of the port geometric throat (minimum) since the pressures of figure 34 indicate identical blocker pressure distributions for both ports up to that point. The additional pressure measurements on the external portion of the upper port indicate that the pressure on the overhanging piece of the blocker is below ambient at NPR up to 3.0 and above ambient at NPR above 4.0. Since the lower port has no overhanging blocker piece to generate a canceling force, it is likely that that normal force (which is zero at NPR = 3.0) shown in figure 23 results from the pressure differential across this piece or from the turning influence of this piece on the jet efflux.

VERTICAL TAKEOFF OR LANDING NOZZLES

The internal performance of the four vertical takeoff or landing nozzle configurations (fig. 8) is shown in figure 24. The nozzle pressure ratio test range for these nozzles was restricted because the combination of the displacement of the nozzle exit from the force balance moment reference center and the nearly vertical thrust vector produced large pitching moments and the balance pitching moment limit was rapidly reached.

Although balance limitations did not permit testing to a high enough nozzle pressure ratio to reach a constant level of discharge coefficient it is apparent from the data trends of figure 24 that discharge coefficient would likely be less than 0.9 for all configurations. In the range of nozzle pressure ratios tested, configurations V1 and V3, which both had the rounded lower lip, had significantly higher discharge coefficients than configurations V2 and V4. This result is consistent with results obtained from thrust-reverser-port investigations (ref. 16) which have shown that port corner shape has a large effect on discharge coefficient when flow is being turned into the port passage through large angles.

Thrust-vector angle was 80° or greater for all four configurations at a nozzle pressure ratio of 3.0. Configurations V3 and V4 which incorporated blocker 2 turned the flow 85° at a nozzle pressure ratio of 3.0 even though the blocker terminal angle (at the nozzle exit) was 11° less than the terminal angle of blocker 1 (see fig. 9(a)). This increased turning (despite the smaller terminal angle) can be attributed to the relatively longer flow passage (fig. 8) provided by blocker 2 after the internal flow has been turned toward the nozzle port exit. The longer passage allows the flow to stabilize and become more uniformly directed in the desired vertical direction. This indicates that after turning a flow through a large angle some passage length is needed to produce flow in the intended direction. Alternatively, with little or no passage length, it might be desirable to have some blocker variable geometry capability at the nozzle exit so that the terminal angle can be varied to modulate the thrust direction.

CONCLUSIONS

Static internal performance of a multifunction nozzle having some of the geometric characteristics of both two-dimensional convergent-divergent and single expansion ramp nozzles has been investigated in the static test facility of the Langley 16-Foot Transonic Tunnel. The internal expansion portion of the nozzle geometry consisted of two symmetrical flat surfaces of equal length, and the external expansion portion of the nozzle geometry consisted of a single aft flap. The aft flap could be varied in angle independently of the upper internal expansion surface to which it was attached. The effects of internal expansion ratio, nozzle thrust-vector angle (-30° to 30°), aft flap shape, aft flap angle, and sidewall containment were determined for dry and partial afterburning power settings. In addition, a partial afterburning power setting nozzle, a fully deployed thrust reverser, and four vertical takeoff or landing nozzle configurations were investigated. Results of the study have led to the following conclusions:

1. Internal performance for nozzle configurations in which the geometric thrust-vector angle was greater than or equal to zero was typical of nonaxisymmetric two-dimensional convergent-divergent performance in that a single performance peak was measured. Internal performance data for nozzle configurations in which geometric thrust-vector angle was less than zero generally indicated two resultant thrust peaks (characteristic of external expansion ramp nozzles).

2. Nozzle discharge coefficient was dependent on geometric thrust-vector angle and power setting, but nearly independent of whether flow was vectored up or down.

3. Resultant thrust ratio was nearly independent of geometric thrust-vector angle.

4. The nozzle of the present investigation provided effective exhaust flow turning throughout the entire range of geometric thrust-vector angles.

5. The thrust-reverser configuration provided levels of reverse thrust well in excess of 50 percent; however, because of upper/lower port asymmetry, normal force and pitching moment were also generated.

6. Vertical takeoff or landing nozzle configurations with the longest flow passage in the throat area provided the highest levels of flow turning. The rounded lower flap corner provided significantly higher nozzle discharge coefficients than the sharp lower flap corner.

NASA Langley Research Center
Hampton, VA 23665-5225
December 6, 1985

REFERENCES

1. Schmeer, James W.; Lauer, Rodney F., Jr.; and Berrier, Bobby L.: Performance of Blow-in-Door Ejector Nozzles Installed on a Twin-Jet Variable-Wing-Sweep Fighter Airplane Model. NASA TM X-1383, 1967.

2. Reubush, David E.; and Mercer, Charles E.: Effects of Nozzle Interfairing Modifications on Longitudinal Aerodynamic Characteristics of a Twin-Jet, Variable-Wing-Sweep Fighter Model. NASA TN D-7817, 1975.

3. Maiden, Donald L.; and Berrier, Bobby L.: Effect of Airframe Modifications on Longitudinal Aerodynamic Characteristics of a Fixed-Wing, Twin-Jet Fighter Airplane Model. NASA TM X-2523, 1972.

4. Capone, Francis J.; and Berrier, Bobby L.: Investigation of Axisymmetric and Nonaxisymmetric Nozzles Installed on a 0.10-Scale F-18 Prototype Airplane Model. NASA TP-1638, 1980.

5. Nelson, B. D.; and Nicolai, L. M.: Application of Multi-Function Nozzles to Advanced Fighters. AIAA-81-2618, Dec. 1981.

6. Wallace, Hoyt W.; and Bowers, Douglas L.: Advanced Nozzle Integration for Air Combat Fighter Application. AIAA-82-1135, June 1982.

7. Berrier, Bobby L.; and Re, Richard J.: Effect of Several Geometric Parameters on the Static Internal Performance of Three Nonaxisymmetric Nozzle Concepts. NASA TP-1468, 1979.

8. Mason, Mary L.; Putnam, Lawrence E.; and Re, Richard J.: The Effect of Throat Contouring on Two-Dimensional Converging-Diverging Nozzles at Static Conditions. NASA TP-1704, 1980.

9. Capone, Francis J.: Static Performance of Five Twin-Engine Nonaxisymmetric Nozzles With Vectoring and Reversing Capability. NASA TP-1224, 1978.

10. Re, Richard J.; and Leavitt, Laurence D.: Static Internal Performance Including Thrust Vectoring and Reversing of Two-Dimensional Convergent-Divergent Nozzles. NASA TP-2253, 1984.

11. Re, Richard J.; and Berrier, Bobby L.: Static Internal Performance of Single Expansion-Ramp Nozzles With Thrust Vectoring and Reversing. NASA TP-1962, 1982.

12. Berrier, Bobby L.; and Leavitt, Laurence D.: Static Internal Performance of Single Expansion-Ramp Nozzles With Thrust-Vectoring Capability up to 60°. NASA TP-2364, 1984.

13. Re, Richard J.; and Leavitt, Laurence D.: Static Internal Performance of Single-Expansion-Ramp Nozzles With Various Combinations of Internal Geometric Parameters. NASA TM-86270, 1984.

14. Peddrew, Kathryn H., compiler: A User's Guide to the Langley 16-Foot Transonic Tunnel. NASA TM-83186, 1981.

15. Putnam, Lawrence E.; and Strong, Edward G.: Internal Pressure Distributions for a Two-Dimensional Thrust-Reversing Nozzle Operating at a Free-Stream Mach Number of Zero. NASA TM-85655, 1983.

16. Re, Richard J.; and Mason, Mary L.: Port Geometry Effects on Thrust Reverser Static Performance. AIAA-85-1345, July 1985.

TABLE I.- GEOMETRIC PARAMETERS OF UNVECTORED AND VECTORED NOZZLE CONFIGURATIONS

(a) Afterburning power nozzles

Nozzle configuration	Flaps						Aft flap			Side-walls	Surface pressures	Internal performance
				Unvectored								
	δ_v, deg	δ_u, deg	δ_l, deg	ρ, deg	A_e/A_t	Design NPR	Surface shape	α, deg	σ, deg		Table	Figure
A1FS	-30	32.7	-27.3	2.7	1.10	3.05	Flat	32.7	32.7	Short	II(a)	15(a)
	-15	17.7	-12.3					17.7	17.7		II(b)	15(a)
	0	2.7	2.7					-8.3	-8.3		II(c)	13(a)
								-2.8	-2.8		II(d)	
								0	0		II(e)	
								2.7	2.7		II(f)	
	15	-12.3	17.7					-12.3	-12.3		II(g)	15(a)
	30	-27.3	32.7					-27.3	-27.3		II(h)	15(a)
A1FL	-30	32.7	-27.3					32.7	32.7	Long	II(i)	15(c)
	0	2.7	2.7					2.7	2.7		II(j)	
	30	-27.3	32.7					-27.3	-27.3		II(k)	
A1CS	-30	32.7	-27.3				Curved	32.7	21.7	Short	II(l)	15(b)
	-15	17.7	-12.3					17.7	6.7		II(m)	
	0	2.7	2.7					2.7	-8.3		II(n)	
	15	-12.3	17.7					-12.3	-23.3		II(o)	
	30	-27.3	32.7					-27.3	-38.3		II(p)	
A2FS	0	11.0	11.0	11.0	1.40	5.43	Flat	0	0		II(q)	13(b)
								5.5	5.5		II(r)	
								11.0	11.0		II(s)	
A2CS							Curved	0	-11.0		II(t)	14(a)
								5.5	-5.5		II(u)	
								11.0	0		II(v)	
A3FS	4.15	2.7		6.85	1.25	4.25	Flat	-8.3	-8.3		II(w)	13(c)
								-2.8	-2.8		II(x)	
								0	0		II(y)	
								2.7	2.7		II(z)	
	-4.15	11.0	2.7					0	0		II(aa)	13(d)
								5.5	5.5		II(bb)	
								11.0	11.0		II(cc)	
A3FL	4.15	2.7	11.0					2.7	2.7	Long	II(dd)	17
A3CS							Curved	-8.3	-19.3	Short	II(ee)	14(b)
								-2.8	-13.8		II(ff)	
								2.7	-8.3		II(gg)	
	-4.15	11.0	2.7					11.0	0		II(hh)	16

TABLE I.- Concluded

(b) Partial afterburning and dry power nozzles

Nozzle configuration	Flaps						Aft flap			Side-walls	Surface pressures	Internal performance
				Unvectored								
	δ_v, deg	δ_u, deg	δ_l, deg	ρ, deg	A_e/A_t	Design NPR	Surface shape	α, deg	σ, deg		Table	Figure
P1FS	-0.60	2.7	1.5	2.1	1.10	3.05	Flat	-8.3	-8.3	Short	III(a)	18(a)
↓	↓	↓	↓	↓	↓	↓	↓	-2.8	-2.8	↓	III(b)	↓
↓	↓	↓	↓	↓	↓	↓	↓	0	0	↓	III(c)	↓
↓	↓	↓	↓	↓	↓	↓	↓	2.7	2.7	↓	III(d)	↓
P1CS	↓	↓	↓	↓	↓	↓	Curved	2.7	-8.3	↓	III(e)	20
P2FS	-4.75	11.0	↓	6.25	1.25	4.25	Flat	0	0	↓	III(f)	18(b)
↓	↓	↓	↓	↓	↓	↓	↓	5.5	5.5	↓	III(g)	↓
↓	↓	↓	↓	↓	↓	↓	↓	11.0	11.0	↓	III(h)	↓
P2CS	↓	↓	↓	↓	↓	↓	Curved	5.5	-5.5	↓	III(i)	19
↓	↓	↓	↓	↓	↓	↓	↓	8.3	-2.7	↓	III(j)	↓
↓	↓	↓	↓	↓	↓	↓	↓	11.0	0	↓	III(k)	↓
D1CS	-30	31.5	-28.5	1.5	1.10	3.05	↓	31.5	20.5	↓	III(l)	22
↓	-15	16.5	-13.5	↓	↓	↓	↓	16.5	5.5	↓	III(m)	↓
↓	0	1.5	1.5	↓	↓	↓	↓	1.5	-9.5	↓	III(n)	↓
↓	15	-13.5	16.5	↓	↓	↓	↓	-13.5	-24.5	↓	III(o)	↓
↓	30	-28.5	31.5	↓	↓	↓	↓	-28.5	-39.5	↓	III(p)	↓
D1FS	-30	31.5	-28.5	↓	↓	↓	Flat	31.5	31.5	↓	III(q)	21(a)
↓	-15	16.5	-13.5	↓	↓	↓	↓	16.5	16.5	↓	III(r)	↓
↓	0	1.5	1.5	↓	↓	↓	↓	1.5	1.5	↓	III(s)	↓
↓	15	-13.5	16.5	↓	↓	↓	↓	-13.5	-13.5	↓	III(t)	↓
↓	30	-28.5	31.5	↓	↓	↓	↓	-28.5	-28.5	↓	III(u)	↓
↓	-30	31.5	-28.5	↓	↓	↓	↓	26.0	26.0	↓	III(v)	↓
↓	-15	16.5	-13.5	↓	↓	↓	↓	11.0	11.0	↓	III(w)	↓
↓	0	1.5	1.5	↓	↓	↓	↓	-4.0	-4.0	↓	III(x)	↓
↓	15	-13.5	16.5	↓	↓	↓	↓	-19.0	-19.0	↓	III(y)	↓
↓	30	-28.5	31.5	↓	↓	↓	↓	-34.0	-34.0	↓	III(z)	↓
D1FL	-30	31.5	-28.5	↓	↓	↓	↓	31.5	31.5	Long	III(aa)	21(b)
↓	0	1.5	1.5	↓	↓	↓	↓	1.5	1.5	↓	III(bb)	↓
↓	30	-28.5	31.5	↓	↓	↓	↓	-28.5	-28.5	↓	III(cc)	↓

TABLE II.- RATIO OF INTERNAL STATIC PRESSURE TO JET TOTAL PRESSURE FOR AFTERBURNING POWER NOZZLE CONFIGURATIONS

(a) Configuration A1FS, $\delta_v = -30°$

NPR	$p/p_{t,j}$ at $x'/\ell_{f,nom}$ of -														
	-.609	-.498	-.387	-.277	-.166	.059	.280	.502	.723	.945	-.609	-.498	-.387	-.277	-.166
	Upper flap										Lower flap				
2.020	.123	.193	.353	.456	.523	.535	.513	.503	.501	.481	.895	.843	.782	.720	.653
2.528	.123	.183	.262	.335	.365	.424	.512	.407	.329	.383	.895	.842	.781	.719	.652
3.025	.122	.182	.261	.333	.365	.320	.226	.421	.390	.296	.894	.841	.780	.719	.651
3.325	.121	.182	.261	.332	.365	.321	.224	.301	.372	.327	.894	.841	.779	.719	.650
3.709	.122	.182	.261	.331	.365	.322	.223	.153	.262	.295	.895	.841	.780	.720	.651
4.042	.121	.182	.261	.330	.364	.322	.223	.152	.178	.228	.895	.841	.779	.719	.650
5.041	.121	.183	.261	.329	.364	.323	.223	.152	.105	.184	.895	.841	.780	.719	.651
5.345	.121	.183	.261	.329	.364	.324	.223	.152	.105	.172	.895	.842	.780	.719	.651

(b) Configuration A1FS, $\delta_v = -15°$

NPR	$p/p_{t,j}$ at $x'/\ell_{f,nom}$ of -														
	-.609	-.498	-.387	-.277	-.166	.059	.230	.502	.723	.945	-.609	-.498	-.387	-.277	-.166
	Upper flap										Lower flap				
1.995	.169	.241	.301	.371	.525	.553	.517	.507	.506	.486	.702	.681	.617	.551	.484
2.502	.168	.242	.301	.349	.369	.399	.510	.408	.330	.356	.701	.680	.615	.550	.483
3.027	.169	.242	.301	.347	.368	.374	.316	.390	.363	.267	.700	.680	.615	.550	.483
3.332	.170	.241	.301	.346	.368	.374	.313	.223	.347	.283	.701	.680	.615	.550	.483
3.713	.170	.241	.301	.345	.368	.375	.312	.218	.150	.271	.701	.680	.615	.550	.483
4.003	.170	.241	.301	.345	.369	.375	.312	.217	.145	.231	.701	.681	.615	.550	.483
5.001	.170	.241	.301	.345	.369	.376	.311	.215	.141	.164	.701	.681	.616	.550	.483
6.007	.171	.240	.301	.345	.369	.377	.311	.216	.141	.102	.701	.682	.617	.551	.484
6.592	.171	.240	.301	.344	.369	.377	.311	.216	.141	.096	.701	.682	.617	.551	.485

TABLE II.- Continued

(c) Configuration A1FS, $\delta_v = 0°$, $\alpha = -8.3°$

NPR	$p/p_{t,j}$ at $x'/z_{f,nom}$ of -														
	-.609	-.498	-.387	-.277	-.166	.033	.255	.476	.697	.919	-.609	-.498	-.387	-.277	-.166
	Upper flap										Lower flap				
2.004	.286	.385	.431	.397	.391	.589	.590	.529	.513	.502	.306	.381	.435	.397	.341
2.522	.286	.386	.431	.395	.342	.540	.557	.474	.374	.311	.305	.379	.434	.396	.341
3.013	.286	.385	.431	.394	.343	.528	.477	.441	.399	.315	.305	.379	.433	.397	.340
3.332	.286	.390	.432	.394	.343	.527	.471	.375	.315	.327	.306	.379	.433	.397	.340
3.739	.287	.391	.432	.394	.343	.526	.466	.368	.297	.210	.306	.378	.433	.397	.340
3.995	.287	.391	.432	.394	.343	.526	.464	.365	.276	.206	.306	.378	.433	.397	.340
5.028	.286	.391	.432	.393	.342	.526	.462	.357	.268	.177	.306	.378	.432	.398	.339
6.012	.286	.390	.432	.393	.342	.526	.461	.356	.265	.174	.306	.379	.432	.398	.339
6.023	.286	.390	.432	.393	.342	.526	.461	.356	.264	.174	.305	.378	.432	.398	.339
6.557	.286	.390	.432	.393	.342	.527	.461	.356	.264	.174	.306	.379	.433	.399	.339

(d) Configuration A1FS, $\delta_v = 0°$, $\alpha = -2.8°$

NPR	$p/p_{t,j}$ at $x'/z_{f,nom}$ of -														
	-.609	-.498	-.387	-.277	-.166	.044	.266	.487	.708	.930	-.609	-.498	-.387	-.277	-.166
	Upper flap										Lower flap				
2.022	.286	.385	.431	.397	.343	.539	.561	.514	.503	.495	.305	.381	.435	.397	.341
2.515	.286	.386	.431	.395	.342	.393	.478	.502	.412	.334	.304	.380	.434	.396	.341
3.037	.288	.388	.431	.394	.342	.385	.401	.332	.329	.406	.305	.379	.433	.397	.340
3.335	.288	.390	.432	.394	.343	.385	.397	.323	.303	.237	.305	.379	.433	.397	.340
3.745	.287	.391	.432	.393	.343	.384	.395	.313	.250	.193	.305	.379	.433	.397	.340
3.711	.288	.391	.432	.394	.343	.384	.395	.314	.251	.194	.305	.379	.433	.397	.340
4.038	.287	.391	.432	.394	.343	.383	.395	.310	.245	.190	.305	.379	.433	.397	.340
5.027	.286	.391	.432	.393	.343	.380	.394	.307	.236	.160	.305	.379	.432	.398	.339
6.010	.286	.390	.432	.393	.342	.378	.394	.307	.234	.158	.306	.378	.432	.398	.339
6.561	.286	.390	.432	.393	.342	.376	.394	.307	.234	.157	.306	.378	.432	.399	.339

TABLE II.- Continued

(e) Configuration A1FS, $\delta_v = 0°$, $\alpha = 0°$

NPR	$p/p_{t,j}$ at $x'/Z_{f,nom}$ of -														
	-.609	-.498	-.387	-.277	-.166	.052	.273	.494	.716	.937	-.609	-.498	-.387	-.277	-.166
	Upper flap										Lower flap				
2.012	.288	.386	.431	.397	.343	.517	.552	.516	.506	.498	.304	.383	.435	.397	.341
2.536	.288	.386	.431	.395	.342	.330	.378	.511	.449	.359	.302	.382	.434	.397	.341
3.030	.288	.388	.431	.394	.342	.328	.359	.305	.317	.386	.303	.380	.433	.397	.340
3.315	.288	.390	.432	.394	.343	.327	.358	.293	.278	.222	.303	.380	.433	.397	.340
3.737	.288	.391	.432	.394	.343	.326	.357	.286	.231	.187	.304	.380	.433	.397	.340
4.049	.287	.391	.432	.393	.343	.326	.357	.285	.224	.161	.304	.380	.432	.397	.340
5.027	.286	.391	.432	.393	.343	.323	.357	.284	.217	.150	.304	.379	.432	.398	.339
6.016	.286	.390	.432	.393	.343	.321	.357	.283	.216	.149	.306	.379	.432	.398	.339
6.769	.286	.390	.432	.393	.343	.320	.357	.283	.216	.149	.305	.379	.432	.399	.339

(f) Configuration A1FS, $\delta_v = 0°$, $\alpha = 2.7°$

NPR	$p/p_{t,j}$ at $x'/Z_{f,nom}$ of -														
	-.609	-.498	-.387	-.277	-.166	.059	.280	.502	.723	.945	-.609	-.498	-.387	-.277	-.166
	Upper flap										Lower flap				
1.999	.288	.386	.431	.398	.343	.492	.544	.523	.512	.503	.307	.387	.436	.398	.342
2.516	.288	.387	.431	.396	.343	.292	.331	.502	.470	.393	.306	.386	.435	.397	.341
3.023	.287	.389	.432	.395	.343	.290	.321	.277	.309	.386	.305	.385	.434	.397	.341
3.319	.287	.390	.432	.394	.343	.289	.320	.266	.226	.214	.305	.385	.434	.397	.340
3.744	.287	.391	.432	.394	.343	.287	.320	.262	.211	.181	.305	.384	.433	.397	.340
4.012	.287	.391	.433	.394	.343	.286	.320	.262	.206	.152	.305	.384	.433	.398	.340
5.028	.286	.390	.432	.393	.343	.283	.319	.261	.201	.142	.304	.384	.432	.398	.339
6.015	.286	.390	.433	.392	.343	.280	.319	.261	.201	.141	.305	.384	.432	.398	.339
6.735	.286	.390	.432	.392	.343	.277	.319	.261	.200	.141	.305	.384	.432	.398	.339

TABLE II.- Continued

(g) Configuration A1FS, $\delta_v = 15°$

NPR	$p/p_{t,j}$ at $x'/l_{f,nom}$ of -														
	-.609	-.498	-.387	-.277	-.166	.059	.280	.502	.723	.945	-.609	-.498	-.387	-.277	-.166
	Upper flap										Lower flap				
2.010	.701	.682	.616	.551	.485	.348	.461	.525	.529	.513	.170	.237	.298	.352	.371
2.544	.701	.681	.616	.551	.485	.349	.245	.374	.425	.453	.170	.237	.299	.350	.370
2.522	.701	.681	.616	.551	.485	.349	.245	.380	.431	.455	.170	.237	.299	.350	.370
3.014	.701	.681	.615	.551	.484	.350	.244	.177	.330	.330	.170	.236	.299	.349	.370
3.334	.701	.681	.615	.551	.484	.351	.244	.177	.298	.281	.170	.236	.300	.348	.369
3.723	.701	.681	.615	.551	.484	.352	.244	.177	.287	.231	.170	.236	.300	.347	.370
3.989	.701	.682	.616	.551	.485	.352	.244	.177	.286	.220	.170	.236	.301	.347	.369
4.015	.701	.681	.616	.551	.485	.352	.244	.177	.285	.220	.170	.236	.301	.347	.369
5.035	.701	.682	.616	.551	.485	.354	.244	.177	.284	.217	.173	.236	.301	.345	.369
6.013	.701	.682	.617	.551	.486	.355	.244	.178	.283	.216	.174	.236	.300	.345	.369
6.361	.701	.683	.617	.552	.486	.356	.244	.178	.283	.216	.174	.236	.300	.345	.369

(h) Configuration A1FS, $\delta_v = 30°$

NPR	$p/p_{t,j}$ at $x'/l_{f,nom}$ of -														
	-.609	-.498	-.387	-.277	-.166	.059	.280	.502	.723	.945	-.609	-.498	-.387	-.277	-.166
	Upper flap										Lower flap				
1.984	.895	.843	.782	.724	.662	.480	.391	.523	.541	.500	.312	.318	.342	.392	.440
2.519	.895	.842	.779	.720	.655	.460	.346	.241	.377	.422	.124	.186	.260	.339	.382
3.000	.895	.842	.779	.721	.655	.461	.346	.241	.176	.325	.124	.185	.260	.337	.381
3.337	.896	.843	.779	.721	.655	.466	.346	.241	.175	.299	.123	.184	.261	.337	.381
3.711	.896	.843	.779	.721	.655	.470	.346	.241	.175	.291	.123	.183	.262	.336	.381
4.029	.896	.843	.779	.721	.655	.473	.346	.242	.175	.290	.123	.183	.262	.336	.381
4.637	.896	.843	.779	.721	.655	.474	.346	.242	.175	.289	.123	.183	.262	.335	.380

TABLE II.- Continued

(i) Configuration A1FL, $\delta_v = -30°$

NPR	$p/p_{t,j}$ at $x'/\ell_{f,nom}$ of -														
	-.609	-.498	-.387	-.277	-.166	.059	.280	.502	.723	.945	-.609	-.498	-.387	-.277	-.166
	Upper flap										Lower flap				
2.000	.123	.184	.259	.435	.527	.571	.525	.505	.503	.477	.895	.842	.780	.720	.655
2.532	.122	.183	.260	.335	.371	.322	.476	.464	.389	.345	.895	.841	.777	.719	.653
3.017	.121	.182	.260	.333	.370	.323	.225	.354	.385	.321	.895	.841	.778	.719	.653
3.332	.121	.182	.261	.332	.370	.323	.225	.258	.323	.316	.895	.841	.778	.719	.653
3.738	.121	.182	.261	.331	.370	.324	.225	.160	.247	.271	.895	.841	.778	.719	.653
4.029	.121	.182	.261	.331	.369	.325	.225	.160	.131	.239	.896	.842	.778	.720	.653
5.043	.120	.182	.262	.330	.369	.326	.224	.160	.120	.172	.896	.842	.778	.720	.653
6.014	.121	.183	.262	.330	.368	.329	.225	.160	.119	.096	.897	.842	.778	.720	.653
6.902	.122	.183	.262	.329	.368	.330	.225	.160	.119	.088	.897	.842	.779	.720	.654

(j) Configuration A1FL, $\delta_v = 0°$

NPR	$p/p_{t,j}$ at $x'/\ell_{f,nom}$ of -														
	-.609	-.498	-.387	-.277	-.166	.059	.280	.502	.723	.945	-.609	-.498	-.387	-.277	-.166
	Upper flap										Lower flap				
2.008	.289	.386	.431	.396	.342	.361	.523	.540	.517	.500	.297	.383	.439	.400	.345
2.516	.289	.389	.432	.394	.342	.294	.319	.268	.495	.489	.295	.382	.438	.399	.344
3.031	.286	.390	.432	.393	.342	.293	.319	.266	.297	.278	.294	.383	.437	.399	.344
3.325	.288	.390	.433	.393	.342	.292	.319	.266	.239	.225	.294	.383	.437	.399	.344
3.720	.288	.391	.433	.393	.342	.291	.319	.266	.237	.219	.294	.383	.437	.399	.344
4.015	.288	.391	.433	.393	.342	.291	.319	.266	.237	.188	.293	.383	.436	.399	.344
5.025	.287	.390	.433	.393	.341	.288	.318	.265	.236	.187	.293	.383	.435	.400	.344
6.006	.286	.390	.433	.393	.341	.285	.317	.265	.236	.187	.292	.382	.435	.400	.343
6.637	.286	.389	.433	.393	.341	.282	.317	.265	.236	.187	.292	.381	.435	.400	.343

TABLE II.- Continued

(k) Configuration A1FL, $\delta_v = 30°$

NPR	$p/p_{t,j}$ at $x'/z_{f,nom}$ of -														
	-.609	-.498	-.387	-.277	-.166	.059	.280	.502	.723	.945	-.609	-.498	-.387	-.277	-.166
	Upper flap										Lower flap				
2.010	.895	.843	.781	.721	.655	.479	.347	.242	.399	.481	.125	.186	.260	.342	.382
2.509	.895	.842	.779	.720	.654	.479	.346	.242	.331	.371	.124	.184	.262	.339	.381
3.002	.895	.842	.778	.720	.654	.480	.345	.242	.177	.301	.123	.183	.263	.337	.380
3.306	.895	.842	.779	.720	.654	.480	.345	.242	.176	.297	.123	.183	.263	.336	.380
3.709	.896	.842	.779	.721	.654	.481	.346	.242	.176	.295	.123	.183	.263	.336	.380
4.042	.896	.842	.779	.720	.654	.481	.345	.242	.176	.294	.122	.183	.263	.335	.380
4.596	.896	.842	.779	.720	.654	.482	.345	.242	.175	.293	.122	.183	.262	.335	.380

(l) Configuration A1CS, $\delta_v = -30°$

NPR	$p/p_{t,j}$ at $x'/z_{f,nom}$ of -														
	-.609	-.498	-.387	-.277	-.166	.065	.286	.507	.729	.950	-.609	-.498	-.387	-.277	-.166
	Upper flap										Lower flap				
2.008	.288	.300	.330	.387	.439	.527	.560	.567	.559	.521	.899	.844	.781	.720	.653
2.528	.123	.184	.257	.333	.360	.503	.551	.473	.437	.468	.898	.842	.779	.719	.650
3.016	.123	.183	.257	.331	.360	.322	.406	.514	.454	.370	.897	.841	.778	.718	.649
3.308	.123	.182	.258	.330	.360	.322	.253	.417	.479	.403	.897	.842	.778	.718	.649
3.721	.123	.182	.258	.330	.360	.322	.252	.198	.375	.407	.897	.842	.778	.719	.649
4.010	.122	.181	.258	.329	.359	.322	.252	.195	.302	.350	.897	.841	.778	.719	.649
5.018	.122	.182	.260	.327	.359	.322	.252	.194	.146	.113	.896	.841	.778	.718	.649
6.034	.124	.182	.259	.326	.358	.321	.252	.195	.145	.112	.896	.841	.778	.718	.650

TABLE II.- Continued

(m) Configuration A1CS, $\delta_v = -15°$

NPR	$p/p_{t,j}$ at $x'/\ell_{f,nom}$ of -														
	-.609	-.498	-.387	-.277	-.166	.065	.286	.507	.729	.950	-.609	-.498	-.387	-.277	-.166
	Upper flap										Lower flap				
2.022	.171	.237	.300	.356	.523	.581	.568	.568	.562	.522	.701	.682	.615	.555	.487
2.528	.171	.236	.301	.352	.372	.476	.550	.473	.414	.484	.700	.681	.615	.554	.487
3.029	.170	.236	.301	.350	.372	.381	.350	.522	.429	.373	.700	.681	.614	.553	.488
3.344	.171	.236	.301	.349	.372	.381	.346	.276	.467	.363	.701	.682	.615	.553	.488
3.296	.171	.236	.302	.350	.372	.382	.346	.278	.465	.361	.701	.682	.615	.554	.488
3.720	.171	.237	.302	.349	.372	.381	.345	.267	.266	.394	.701	.682	.615	.554	.489
4.025	.171	.237	.301	.348	.372	.381	.344	.265	.192	.326	.701	.682	.616	.554	.489
5.017	.174	.237	.301	.347	.371	.380	.343	.264	.186	.139	.701	.682	.617	.554	.490
6.003	.174	.237	.300	.346	.371	.380	.344	.264	.185	.138	.701	.683	.618	.555	.491
6.769	.174	.237	.300	.345	.371	.380	.343	.265	.185	.138	.701	.684	.619	.555	.492

(n) Configuration A1CS, $\delta_v = 0°$

NPR	$p/p_{t,j}$ at $x'/\ell_{f,nom}$ of -														
	-.609	-.498	-.387	-.277	-.166	.065	.286	.507	.729	.950	-.609	-.498	-.387	-.277	-.166
	Upper flap										Lower flap				
2.009	.288	.385	.431	.395	.342	.511	.581	.577	.562	.529	.297	.389	.439	.399	.343
2.537	.288	.386	.431	.394	.342	.289	.481	.556	.496	.433	.295	.387	.439	.398	.343
3.016	.287	.388	.432	.393	.342	.290	.362	.345	.482	.499	.295	.389	.437	.398	.343
3.334	.287	.390	.432	.393	.342	.292	.360	.328	.350	.388	.295	.390	.437	.398	.343
3.742	.287	.391	.432	.393	.342	.293	.359	.319	.281	.250	.294	.391	.436	.398	.342
4.054	.287	.391	.432	.393	.342	.294	.359	.317	.272	.242	.295	.391	.435	.398	.342
3.997	.287	.391	.432	.393	.342	.294	.359	.318	.274	.245	.295	.391	.436	.398	.342
5.024	.286	.391	.432	.392	.342	.294	.358	.317	.263	.203	.296	.391	.435	.399	.342
6.034	.286	.390	.432	.392	.342	.291	.358	.317	.261	.200	.297	.391	.435	.399	.342
6.635	.286	.390	.432	.392	.342	.290	.358	.317	.261	.200	.297	.391	.435	.399	.342

TABLE II.- Continued

(o) Configuration A1CS, $\delta_v = 15°$

NPR	$p/p_{t,j}$ at $x'/l_{f,nom}$ of -														
	-.609	-.498	-.387	-.277	-.166	.065	.286	.507	.729	.950	-.609	-.498	-.387	-.277	-.166
	Upper flap										Lower flap				
2.011	.701	.682	.617	.552	.487	.340	.515	.584	.571	.520	.170	.238	.298	.353	.372
2.521	.700	.681	.615	.551	.486	.340	.272	.469	.531	.463	.170	.237	.299	.350	.370
3.018	.701	.681	.615	.551	.487	.340	.272	.305	.439	.452	.170	.236	.299	.349	.370
3.313	.701	.681	.615	.551	.487	.340	.272	.222	.411	.340	.170	.236	.300	.348	.370
3.702	.701	.682	.616	.552	.487	.340	.272	.222	.385	.305	.170	.236	.300	.347	.370
3.984	.701	.682	.616	.552	.487	.340	.272	.222	.378	.282	.170	.236	.300	.347	.370
5.047	.701	.682	.616	.552	.488	.340	.272	.222	.375	.264	.173	.236	.301	.346	.370
5.009	.701	.682	.616	.552	.488	.340	.272	.222	.375	.264	.173	.236	.301	.346	.370
5.563	.701	.682	.617	.552	.489	.340	.272	.223	.375	.264	.174	.236	.300	.345	.370

(p) Configuration A1CS, $\delta_v = 30°$

NPR	$p/p_{t,j}$ at $x'/l_{f,nom}$ of -														
	-.609	-.498	-.387	-.277	-.166	.065	.286	.507	.729	.950	-.609	-.498	-.387	-.277	-.166
	Upper flap										Lower flap				
1.997	.896	.844	.782	.722	.658	.498	.401	.598	.581	.529	.195	.236	.291	.403	.491
2.509	.896	.842	.780	.720	.656	.492	.385	.296	.509	.510	.124	.185	.259	.339	.381
2.993	.895	.842	.779	.720	.655	.491	.385	.296	.354	.441	.123	.184	.260	.337	.380
3.324	.895	.842	.779	.720	.655	.492	.385	.296	.233	.416	.123	.183	.261	.336	.380
3.736	.896	.842	.779	.720	.655	.492	.385	.296	.232	.385	.123	.183	.262	.336	.380
4.055	.896	.842	.779	.720	.655	.492	.385	.297	.232	.381	.123	.182	.262	.335	.380
4.024	.896	.842	.779	.720	.655	.492	.385	.297	.232	.381	.123	.182	.262	.335	.379

TABLE II.- Continued

(q) Configuration A2FS, $\delta_v = 0°$, $\alpha = 0°$

NPR	$p/p_{t,j}$ at $x'/\ell_{f,nom}$ of -														
	-.609	-.498	-.387	-.277	-.166	.033	.255	.476	.697	.919	-.609	-.498	-.387	-.277	-.166
	Upper flap										Lower flap				
2.012	.200	.246	.277	.440	.465	.498	.543	.550	.528	.507	.201	.250	.286	.296	.450
2.508	.201	.245	.279	.276	.252	.388	.513	.484	.419	.386	.200	.249	.285	.279	.250
3.000	.201	.244	.279	.274	.252	.329	.251	.467	.460	.348	.199	.249	.285	.278	.250
3.539	.201	.244	.280	.273	.252	.330	.248	.245	.369	.425	.199	.248	.284	.277	.250
4.037	.201	.245	.280	.273	.252	.331	.248	.183	.146	.296	.199	.249	.284	.277	.250
4.537	.201	.245	.281	.272	.252	.331	.248	.182	.137	.233	.199	.249	.285	.276	.249
5.041	.201	.246	.281	.272	.252	.332	.247	.182	.135	.148	.199	.249	.285	.276	.249
5.334	.201	.246	.281	.272	.252	.332	.247	.182	.134	.141	.198	.249	.284	.276	.249
5.733	.201	.245	.281	.271	.252	.332	.247	.182	.134	.138	.198	.249	.284	.276	.249
6.037	.201	.245	.281	.271	.252	.332	.247	.182	.134	.137	.199	.249	.284	.275	.249
6.757	.201	.245	.281	.271	.252	.331	.247	.182	.133	.136	.199	.249	.284	.275	.248

(r) Configuration A2FS, $\delta_v = 0°$, $\alpha = 5.5°$

NPR	$p/p_{t,j}$ at $x'/\ell_{f,nom}$ of -														
	-.609	-.498	-.387	-.277	-.166	.044	.266	.487	.708	.930	-.609	-.498	-.387	-.277	-.166
	Upper flap										Lower flap				
2.023	.200	.245	.276	.293	.443	.481	.530	.542	.523	.504	.201	.250	.285	.291	.449
2.520	.201	.245	.279	.276	.252	.310	.448	.476	.435	.389	.200	.250	.285	.279	.251
3.015	.201	.244	.280	.275	.252	.256	.324	.386	.429	.360	.200	.249	.284	.278	.250
3.514	.201	.244	.280	.274	.252	.256	.196	.292	.325	.377	.200	.249	.284	.277	.250
4.039	.202	.245	.280	.273	.252	.256	.195	.147	.115	.251	.199	.248	.284	.277	.250
4.541	.201	.245	.281	.272	.252	.257	.195	.147	.112	.193	.199	.249	.284	.276	.249
5.028	.201	.246	.281	.272	.252	.257	.195	.147	.111	.173	.199	.249	.284	.276	.249
5.343	.201	.246	.281	.272	.252	.257	.195	.147	.111	.151	.198	.249	.284	.276	.249
5.724	.201	.246	.281	.272	.252	.258	.195	.147	.111	.101	.199	.249	.284	.276	.249
6.035	.201	.245	.281	.271	.252	.258	.195	.147	.111	.090	.199	.249	.284	.275	.249
6.907	.201	.245	.281	.271	.252	.258	.195	.147	.111	.089	.199	.249	.284	.275	.249

TABLE II.- Continued

(s) Configuration A2FS, $\delta_v = 0°$, $\alpha = 11.0°$

NPR	$p/p_{t,j}$ at $x'/\ell_{f,nom}$ of -														
	-.609	-.498	-.387	-.277	-.166	.059	.280	.502	.723	.945	-.609	-.498	-.387	-.277	-.166
	Upper flap										Lower flap				
1.995	.200	.245	.276	.278	.429	.473	.529	.545	.531	.512	.201	.250	.285	.321	.455
2.531	.200	.245	.279	.276	.251	.347	.383	.435	.447	.413	.200	.249	.285	.279	.250
3.061	.201	.244	.279	.274	.251	.193	.301	.326	.385	.364	.199	.249	.284	.278	.250
3.018	.201	.244	.279	.274	.252	.193	.305	.335	.390	.367	.199	.249	.285	.278	.250
3.567	.201	.244	.280	.273	.252	.194	.152	.261	.281	.338	.199	.249	.285	.277	.250
3.517	.201	.244	.280	.273	.252	.194	.152	.267	.290	.344	.199	.249	.285	.277	.250
4.041	.201	.245	.280	.273	.252	.194	.152	.116	.198	.251	.199	.248	.284	.276	.250
4.542	.201	.245	.281	.272	.252	.194	.151	.116	.162	.199	.199	.249	.284	.276	.249
5.044	.201	.246	.281	.272	.252	.194	.151	.116	.100	.185	.199	.249	.284	.276	.249
5.349	.201	.246	.281	.272	.252	.195	.151	.116	.090	.174	.198	.249	.284	.275	.249
5.732	.201	.245	.281	.271	.252	.195	.151	.116	.090	.161	.198	.249	.284	.275	.249
6.025	.201	.245	.281	.271	.252	.195	.151	.116	.090	.152	.198	.249	.284	.275	.249
7.002	.201	.245	.281	.271	.252	.195	.151	.116	.090	.106	.198	.248	.284	.275	.249

(t) Configuration A2CS, $\delta_v = 0°$, $\alpha = 0°$

NPR	$p/p_{t,j}$ at $x'/\ell_{f,nom}$ of -				
	.037	.258	.479	.700	.921
	Upper flap				
1.999	.515	.571	.591	.572	.527
2.505	.428	.516	.528	.487	.443
3.009	.328	.423	.538	.478	.409
3.504	.329	.278	.424	.519	.471
4.036	.329	.278	.227	.385	.472
4.500	.330	.278	.225	.192	.364
5.036	.330	.278	.224	.184	.327
5.331	.330	.278	.224	.182	.289
5.729	.330	.278	.224	.181	.249
6.011	.330	.278	.224	.181	.240
6.484	.331	.278	.224	.180	.235

TABLE II.- Continued

(u) Configuration A2CS, $\delta_v = 0°$, $\alpha = 5.5°$

NPR	$p/p_{t,j}$ at $x'/\ell_{f,nom}$ of -				
	.051	.272	.493	.715	.936
	Upper flap				
2.022	.494	.549	.576	.562	.520
2.523	.397	.459	.506	.486	.441
3.029	.255	.378	.448	.473	.404
3.514	.255	.219	.369	.427	.440
4.022	.255	.219	.184	.311	.393
4.530	.255	.219	.184	.155	.315
5.038	.255	.219	.184	.152	.249
5.299	.255	.218	.184	.152	.199
5.732	.255	.218	.185	.151	.182
6.032	.255	.219	.185	.151	.180
6.635	.255	.219	.184	.151	.179

(v) Configuration A2CS, $\delta_v = 0°$, $\alpha = 11.0°$

NPR	$p/p_{t,j}$ at $x'/\ell_{f,nom}$ of -				
	.065	.286	.507	.729	.950
	Upper flap				
2.015	.477	.537	.571	.560	.521
2.529	.370	.397	.455	.481	.444
3.048	.193	.327	.362	.420	.398
3.022	.193	.329	.366	.423	.400
3.517	.193	.209	.316	.354	.395
4.022	.193	.172	.147	.276	.337
4.540	.193	.172	.147	.127	.270
5.016	.193	.172	.147	.126	.196
5.314	.193	.172	.147	.126	.129
5.728	.194	.171	.147	.126	.125
6.010	.194	.171	.147	.126	.125
6.839	.193	.171	.146	.125	.124

TABLE II.- Continued

(w) Configuration A3FS, $\delta_v = 4.15°$, $\alpha = -8.3°$

NPR	$p/p_{t,j}$ at $x'/\ell_{f,nom}$ of -														
	-.609	-.498	-.387	-.277	-.166	.033	.255	.476	.697	.919	-.609	-.498	-.387	-.277	-.166
	Upper flap										Lower flap				
2.008	.290	.391	.435	.400	.345	.556	.587	.536	.513	.501	.203	.246	.285	.301	.448
2.503	.289	.391	.436	.398	.344	.422	.453	.523	.423	.359	.202	.245	.285	.278	.252
3.012	.289	.391	.436	.397	.344	.422	.290	.363	.471	.414	.201	.244	.284	.277	.251
3.523	.289	.392	.437	.396	.344	.423	.289	.209	.254	.395	.200	.243	.284	.276	.251
4.044	.288	.393	.436	.396	.344	.423	.289	.208	.228	.239	.200	.243	.284	.275	.250
4.340	.288	.393	.436	.396	.344	.423	.289	.208	.225	.206	.199	.242	.284	.275	.250
4.313	.288	.393	.436	.396	.344	.423	.289	.208	.225	.208	.200	.242	.284	.275	.250
4.701	.287	.393	.436	.396	.344	.423	.289	.208	.223	.189	.199	.243	.284	.274	.250
5.029	.287	.393	.436	.396	.344	.423	.288	.208	.222	.186	.199	.243	.283	.274	.250
6.015	.287	.393	.436	.396	.344	.424	.288	.208	.221	.183	.199	.243	.283	.273	.249
6.481	.287	.393	.436	.396	.344	.424	.288	.208	.220	.183	.198	.243	.283	.273	.249

(x) Configuration A3FS, $\delta_v = 4.15°$, $\alpha = -2.8°$

NPR	$p/p_{t,j}$ at $x'/\ell_{f,nom}$ of -														
	-.609	-.498	-.387	-.277	-.166	.044	.266	.487	.708	.930	-.609	-.498	-.387	-.277	-.166
	Upper flap										Lower flap				
2.001	.289	.390	.434	.400	.345	.517	.563	.531	.514	.504	.203	.246	.285	.302	.454
2.506	.288	.390	.436	.397	.344	.329	.399	.479	.447	.384	.202	.245	.284	.278	.252
3.013	.288	.390	.436	.397	.344	.329	.231	.333	.385	.410	.201	.244	.284	.277	.252
3.521	.288	.392	.437	.396	.344	.330	.231	.170	.243	.343	.200	.243	.284	.276	.251
4.003	.288	.393	.437	.396	.345	.331	.231	.170	.175	.197	.200	.243	.284	.276	.251
4.294	.288	.393	.436	.396	.344	.331	.231	.170	.174	.162	.200	.243	.284	.275	.251
4.707	.287	.393	.436	.396	.344	.332	.231	.170	.173	.156	.199	.243	.284	.274	.250
5.009	.287	.393	.436	.396	.344	.332	.230	.170	.173	.155	.199	.243	.283	.274	.250
6.050	.287	.393	.436	.396	.345	.332	.230	.170	.172	.154	.199	.243	.283	.274	.249
6.537	.287	.393	.436	.396	.344	.333	.230	.170	.171	.154	.198	.243	.283	.273	.249

TABLE II.- Continued

(y) Configuration A3FS, $\delta_v = 4.15°$, $\alpha = 0°$

NPR	$p/p_{t,j}$ at $x'/\ell_{f,nom}$ of -														
	-.609	-.498	-.387	-.277	-.166	.052	.273	.494	.716	.937	-.609	-.498	-.387	-.277	-.166
	Upper flap										Lower flap				
2.004	.289	.389	.435	.400	.345	.488	.549	.532	.516	.504	.203	.246	.285	.301	.456
2.507	.289	.390	.436	.397	.344	.287	.384	.446	.447	.400	.202	.245	.284	.278	.252
3.010	.289	.390	.435	.396	.344	.287	.204	.320	.364	.394	.201	.244	.284	.277	.251
3.531	.288	.391	.436	.395	.344	.288	.204	.152	.241	.313	.200	.243	.284	.276	.251
4.020	.288	.392	.436	.396	.344	.288	.204	.152	.147	.200	.200	.242	.284	.275	.251
4.305	.288	.393	.436	.396	.344	.288	.204	.152	.147	.143	.199	.242	.284	.275	.250
4.743	.287	.393	.436	.395	.344	.289	.203	.152	.147	.138	.199	.243	.284	.274	.250
5.002	.287	.393	.436	.395	.344	.289	.203	.152	.147	.138	.199	.243	.283	.274	.250
5.995	.287	.393	.436	.395	.344	.290	.203	.152	.146	.137	.199	.243	.283	.273	.249
6.681	.287	.393	.436	.396	.344	.291	.203	.152	.145	.137	.199	.243	.283	.273	.249

(z) Configuration A3FS, $\delta_v = 4.15°$, $\alpha = 2.7°$

NPR	$p/p_{t,j}$ at $x'/\ell_{f,nom}$ of -														
	-.609	-.498	-.387	-.277	-.166	.059	.280	.502	.723	.945	-.609	-.498	-.387	-.277	-.166
	Upper flap										Lower flap				
1.997	.289	.389	.435	.400	.345	.473	.534	.534	.519	.506	.203	.246	.284	.309	.457
2.517	.289	.389	.436	.398	.344	.253	.372	.409	.439	.413	.202	.245	.284	.278	.252
3.026	.288	.391	.436	.397	.344	.253	.182	.304	.346	.381	.201	.244	.284	.277	.251
3.532	.288	.392	.437	.396	.344	.254	.182	.136	.234	.303	.200	.243	.284	.276	.251
4.029	.288	.393	.437	.396	.344	.254	.182	.136	.110	.234	.200	.242	.284	.275	.250
4.305	.288	.393	.437	.396	.344	.254	.182	.136	.110	.207	.200	.242	.284	.275	.250
4.741	.287	.393	.437	.396	.344	.254	.182	.136	.110	.125	.199	.243	.283	.274	.250
5.019	.287	.394	.437	.396	.344	.254	.182	.136	.110	.124	.199	.243	.283	.274	.250
6.024	.287	.393	.436	.396	.344	.255	.181	.136	.110	.123	.199	.243	.283	.273	.249
6.744	.287	.393	.436	.396	.344	.255	.181	.136	.109	.123	.198	.242	.283	.273	.249

TABLE II.- Continued

(aa) Configuration A3FS, $\delta_v = -4.15°$, $\alpha = 0°$

NPR	$p/p_{t,j}$ at $x'/\ell_{f,nom}$ of -														
	-.609	-.498	-.387	-.277	-.166	.033	.255	.476	.697	.919	-.609	-.498	-.387	-.277	-.166
	Upper flap										Lower flap				
1.994	.200	.245	.277	.451	.469	.509	.557	.553	.527	.508	.297	.390	.442	.400	.344
2.535	.200	.244	.278	.273	.254	.426	.505	.492	.408	.391	.295	.390	.441	.399	.344
3.031	.201	.243	.279	.271	.251	.330	.481	.526	.447	.337	.295	.392	.439	.399	.344
3.521	.200	.243	.279	.270	.251	.330	.402	.364	.476	.400	.294	.393	.438	.399	.344
4.032	.201	.244	.279	.269	.251	.331	.388	.343	.278	.219	.294	.394	.437	.399	.343
4.357	.201	.244	.279	.269	.251	.331	.386	.330	.270	.205	.295	.394	.437	.399	.343
4.740	.201	.245	.279	.269	.251	.331	.385	.322	.262	.200	.295	.394	.437	.399	.343
5.029	.201	.245	.279	.268	.251	.331	.385	.319	.255	.197	.296	.394	.436	.399	.343
6.015	.200	.245	.280	.267	.251	.332	.384	.317	.242	.185	.297	.394	.436	.400	.343
6.799	.200	.244	.279	.267	.251	.333	.383	.317	.240	.179	.297	.393	.437	.401	.343

(bb) Configuration A3FS, $\delta_v = -4.15°$, $\alpha = 5.5°$

NPR	$p/p_{t,j}$ at $x'/\ell_{f,nom}$ of -														
	-.609	-.498	-.387	-.277	-.166	.044	.266	.487	.708	.930	-.609	-.498	-.387	-.277	-.166
	Upper flap										Lower flap				
2.020	.200	.245	.276	.348	.446	.486	.535	.538	.519	.501	.298	.389	.442	.401	.344
2.527	.201	.244	.278	.273	.251	.398	.465	.477	.405	.392	.296	.390	.440	.400	.344
3.021	.201	.244	.279	.271	.251	.256	.356	.487	.467	.363	.296	.392	.439	.400	.344
3.520	.201	.243	.279	.269	.251	.256	.296	.305	.364	.415	.295	.393	.439	.399	.344
3.992	.201	.244	.279	.269	.251	.257	.295	.274	.245	.204	.295	.394	.438	.400	.344
4.025	.201	.244	.279	.269	.251	.257	.295	.273	.244	.202	.295	.394	.438	.400	.344
4.335	.201	.245	.279	.268	.251	.257	.294	.267	.230	.190	.295	.394	.437	.400	.343
4.720	.201	.245	.279	.268	.251	.257	.294	.265	.215	.180	.296	.394	.437	.400	.343
5.029	.201	.245	.279	.268	.251	.258	.293	.265	.208	.172	.296	.394	.437	.400	.343
6.031	.201	.245	.279	.267	.251	.259	.292	.265	.204	.155	.297	.394	.437	.400	.343
6.882	.201	.244	.279	.267	.251	.259	.292	.265	.203	.152	.297	.394	.437	.401	.343

TABLE II.- Continued

(cc) Configuration A3FS, $\delta_v = -4.15°$, $\alpha = 11.0°$

NPR	$p/p_{t,j}$ at $x'/l_{f,nom}$ of -														
	-.609	-.498	-.387	-.277	-.166	.059	.280	.502	.723	.945	-.609	-.498	-.387	-.277	-.166
	Upper flap										Lower flap				
2.002	.200	.245	.276	.275	.430	.472	.528	.540	.525	.509	.297	.389	.443	.400	.344
2.520	.200	.244	.278	.273	.251	.371	.409	.447	.419	.411	.296	.389	.441	.400	.344
3.015	.201	.244	.279	.271	.250	.194	.328	.380	.427	.369	.295	.392	.440	.400	.344
3.529	.201	.244	.279	.270	.251	.194	.224	.233	.345	.392	.295	.394	.438	.399	.344
4.043	.201	.244	.279	.269	.250	.194	.224	.215	.201	.190	.295	.394	.437	.399	.343
4.007	.201	.244	.279	.269	.250	.194	.224	.215	.204	.194	.295	.394	.438	.399	.344
4.332	.201	.245	.279	.269	.251	.195	.223	.214	.183	.168	.295	.394	.437	.399	.343
4.706	.201	.245	.279	.269	.251	.195	.223	.214	.173	.150	.296	.394	.437	.400	.343
5.004	.201	.245	.280	.268	.251	.195	.223	.214	.171	.139	.296	.394	.437	.400	.343
6.002	.201	.245	.280	.268	.251	.195	.222	.214	.170	.128	.297	.394	.437	.400	.343
7.306	.200	.244	.280	.267	.250	.195	.221	.214	.169	.127	.297	.394	.437	.401	.343

(dd) Configuration A3FL, $\delta_v = 4.15°$

NPR	$p/p_{t,j}$ at $x'/l_{f,nom}$ of -														
	-.609	-.498	-.387	-.277	-.166	.059	.280	.502	.723	.945	-.609	-.498	-.387	-.277	-.166
	Upper flap										Lower flap				
2.020	.290	.389	.435	.400	.345	.251	.422	.498	.530	.508	.202	.245	.284	.299	.457
2.518	.289	.389	.436	.398	.344	.252	.183	.305	.321	.374	.201	.244	.284	.277	.251
3.028	.289	.390	.437	.397	.344	.253	.182	.289	.297	.310	.200	.243	.284	.276	.250
3.553	.288	.392	.437	.396	.344	.253	.182	.134	.246	.265	.200	.242	.284	.275	.250
3.996	.288	.393	.437	.396	.344	.253	.182	.134	.112	.205	.200	.242	.283	.274	.250
4.322	.288	.393	.437	.396	.344	.253	.182	.134	.112	.147	.199	.242	.283	.274	.250
4.738	.287	.393	.437	.396	.344	.253	.181	.134	.113	.143	.199	.243	.283	.273	.250
5.025	.287	.393	.437	.396	.344	.253	.181	.134	.113	.143	.199	.243	.282	.273	.249
6.044	.287	.393	.437	.396	.344	.254	.181	.134	.112	.142	.198	.242	.282	.273	.249
6.689	.287	.393	.436	.396	.344	.254	.181	.134	.112	.142	.198	.242	.282	.273	.249

TABLE II.- Continued

(ee) Configuration A3CS, $\delta_v = 4.15°$, $\alpha = -8.3°$

NPR	$p/p_{t,j}$ at $x'/\ell_{f,nom}$ of -				
	.037	.258	.479	.700	.921
	Upper flap				
2.005	.575	.628	.597	.572	.525
2.511	.424	.564	.555	.481	.469
3.023	.425	.322	.525	.536	.437
3.527	.426	.321	.258	.517	.490
4.008	.427	.321	.256	.337	.455
4.311	.427	.321	.256	.318	.343
4.694	.428	.321	.256	.310	.304
5.007	.426	.321	.256	.308	.286
5.517	.429	.321	.256	.306	.270

(ff) Configuration A3CS, $\delta_v = 4.15°$, $\alpha = -2.8°$

NPR	$p/p_{t,j}$ at $x'/\ell_{f,nom}$ of -				
	.051	.272	.493	.715	.936
	Upper flap				
1.996	.542	.603	.587	.567	.525
2.510	.329	.471	.545	.492	.450
3.009	.330	.258	.434	.508	.461
3.542	.331	.258	.212	.412	.455
4.012	.331	.258	.212	.255	.394
4.352	.331	.257	.212	.251	.284
4.281	.331	.257	.212	.252	.294
4.322	.331	.257	.212	.252	.289
4.693	.332	.257	.212	.250	.245
5.015	.332	.257	.212	.249	.234
6.008	.333	.257	.212	.247	.230
6.385	.334	.257	.213	.247	.230

TABLE II.- Concluded

(gg) Configuration A3CS, $\delta_v = 4.15°$, $\alpha = 2.7°$

NPR	$p/p_{t,j}$ at $x'/\ell_{f,nom}$ of -				
	.065	.286	.507	.729	.950
	Upper flap				
2.012	.492	.561	.578	.560	.518
2.495	.252	.414	.459	.485	.445
3.012	.252	.264	.366	.415	.426
3.294	.252	.202	.319	.370	.405
3.720	.253	.201	.171	.300	.372
4.013	.253	.201	.171	.195	.305
5.027	.253	.201	.171	.194	.197
6.019	.254	.200	.171	.192	.196

(hh) Configuration A3CS, $\delta_v = -4.15°$

NPR	$p/p_{t,j}$ at $x'/\ell_{f,nom}$ of -														
	-.609	-.498	-.387	-.277	-.166	.065	.286	.507	.729	.950	-.609	-.498	-.387	-.277	-.166
	Upper flap										Lower flap				
2.020	.199	.245	.277	.289	.442	.478	.536	.570	.560	.521	.297	.391	.442	.400	.344
2.519	.199	.244	.278	.274	.251	.393	.428	.479	.486	.458	.295	.389	.441	.400	.344
3.019	.200	.244	.279	.272	.251	.280	.365	.429	.468	.406	.295	.391	.440	.400	.344
3.524	.200	.244	.280	.271	.251	.191	.259	.321	.473	.462	.295	.394	.439	.399	.344
4.009	.200	.244	.280	.271	.251	.191	.258	.275	.284	.296	.295	.394	.438	.399	.343
4.314	.200	.244	.280	.270	.251	.191	.257	.270	.262	.256	.295	.394	.437	.399	.343
4.744	.200	.245	.280	.270	.251	.191	.256	.268	.241	.234	.295	.394	.437	.400	.343
5.022	.200	.245	.280	.270	.251	.191	.256	.268	.235	.223	.296	.394	.437	.400	.343
6.025	.200	.245	.280	.269	.251	.191	.255	.267	.230	.199	.297	.394	.437	.400	.343
6.926	.200	.244	.280	.269	.251	.191	.254	.267	.229	.195	.297	.394	.437	.401	.343

TABLE III.- RATIO OF INTERNAL STATIC PRESSURE TO JET TOTAL PRESSURE FOR PARTIAL AFTERBURNING AND DRY POWER NOZZLE CONFIGURATIONS

(a) Configuration P1FS, $\delta_v = -0.60°$, $\alpha = -8.3°$

NPR	$p/p_{t,j}$ at $x'/\ell_{f,nom}$ of -														
	-.609	-.498	-.387	-.277	-.166	.033	.255	.476	.697	.919	-.609	-.498	-.387	-.277	-.166
	Upper flap										Lower flap				
2.015	.432	.570	.498	.418	.336	.547	.579	.519	.506	.498	.226	.314	.377	.393	.391
2.498	.430	.569	.498	.416	.335	.496	.549	.432	.348	.350	.225	.313	.375	.391	.384
3.006	.432	.569	.498	.414	.335	.481	.513	.405	.330	.238	.224	.313	.374	.389	.383
3.293	.434	.569	.499	.414	.335	.473	.509	.381	.322	.228	.224	.313	.373	.389	.383
3.695	.437	.569	.499	.413	.334	.463	.504	.379	.249	.213	.224	.314	.372	.389	.382
3.998	.440	.569	.499	.413	.334	.458	.502	.377	.240	.207	.223	.314	.372	.388	.382
5.009	.449	.569	.499	.413	.334	.450	.497	.372	.235	.145	.222	.313	.371	.387	.381
5.987	.456	.570	.499	.413	.333	.446	.497	.370	.231	.142	.222	.313	.370	.386	.381
7.001	.458	.570	.499	.413	.333	.438	.497	.371	.230	.140	.221	.312	.370	.386	.381
7.423	.458	.570	.499	.413	.334	.434	.497	.371	.230	.140	.220	.312	.369	.386	.381

(b) Configuration P1FS, $\delta_v = -0.60°$, $\alpha = -2.8°$

NPR	$p/p_{t,j}$ at $x'/\ell_{f,nom}$ of -														
	-.609	-.498	-.387	-.277	-.166	.044	.266	.487	.708	.930	-.609	-.498	-.387	-.277	-.166
	Upper flap										Lower flap				
2.005	.432	.571	.497	.418	.335	.497	.549	.522	.510	.501	.226	.314	.377	.393	.385
2.992	.433	.569	.499	.415	.334	.305	.448	.367	.439	.287	.224	.313	.374	.390	.383
3.306	.434	.569	.499	.414	.334	.296	.438	.364	.265	.345	.224	.313	.373	.389	.383
3.698	.437	.569	.499	.414	.334	.283	.434	.358	.229	.200	.224	.313	.373	.389	.382
3.995	.440	.569	.499	.414	.334	.278	.433	.354	.225	.157	.223	.313	.372	.388	.382
5.012	.449	.570	.499	.413	.334	.272	.433	.350	.215	.134	.221	.313	.371	.387	.381
6.026	.456	.570	.499	.413	.333	.270	.433	.350	.214	.131	.222	.312	.370	.386	.381
7.006	.459	.570	.499	.413	.333	.269	.433	.351	.213	.130	.221	.312	.370	.386	.381
7.990	.459	.570	.499	.413	.333	.270	.434	.352	.213	.130	.220	.311	.369	.385	.381

TABLE III.- Continued

(c) Configuration P1FS, $\delta_v = -0.60°$, $\alpha = 0°$

NPR	$p/p_{t,j}$ at $x'/\ell_{f,nom}$ of -														
	-.609	-.498	-.387	-.277	-.166	.052	.273	.494	.716	.937	-.609	-.498	-.387	-.277	-.166
	Upper flap										Lower flap				
1.992	.432	.570	.497	.424	.336	.481	.534	.529	.516	.506	.225	.313	.376	.393	.386
2.525	.431	.569	.498	.426	.335	.288	.470	.497	.388	.335	.224	.313	.375	.390	.384
2.995	.432	.569	.498	.415	.335	.275	.396	.359	.434	.342	.224	.312	.374	.389	.383
3.304	.434	.569	.499	.414	.334	.268	.392	.348	.232	.391	.224	.312	.373	.389	.383
3.689	.437	.569	.499	.414	.334	.260	.390	.333	.220	.175	.224	.313	.372	.388	.383
3.994	.440	.569	.499	.414	.334	.251	.390	.329	.215	.139	.223	.313	.372	.388	.382
4.987	.449	.570	.500	.413	.334	.238	.389	.327	.205	.127	.221	.313	.371	.387	.382
6.006	.456	.570	.499	.413	.334	.235	.389	.326	.204	.125	.221	.312	.370	.386	.381
7.010	.459	.570	.499	.413	.334	.234	.389	.327	.204	.125	.221	.312	.370	.386	.381
8.047	.459	.570	.499	.413	.333	.233	.389	.327	.204	.125	.220	.311	.369	.385	.381

(d) Configuration P1FS, $\delta_v = -0.60°$, $\alpha = 2.7°$

NPR	$p/p_{t,j}$ at $x'/\ell_{f,nom}$ of -														
	-.609	-.498	-.387	-.277	-.166	.059	.280	.502	.723	.945	-.609	-.498	-.387	-.277	-.166
	Upper flap										Lower flap				
1.999	.432	.570	.497	.418	.336	.465	.508	.529	.519	.507	.225	.313	.376	.392	.385
2.509	.431	.569	.498	.416	.335	.264	.432	.500	.419	.345	.224	.313	.375	.390	.384
3.011	.432	.569	.498	.415	.335	.250	.348	.334	.377	.405	.224	.312	.374	.389	.383
3.310	.434	.569	.498	.414	.334	.244	.347	.313	.220	.364	.224	.312	.373	.389	.383
3.703	.437	.569	.499	.414	.334	.237	.346	.302	.209	.158	.224	.313	.372	.388	.382
4.005	.440	.569	.499	.414	.334	.231	.346	.300	.202	.163	.223	.313	.372	.388	.382
5.011	.449	.570	.499	.415	.334	.212	.345	.299	.196	.121	.221	.313	.371	.387	.381
6.017	.457	.570	.499	.413	.334	.207	.343	.298	.195	.119	.221	.312	.370	.386	.381
7.015	.460	.570	.499	.413	.334	.205	.343	.298	.195	.119	.221	.312	.370	.386	.381
8.017	.460	.570	.499	.413	.333	.203	.342	.298	.195	.119	.220	.311	.369	.386	.381

TABLE III.- Continued

(e) Configuration P1CS, $\delta_v = -0.60°$

NPR	$p/p_{t,j}$ at $x'/\ell_{f,nom}$ of -														
	-.609	-.498	-.387	-.277	-.166	.065	.286	.507	.729	.950	-.609	-.498	-.387	-.277	-.166
	Upper flap										Lower flap				
1.995	.434	.570	.496	.415	.335	.474	.537	.571	.561	.527	.225	.314	.376	.392	.384
2.550	.433	.569	.496	.415	.334	.250	.477	.529	.447	.424	.224	.313	.374	.390	.382
3.000	.435	.569	.497	.415	.334	.218	.402	.404	.519	.420	.224	.314	.373	.389	.382
3.305	.436	.569	.498	.414	.334	.218	.396	.390	.340	.476	.224	.313	.373	.389	.381
3.777	.440	.569	.497	.415	.333	.219	.394	.370	.262	.257	.223	.313	.371	.387	.381
3.696	.440	.569	.498	.414	.334	.219	.394	.373	.264	.290	.224	.314	.372	.388	.381
4.018	.443	.569	.498	.413	.334	.219	.394	.367	.257	.203	.223	.314	.372	.388	.381
5.037	.454	.570	.498	.413	.333	.219	.393	.365	.245	.172	.221	.313	.371	.387	.380
6.036	.462	.571	.499	.413	.333	.219	.392	.365	.244	.168	.221	.312	.370	.386	.380
7.048	.463	.570	.499	.414	.334	.219	.391	.366	.244	.168	.220	.312	.370	.386	.380
7.007	.463	.570	.499	.414	.334	.219	.391	.366	.244	.168	.221	.312	.370	.386	.380
7.527	.463	.571	.499	.414	.334	.219	.391	.366	.244	.169	.220	.312	.369	.386	.380

(f) Configuration P2FS, $\delta_v = -4.75°$, $\alpha = 0°$

NPR	$p/p_{t,j}$ at $x'/\ell_{f,nom}$ of -														
	-.609	-.498	-.387	-.277	-.166	.033	.255	.476	.697	.919	-.609	-.498	-.387	-.277	-.166
	Upper flap										Lower flap				
2.006	.258	.362	.387	.330	.488	.517	.551	.537	.516	.505	.219	.296	.317	.287	.452
2.505	.258	.364	.388	.328	.274	.413	.517	.459	.385	.390	.218	.296	.316	.282	.233
3.020	.259	.365	.388	.327	.274	.316	.377	.507	.428	.312	.218	.296	.315	.281	.233
3.525	.259	.367	.389	.326	.274	.318	.304	.307	.441	.393	.218	.296	.315	.281	.233
4.011	.259	.368	.389	.326	.275	.318	.304	.277	.244	.309	.217	.296	.315	.280	.233
4.352	.258	.368	.389	.325	.274	.319	.305	.274	.229	.239	.216	.296	.314	.280	.233
4.725	.258	.368	.389	.325	.274	.319	.304	.273	.213	.226	.216	.296	.314	.280	.232
5.022	.258	.368	.389	.325	.275	.320	.304	.273	.208	.177	.217	.296	.314	.279	.232
6.019	.258	.368	.389	.324	.275	.321	.302	.272	.206	.151	.217	.296	.314	.279	.232
7.033	.258	.368	.389	.324	.275	.322	.301	.272	.205	.150	.216	.295	.313	.279	.232
8.042	.258	.368	.389	.324	.275	.323	.300	.272	.205	.150	.216	.295	.313	.279	.232

TABLE III.- Continued

(g) Configuration P2FS, $\delta_v = -4.75°$, $\alpha = 5.5°$

NPR	$p/p_{t,j}$ at $x'/\ell_{f,nom}$ of -														
	-.609	-.498	-.387	-.277	-.166	.044	.266	.487	.708	.930	-.609	-.498	-.387	-.277	-.166
	Upper flap										Lower flap				
1.988	.258	.362	.387	.331	.444	.497	.536	.535	.520	.510	.220	.296	.318	.301	.458
2.525	.259	.365	.389	.329	.275	.356	.432	.453	.405	.418	.219	.296	.317	.282	.233
2.994	.259	.365	.389	.327	.274	.244	.335	.416	.439	.345	.218	.296	.316	.281	.233
3.536	.259	.367	.389	.326	.274	.245	.202	.223	.385	.405	.218	.296	.315	.281	.233
4.037	.259	.368	.390	.326	.275	.245	.203	.216	.198	.278	.218	.296	.315	.280	.233
4.337	.258	.368	.389	.325	.275	.245	.205	.216	.181	.223	.217	.296	.315	.280	.233
4.738	.258	.368	.390	.325	.275	.246	.207	.215	.175	.146	.217	.296	.315	.280	.232
5.035	.258	.368	.389	.325	.275	.246	.208	.215	.174	.134	.217	.296	.314	.279	.232
6.046	.258	.368	.389	.324	.275	.247	.206	.215	.173	.127	.217	.296	.314	.279	.232
7.038	.259	.368	.389	.324	.275	.247	.202	.215	.173	.127	.217	.295	.313	.279	.232

(h) Configuration P2FS, $\delta_v = -4.75°$, $\alpha = 11.0°$

NPR	$p/p_{t,j}$ at $x'/\ell_{f,nom}$ of -														
	-.609	-.498	-.387	-.277	-.166	.059	.280	.502	.723	.945	-.609	-.498	-.387	-.277	-.166
	Upper flap										Lower flap				
2.004	.258	.363	.387	.330	.283	.468	.518	.531	.521	.509	.220	.298	.318	.300	.457
2.481	.259	.365	.388	.328	.275	.346	.374	.413	.450	.428	.219	.297	.317	.283	.234
3.010	.259	.366	.389	.327	.275	.185	.293	.334	.390	.366	.219	.296	.316	.281	.233
3.496	.259	.367	.389	.326	.275	.185	.135	.277	.326	.360	.219	.296	.315	.281	.233
4.001	.259	.368	.389	.326	.275	.185	.135	.166	.157	.284	.218	.296	.315	.280	.233
4.324	.259	.368	.389	.325	.275	.185	.135	.166	.144	.158	.217	.296	.315	.280	.233
4.719	.258	.368	.389	.325	.275	.186	.135	.166	.143	.130	.218	.296	.315	.280	.233
5.031	.258	.369	.389	.325	.275	.186	.135	.166	.142	.109	.218	.296	.315	.280	.233
6.008	.259	.368	.389	.324	.275	.187	.135	.166	.142	.106	.218	.296	.314	.279	.232
7.058	.259	.368	.389	.324	.275	.187	.134	.166	.141	.105	.217	.296	.314	.279	.232
8.028	.259	.368	.390	.324	.275	.187	.134	.166	.141	.105	.216	.295	.314	.279	.232

TABLE III.- Continued

(i) Configuration P2CS, $\delta_v = -4.75°$, $\alpha = 5.5°$

NPR	$p/p_{t,j}$ at $x'/\ell_{f,nom}$ of -				
	.051	.272	.493	.715	.936
	Upper flap				
2.009	.505	.556	.573	.558	.518
2.528	.399	.458	.498	.489	.437
2.999	.245	.399	.472	.465	.369
3.509	.245	.257	.388	.510	.462
4.044	.245	.258	.276	.281	.449
4.341	.245	.259	.274	.260	.319
4.682	.245	.260	.273	.242	.280
4.730	.245	.260	.273	.240	.278
5.012	.245	.260	.273	.235	.257
6.035	.245	.258	.273	.232	.187
7.050	.245	.256	.273	.231	.186
8.055	.246	.254	.273	.231	.186

(j) Configuration P2CS, $\delta_v = -4.75°$, $\alpha = 8.3°$

NPR	$p/p_{t,j}$ at $x'/\ell_{f,nom}$ of -				
	.058	.279	.501	.722	.943
	Upper flap				
2.008	.493	.546	.568	.556	.517
2.510	.384	.425	.474	.489	.434
3.001	.213	.360	.418	.451	.376
3.506	.213	.207	.371	.472	.460
3.989	.213	.208	.243	.268	.431
4.001	.213	.208	.243	.264	.426
4.309	.213	.210	.242	.236	.321
4.698	.213	.212	.242	.219	.270
5.034	.213	.212	.241	.216	.192
6.054	.212	.210	.241	.215	.172
7.056	.213	.207	.241	.214	.172
7.983	.213	.204	.242	.214	.172

TABLE III.- Continued

(k) Configuration P2CS, $\delta_v = -4.75°$, $\alpha = 11.0°$

NPR	$p/p_{t,j}$ at $x'/\ell_{f,nom}$ of -				
	.065	.286	.507	.729	.950
	Upper flap				
2.031	.475	.529	.559	.551	.512
2.542	.364	.392	.440	.478	.439
3.014	.203	.325	.375	.429	.380
3.536	.185	.167	.351	.419	.434
4.038	.185	.167	.214	.238	.380
4.315	.185	.169	.214	.211	.322
4.729	.185	.170	.214	.198	.195
5.047	.185	.170	.213	.197	.174
6.014	.185	.168	.214	.196	.160
7.029	.185	.165	.214	.196	.160
8.048	.185	.162	.214	.196	.160

TABLE III.- Continued

(l) Configuration D1CS, $\delta_v = -30°$

NPR	$p/p_{t,j}$ at $x'/\ell_{f,nom}$ of -														
	-.609	-.498	-.387	-.277	-.166	.065	.286	.507	.729	.950	-.609	-.498	-.387	-.277	-.166
	Upper flap										Lower flap				
1.999	.194	.324	.413	.566	.548	.500	.552	.553	.548	.519	.864	.829	.740	.624	.481
2.506	.192	.326	.411	.403	.494	.399	.426	.508	.417	.433	.866	.827	.739	.623	.480
3.035	.191	.327	.411	.401	.358	.380	.276	.439	.477	.340	.868	.827	.739	.623	.480
3.306	.192	.327	.410	.400	.358	.394	.253	.329	.462	.388	.868	.827	.739	.623	.480
3.715	.194	.327	.410	.400	.358	.234	.249	.195	.403	.434	.870	.827	.739	.624	.480
3.987	.195	.327	.410	.400	.358	.233	.259	.179	.330	.406	.870	.827	.739	.624	.479
5.015	.195	.326	.409	.399	.358	.233	.150	.177	.122	.116	.872	.826	.740	.624	.479
6.032	.194	.325	.408	.399	.358	.234	.150	.104	.123	.089	.873	.827	.740	.625	.479
8.028	.192	.323	.406	.399	.358	.234	.150	.105	.076	.078	.879	.827	.741	.626	.480
10.041	.191	.322	.404	.399	.359	.235	.151	.105	.076	.058	.882	.828	.742	.628	.482

(m) Configuration D1CS, $\delta_v = -15°$

NPR	$p/p_{t,j}$ at $x'/\ell_{f,nom}$ of -														
	-.609	-.498	-.387	-.277	-.166	.065	.286	.507	.729	.950	-.609	-.498	-.387	-.277	-.166
	Upper flap										Lower flap				
2.015	.228	.347	.416	.407	.454	.530	.546	.548	.543	.517	.693	.649	.532	.410	.307
2.538	.228	.349	.416	.405	.362	.279	.522	.428	.430	.473	.695	.648	.531	.408	.306
3.005	.228	.350	.417	.403	.362	.274	.314	.511	.438	.324	.700	.648	.530	.407	.307
3.300	.229	.350	.417	.403	.362	.273	.274	.347	.502	.375	.702	.648	.530	.408	.307
3.677	.229	.350	.417	.402	.362	.273	.250	.221	.414	.462	.703	.647	.531	.407	.306
3.726	.229	.350	.417	.402	.362	.273	.249	.218	.394	.461	.703	.647	.531	.407	.306
3.997	.228	.349	.417	.402	.362	.273	.242	.194	.206	.416	.702	.648	.531	.407	.306
4.964	.229	.348	.417	.400	.362	.273	.236	.159	.131	.129	.700	.648	.531	.407	.306
4.998	.229	.348	.416	.400	.362	.273	.236	.159	.129	.126	.699	.647	.531	.407	.306
6.036	.229	.347	.416	.400	.362	.273	.232	.158	.107	.089	.699	.648	.532	.407	.306
8.037	.227	.346	.415	.399	.362	.274	.226	.159	.106	.076	.699	.648	.533	.407	.306
10.029	.226	.345	.413	.399	.362	.275	.225	.160	.106	.076	.699	.648	.534	.408	.307

TABLE III.- Continued

(n) Configuraton D1CS, $\delta_v = 0°$

NPR	$p/p_{t,j}$ at $x'/\ell_{f,nom}$ of -														
	-.609	-.498	-.387	-.277	-.166	.065	.286	.507	.729	.950	-.609	-.498	-.387	-.277	-.166
	Upper flap										Lower flap				
1.959	.320	.452	.361	.392	.358	.542	.575	.568	.561	.531	.325	.458	.363	.367	.349
2.014	.320	.452	.361	.391	.358	.523	.565	.556	.549	.520	.324	.458	.362	.367	.348
2.519	.320	.453	.361	.389	.357	.341	.530	.449	.429	.478	.324	.457	.361	.372	.349
3.018	.320	.451	.361	.388	.357	.339	.324	.474	.441	.350	.323	.456	.360	.374	.348
3.339	.321	.451	.362	.388	.357	.340	.324	.300	.446	.431	.322	.456	.360	.375	.348
3.712	.320	.450	.362	.387	.357	.339	.323	.258	.268	.393	.320	.455	.360	.375	.347
4.016	.319	.449	.362	.387	.357	.339	.323	.241	.222	.350	.318	.454	.360	.376	.347
5.030	.321	.450	.362	.385	.356	.337	.322	.236	.155	.143	.317	.453	.359	.376	.346
6.046	.321	.450	.362	.384	.356	.336	.322	.236	.145	.105	.316	.453	.359	.375	.346
8.036	.320	.450	.362	.384	.356	.332	.323	.237	.145	.098	.314	.453	.360	.371	.346
10.041	.319	.450	.363	.384	.356	.322	.324	.239	.145	.098	.314	.453	.361	.364	.346

(o) Configuration D1CS, $\delta_v = 15°$

NPR	$p/p_{t,j}$ at $x'/\ell_{f,nom}$ of -														
	-.609	-.498	-.387	-.277	-.166	.065	.286	.507	.729	.950	-.609	-.498	-.387	-.277	-.166
	Upper flap										Lower flap				
2.029	.694	.650	.532	.408	.308	.462	.563	.559	.547	.517	.229	.343	.421	.410	.371
2.493	.696	.649	.531	.407	.307	.383	.537	.467	.431	.487	.229	.344	.421	.408	.368
3.009	.700	.648	.530	.406	.307	.382	.373	.494	.383	.338	.230	.344	.421	.406	.368
3.321	.703	.648	.530	.406	.307	.381	.374	.342	.327	.379	.230	.345	.421	.406	.367
3.709	.704	.648	.531	.406	.303	.380	.371	.325	.299	.314	.230	.350	.419	.405	.367
4.017	.702	.648	.531	.407	.304	.379	.374	.324	.294	.204	.229	.346	.421	.403	.366
5.019	.699	.648	.531	.407	.304	.375	.371	.325	.184	.198	.230	.345	.418	.402	.366
6.024	.698	.648	.532	.407	.303	.374	.372	.325	.184	.118	.230	.344	.417	.401	.365
8.025	.698	.648	.533	.408	.304	.369	.374	.326	.184	.118	.229	.346	.413	.401	.366

TABLE III.- Continued

(p) Configuration D1CS, $\delta_v = 30°$

NPR	$p/p_{t,j}$ at $x'/\ell_{f,nom}$ of -														
	-.609	-.498	-.387	-.277	-.166	.065	.286	.507	.729	.950	-.609	-.498	-.387	-.277	-.166
	Upper flap										Lower flap				
2.000	.876	.829	.741	.625	.481	.406	.525	.572	.553	.516	.195	.325	.414	.406	.480
2.529	.875	.828	.740	.624	.480	.260	.437	.527	.426	.419	.192	.325	.414	.404	.362
3.022	.876	.828	.740	.623	.479	.260	.423	.400	.422	.352	.192	.325	.414	.403	.362
3.318	.876	.827	.740	.624	.479	.260	.421	.394	.432	.320	.192	.326	.413	.402	.362
3.707	.876	.827	.739	.624	.479	.260	.421	.392	.295	.276	.192	.326	.413	.401	.362
4.007	.876	.827	.740	.624	.479	.260	.420	.391	.266	.257	.192	.326	.412	.401	.362
5.032	.877	.827	.740	.624	.479	.260	.418	.392	.265	.165	.194	.325	.411	.399	.361
6.017	.876	.827	.740	.625	.480	.260	.417	.393	.264	.154	.194	.324	.410	.398	.360

(q) Configuration D1FS, $\delta_v = -30°$, $\alpha = 31.5°$

NPR	$p/p_{t,j}$ at $x'/\ell_{f,nom}$ of -														
	-.609	-.498	-.387	-.277	-.166	.059	.280	.502	.723	.945	-.609	-.498	-.387	-.277	-.166
	Upper flap										Lower flap				
2.010	.194	.323	.412	.563	.548	.473	.517	.503	.502	.501	.874	.828	.740	.624	.481
2.526	.191	.325	.412	.402	.464	.397	.372	.396	.467	.369	.874	.827	.739	.623	.480
3.061	.191	.325	.411	.401	.358	.387	.249	.334	.351	.375	.875	.827	.739	.623	.480
2.992	.191	.325	.411	.401	.359	.381	.258	.356	.394	.354	.875	.827	.739	.623	.480
3.303	.191	.325	.411	.401	.358	.397	.230	.207	.326	.432	.875	.827	.739	.624	.480
3.752	.190	.326	.410	.400	.358	.244	.229	.154	.207	.335	.876	.826	.739	.624	.479
4.021	.191	.327	.411	.400	.358	.244	.236	.142	.124	.262	.876	.826	.739	.624	.480
5.039	.194	.326	.410	.398	.357	.245	.137	.143	.108	.185	.876	.826	.740	.625	.479
6.011	.194	.326	.409	.398	.357	.246	.137	.083	.092	.156	.876	.827	.740	.626	.480
8.027	.192	.324	.407	.398	.357	.247	.137	.083	.059	.120	.877	.827	.742	.628	.480
10.065	.191	.323	.405	.398	.358	.249	.137	.083	.054	.093	.881	.828	.744	.630	.481

TABLE III.- Continued

(r) Configuration D1FS, $\delta_v = -15°$, $\alpha = 16.5°$

NPR	$p/p_{t,j}$ at $x'/l_{f,nom}$ of -														
	-.609	-.498	-.387	-.277	-.166	.059	.280	.502	.723	.945	-.609	-.498	-.387	-.277	-.166
	Upper flap										Lower flap				
2.020	.229	.349	.415	.406	.442	.487	.509	.495	.497	.504	.694	.649	.532	.410	.308
2.521	.229	.350	.416	.403	.362	.273	.489	.409	.360	.389	.696	.649	.531	.409	.307
3.007	.229	.350	.417	.402	.362	.274	.277	.357	.459	.346	.700	.648	.531	.408	.307
3.301	.230	.349	.417	.401	.362	.274	.241	.215	.385	.420	.703	.648	.531	.408	.307
3.731	.229	.349	.417	.400	.362	.274	.211	.171	.163	.327	.703	.647	.530	.407	.306
3.999	.228	.348	.417	.400	.362	.275	.207	.150	.133	.246	.703	.648	.531	.407	.306
5.007	.230	.347	.416	.398	.361	.275	.204	.129	.108	.187	.699	.647	.531	.407	.306
6.009	.229	.346	.416	.398	.361	.276	.201	.129	.079	.155	.699	.648	.532	.407	.306
8.060	.227	.345	.415	.398	.361	.278	.199	.129	.078	.111	.698	.648	.533	.407	.306
8.010	.228	.345	.415	.398	.361	.278	.199	.129	.078	.112	.698	.648	.533	.407	.306
10.023	.227	.344	.414	.398	.362	.278	.199	.130	.078	.049	.699	.649	.534	.408	.307

(s) Configuration D1FS, $\delta_v = 0°$, $\alpha = 1.5°$

NPR	$p/p_{t,j}$ at $x'/l_{f,nom}$ of -														
	-.609	-.498	-.387	-.277	-.166	.059	.280	.502	.723	.945	-.609	-.498	-.387	-.277	-.166
	Upper flap										Lower flap				
2.022	.327	.449	.361	.390	.357	.495	.524	.507	.504	.498	.323	.457	.362	.364	.348
2.518	.326	.449	.362	.389	.357	.337	.464	.455	.361	.356	.323	.456	.361	.368	.348
3.007	.326	.448	.362	.387	.357	.335	.288	.299	.380	.396	.322	.455	.360	.369	.347
3.323	.326	.448	.363	.387	.357	.336	.288	.229	.256	.345	.321	.454	.360	.370	.348
3.717	.327	.447	.363	.386	.357	.336	.288	.217	.181	.276	.320	.454	.360	.371	.347
4.033	.327	.448	.363	.386	.357	.337	.287	.197	.144	.145	.318	.453	.360	.372	.347
5.017	.327	.449	.363	.385	.356	.337	.287	.197	.115	.184	.317	.453	.359	.374	.346
6.034	.326	.449	.363	.384	.355	.336	.287	.197	.114	.149	.316	.452	.359	.373	.345
8.045	.321	.449	.364	.384	.356	.335	.287	.198	.114	.068	.315	.453	.360	.371	.346
10.048	.321	.449	.364	.384	.356	.328	.288	.199	.114	.068	.314	.453	.360	.366	.346

TABLE III.- Continued

(t) Configuration D1FS, $\delta_v = 15°$, $\alpha = -13.5°$

NPR	$p/p_{t,j}$ at $x'/l_{f,nom}$ of -														
	-.609	-.498	-.387	-.277	-.166	.059	.280	.502	.723	.945	-.609	-.498	-.387	-.277	-.166
	Upper flap										Lower flap				
2.020	.694	.649	.532	.410	.309	.414	.533	.509	.503	.506	.229	.347	.415	.406	.363
2.529	.696	.648	.531	.409	.307	.364	.352	.438	.363	.371	.228	.348	.415	.403	.361
3.009	.700	.648	.530	.408	.308	.364	.332	.380	.316	.388	.228	.348	.416	.402	.362
3.296	.703	.648	.530	.408	.308	.364	.331	.267	.269	.288	.228	.347	.417	.401	.362
3.707	.703	.648	.530	.408	.307	.364	.331	.265	.244	.173	.228	.347	.416	.401	.362
4.019	.701	.648	.531	.408	.307	.364	.330	.265	.180	.153	.229	.346	.416	.400	.361
5.016	.699	.647	.531	.408	.307	.364	.330	.265	.153	.141	.230	.345	.416	.399	.361
6.005	.698	.648	.531	.408	.307	.364	.330	.264	.153	.089	.229	.344	.415	.398	.361
7.993	.698	.648	.533	.408	.307	.363	.330	.265	.153	.088	.228	.343	.414	.398	.361
8.033	.697	.648	.533	.408	.307	.363	.330	.265	.153	.088	.228	.343	.414	.398	.361
9.259	.698	.648	.533	.408	.308	.362	.330	.265	.154	.089	.227	.343	.413	.398	.362

(u) Configuration D1FS, $\delta_v = 30°$, $\alpha = -28.5°$

NPR	$p/p_{t,j}$ at $x'/l_{f,nom}$ of -														
	-.609	-.498	-.387	-.277	-.166	.059	.280	.502	.723	.945	-.609	-.498	-.387	-.277	-.166
	Upper flap										Lower flap				
2.001	.875	.829	.741	.625	.482	.262	.460	.524	.520	.502	.195	.324	.412	.406	.362
2.530	.875	.828	.740	.624	.481	.262	.369	.496	.413	.353	.192	.324	.411	.403	.361
3.036	.875	.827	.740	.623	.480	.262	.366	.325	.438	.295	.191	.324	.411	.402	.361
3.018	.875	.827	.740	.623	.480	.262	.366	.325	.443	.297	.192	.323	.411	.402	.361
3.321	.875	.827	.740	.624	.480	.262	.365	.323	.262	.285	.192	.324	.411	.401	.361
3.696	.876	.827	.740	.624	.480	.263	.365	.322	.235	.253	.191	.324	.411	.401	.360
3.982	.876	.827	.740	.624	.480	.263	.364	.322	.234	.171	.192	.326	.410	.400	.360
4.023	.875	.827	.739	.624	.479	.263	.364	.321	.234	.160	.192	.326	.410	.400	.360
5.038	.876	.827	.740	.625	.480	.264	.362	.320	.235	.120	.194	.326	.409	.398	.359
6.029	.877	.827	.740	.626	.480	.264	.361	.320	.235	.120	.194	.325	.408	.398	.359
6.943	.878	.827	.741	.627	.480	.265	.360	.320	.235	.120	.193	.324	.407	.398	.359

TABLE III.- Continued

(v) Configuration D1FS, $\delta_v = -30°$, $\alpha = 26.0°$

NPR	$p/p_{t,j}$ at $x'/\ell_{f,nom}$ of -														
	-.609	-.498	-.387	-.277	-.166	.044	.266	.487	.708	.930	-.609	-.498	-.387	-.277	-.166
	Upper flap										Lower flap				
2.012	.193	.321	.412	.565	.563	.566	.505	.503	.503	.500	.873	.828	.740	.624	.481
2.528	.191	.324	.411	.402	.463	.519	.412	.347	.449	.427	.874	.827	.739	.623	.481
3.035	.190	.324	.411	.401	.358	.469	.319	.358	.286	.293	.874	.826	.739	.623	.480
3.318	.190	.324	.411	.401	.358	.473	.283	.294	.285	.308	.875	.826	.739	.624	.480
3.710	.190	.324	.410	.400	.358	.315	.274	.198	.328	.278	.875	.826	.739	.624	.480
3.996	.190	.325	.410	.400	.358	.315	.284	.179	.171	.301	.876	.826	.739	.624	.480
5.065	.193	.326	.409	.398	.357	.316	.170	.169	.106	.174	.876	.826	.739	.625	.479
5.017	.193	.326	.409	.398	.357	.316	.170	.169	.108	.175	.875	.826	.740	.625	.480
6.044	.193	.325	.408	.398	.357	.317	.170	.100	.106	.148	.876	.826	.740	.626	.480
8.068	.192	.324	.407	.398	.357	.320	.170	.100	.064	.113	.877	.827	.742	.628	.480
8.015	.192	.324	.407	.398	.357	.320	.170	.100	.064	.113	.876	.827	.742	.628	.480
10.039	.191	.323	.405	.399	.358	.323	.171	.101	.064	.078	.880	.828	.744	.630	.481

(w) Configuration D1FS, $\delta_v = -15°$, $\alpha = 11.0°$

NPR	$p/p_{t,j}$ at $x'/\ell_{f,nom}$ of -														
	-.609	-.498	-.387	-.277	-.166	.044	.266	.487	.708	.930	-.609	-.498	-.387	-.277	-.166
	Upper flap										Lower flap				
2.024	.228	.345	.416	.406	.501	.577	.504	.496	.496	.509	.694	.649	.532	.410	.308
2.517	.228	.349	.416	.403	.363	.480	.483	.352	.344	.484	.696	.649	.531	.409	.307
3.025	.229	.349	.416	.402	.363	.350	.352	.456	.340	.278	.701	.648	.531	.408	.307
3.297	.229	.349	.417	.401	.362	.352	.312	.277	.328	.312	.703	.648	.531	.408	.307
3.703	.229	.349	.417	.400	.362	.353	.284	.213	.244	.313	.704	.647	.531	.407	.306
4.014	.228	.348	.417	.400	.362	.355	.280	.190	.178	.254	.702	.648	.531	.407	.306
5.022	.229	.346	.416	.398	.362	.357	.274	.152	.112	.158	.699	.647	.531	.407	.306
6.037	.229	.346	.416	.398	.361	.358	.270	.151	.091	.152	.699	.647	.532	.407	.306
8.033	.227	.345	.415	.398	.362	.359	.264	.151	.090	.084	.698	.648	.533	.407	.306
10.038	.227	.344	.414	.398	.362	.360	.260	.152	.089	.056	.699	.649	.535	.408	.307

TABLE III.- Continued

(x) Configuration D1FS, $\delta_v = 0°$, $\alpha = -4.0°$

NPR	$p/p_{t,j}$ at $x'/\ell_{f,nom}$ of -														
	-.609	-.498	-.387	-.277	-.166	.044	.266	.487	.708	.930	-.609	-.498	-.387	-.277	-.166
	Upper flap										Lower flap				
1.979	.319	.450	.362	.391	.358	.566	.536	.515	.513	.509	.324	.457	.361	.361	.348
2.006	.319	.451	.363	.392	.357	.561	.530	.508	.506	.502	.324	.457	.361	.361	.349
2.551	.319	.450	.363	.389	.357	.438	.515	.358	.343	.462	.323	.457	.360	.367	.348
2.513	.319	.450	.363	.389	.357	.441	.510	.364	.352	.480	.323	.457	.361	.367	.348
3.020	.320	.450	.363	.388	.357	.435	.360	.435	.277	.323	.323	.456	.360	.371	.348
3.325	.320	.450	.363	.388	.357	.435	.359	.300	.272	.247	.322	.455	.360	.371	.347
3.717	.319	.449	.363	.388	.357	.435	.358	.246	.240	.180	.320	.455	.360	.372	.348
4.020	.319	.449	.364	.388	.357	.436	.358	.238	.195	.143	.318	.454	.360	.373	.348
5.045	.321	.449	.363	.385	.356	.435	.357	.222	.134	.109	.317	.453	.359	.375	.346
6.028	.320	.450	.363	.384	.356	.434	.361	.222	.124	.118	.315	.453	.359	.374	.345
8.082	.320	.450	.364	.384	.356	.428	.362	.223	.123	.072	.314	.453	.360	.370	.346
8.055	.320	.450	.364	.384	.356	.428	.362	.223	.123	.072	.314	.453	.360	.370	.346

(y) Configuration D1FS, $\delta_v = 15°$, $\alpha = -19.0°$

NPR	$p/p_{t,j}$ at $x'/\ell_{f,nom}$ of -														
	-.609	-.498	-.387	-.277	-.166	.044	.266	.487	.708	.930	-.609	-.498	-.387	-.277	-.166
	Upper flap										Lower flap				
1.994	.696	.649	.532	.410	.308	.492	.546	.512	.507	.507	.230	.347	.414	.406	.362
2.475	.698	.649	.531	.409	.307	.460	.519	.386	.362	.470	.229	.349	.415	.404	.361
3.028	.702	.648	.530	.408	.307	.457	.409	.387	.245	.296	.228	.348	.416	.402	.361
3.312	.703	.648	.530	.408	.307	.457	.408	.368	.221	.250	.228	.347	.417	.401	.361
3.734	.703	.648	.530	.408	.307	.457	.407	.299	.215	.209	.229	.347	.416	.401	.361
4.003	.702	.648	.530	.408	.307	.456	.407	.299	.220	.194	.230	.347	.416	.401	.360
5.025	.699	.648	.530	.408	.306	.456	.407	.300	.159	.126	.231	.346	.415	.399	.360
6.021	.698	.648	.531	.408	.306	.456	.407	.300	.159	.090	.230	.345	.415	.398	.361
7.977	.697	.648	.533	.408	.307	.455	.408	.302	.159	.090	.228	.343	.414	.398	.361

TABLE III.- Continued

(z) Configuration D1FS, $\delta_v = 30°$, $\alpha = -34.0°$

NPR	$p/p_{t,j}$ at $x'/\ell_{f,nom}$ of -														
	-.609	-.498	-.387	-.277	-.166	.044	.266	.487	.708	.930	-.609	-.498	-.387	-.277	-.166
	Upper flap										Lower flap				
2.010	.877	.828	.741	.624	.481	.464	.569	.508	.498	.495	.194	.323	.412	.521	.579
2.516	.877	.827	.740	.623	.481	.343	.480	.455	.346	.374	.192	.324	.412	.404	.358
3.009	.877	.826	.739	.623	.480	.343	.472	.400	.258	.281	.191	.325	.412	.402	.358
3.318	.877	.826	.739	.624	.480	.344	.471	.396	.244	.182	.190	.326	.412	.402	.358
3.714	.877	.826	.739	.624	.480	.344	.472	.394	.226	.200	.191	.327	.412	.401	.358
4.001	.878	.826	.739	.624	.480	.345	.472	.394	.225	.139	.191	.328	.411	.400	.358
5.039	.877	.826	.740	.625	.480	.347	.472	.395	.224	.120	.194	.327	.410	.399	.357
6.048	.877	.826	.740	.626	.480	.348	.472	.394	.223	.120	.194	.326	.409	.398	.357

(aa) Configuration D1FL, $\delta_v = -30°$

NPR	$p/p_{t,j}$ at $x'/\ell_{f,nom}$ of -														
	-.609	-.498	-.387	-.277	-.166	.059	.280	.502	.723	.945	-.609	-.498	-.387	-.277	-.166
	Upper flap										Lower flap				
2.005	.195	.323	.414	.564	.550	.474	.517	.505	.503	.502	.873	.828	.740	.624	.482
2.524	.192	.324	.414	.404	.464	.397	.381	.390	.463	.392	.874	.827	.739	.624	.481
3.041	.191	.324	.413	.402	.359	.385	.257	.330	.316	.399	.875	.827	.739	.623	.481
3.033	.190	.324	.413	.402	.359	.384	.258	.331	.322	.395	.874	.827	.739	.623	.481
3.307	.190	.323	.413	.402	.359	.396	.234	.244	.280	.380	.875	.827	.739	.624	.481
3.696	.190	.324	.412	.401	.359	.245	.230	.169	.226	.297	.875	.827	.739	.624	.480
4.001	.191	.326	.412	.401	.359	.245	.238	.154	.159	.205	.875	.827	.739	.624	.480
5.019	.194	.327	.410	.399	.357	.246	.138	.151	.100	.183	.875	.826	.740	.625	.480
6.006	.194	.326	.409	.399	.357	.246	.138	.086	.105	.151	.875	.827	.740	.626	.481
7.979	.193	.324	.407	.399	.358	.248	.138	.086	.061	.118	.878	.827	.742	.628	.482
9.998	.191	.323	.405	.399	.358	.249	.138	.087	.061	.071	.882	.828	.743	.630	.482

TABLE III.- Concluded

(bb) Configuration D1FL, $\delta_v = 0°$

NPR	$p/p_{t,j}$ at $x'/l_{f,nom}$ of -														
	-.609	-.498	-.387	-.277	-.166	.059	.280	.502	.723	.945	-.609	-.498	-.387	-.277	-.166
	Upper flap										Lower flap				
2.000	.324	.448	.360	.390	.356	.469	.535	.511	.505	.502	.323	.457	.362	.373	.348
2.517	.324	.448	.361	.388	.356	.338	.377	.498	.371	.354	.323	.456	.361	.375	.348
3.017	.324	.449	.361	.387	.355	.336	.289	.304	.354	.417	.322	.455	.360	.374	.347
3.314	.324	.449	.362	.386	.356	.337	.289	.234	.294	.289	.322	.455	.360	.374	.347
3.721	.323	.448	.362	.386	.356	.337	.289	.219	.212	.229	.320	.454	.359	.374	.347
4.039	.323	.448	.362	.386	.356	.338	.289	.200	.164	.199	.318	.453	.359	.374	.347
5.065	.322	.449	.362	.385	.357	.336	.288	.202	.125	.159	.316	.453	.359	.375	.346
6.071	.321	.449	.362	.384	.357	.336	.289	.202	.125	.092	.315	.453	.359	.373	.346
6.039	.322	.449	.362	.384	.357	.336	.290	.203	.125	.088	.315	.453	.359	.373	.346
8.065	.321	.449	.363	.383	.357	.331	.292	.203	.125	.083	.314	.453	.359	.369	.346
9.633	.320	.449	.363	.383	.356	.316	.289	.203	.125	.083	.313	.453	.360	.362	.346

(cc) Configuration D1FL, $\delta_v = 30°$

NPR	$p/p_{t,j}$ at $x'/l_{f,nom}$ of -														
	-.609	-.498	-.387	-.277	-.166	.059	.280	.502	.723	.945	-.609	-.498	-.387	-.277	-.166
	Upper flap										Lower flap				
2.035	.875	.828	.741	.625	.482	.263	.402	.540	.506	.483	.195	.324	.413	.406	.361
2.532	.875	.827	.740	.623	.481	.262	.368	.419	.449	.361	.193	.323	.412	.404	.360
2.506	.875	.827	.740	.623	.481	.262	.368	.445	.452	.370	.193	.323	.412	.404	.360
3.006	.875	.827	.739	.623	.480	.263	.367	.319	.434	.313	.192	.323	.412	.402	.360
3.281	.876	.827	.740	.624	.480	.263	.366	.319	.279	.271	.192	.324	.412	.402	.360
3.723	.876	.827	.739	.624	.480	.263	.367	.319	.247	.282	.192	.325	.411	.401	.360
4.015	.876	.826	.739	.624	.479	.263	.366	.319	.246	.255	.192	.327	.410	.401	.359
5.022	.876	.826	.740	.624	.479	.264	.364	.319	.246	.141	.194	.326	.409	.399	.359
6.002	.876	.826	.740	.625	.480	.265	.362	.319	.246	.141	.194	.325	.408	.399	.358

TABLE IV.- RATIO OF INTERNAL STATIC PRESSURE TO JET TOTAL PRESSURE ON THRUST REVERSER

NPR	$p/p_{t,j}$ at y, in., of -										
	2.58	2.00	1.70	1.34	.89	.44	0.0	-.44	-.89	-1.34	-1.70
1.505	.634	.636	.866	.978	.998	.998	.997	.999	.997	.977	.860
2.004	.462	.513	.834	.973	.997	.997	.996	.999	.996	.971	.822
2.502	.367	.485	.824	.971	.996	.996	.994	.999	.997	.970	.812
2.996	.310	.472	.819	.971	.996	.996	.993	1.000	.997	.969	.810
4.014	.241	.465	.818	.972	.996	.995	.991	.999	.996	.969	.806
5.014	.215	.464	.819	.973	.996	.996	.986	1.000	.996	.969	.808
5.969	.222	.465	.820	.974	.996	.996	.980	.999	.995	.970	.810
7.019	.238	.465	.822	.976	.996	.996	.971	1.000	.994	.972	.813

TABLE V.- RATIO OF INTERNAL STATIC PRESSURE TO JET TOTAL PRESSURE ON VERTICAL TAKEOFF AND LANDING NOZZLE

[See figure 12 for location of pressure orifices]

(a) Configuration V1

NPR	$p/p_{t,j}$ at -										
	PRB1	PRB2	PRB3	PRB4	PRB5	PRB6	PRB7	PRB8	PRLF1	PRLF2	PRLF3
	Blocker 1								Lower flap 1		
1.495	.931	.943	.961	.954	.963	.979	.969	.912	.653	.659	.654
1.749	.917	.932	.954	.945	.956	.972	.960	.891	.546	.552	.550
1.757	.917	.932	.954	.945	.956	.971	.959	.891	.542	.548	.545
1.993	.910	.926	.951	.942	.951	.967	.954	.880	.472	.476	.474
2.267	.905	.922	.948	.939	.949	.966	.952	.873	.416	.414	.411
2.499	.902	.919	.946	.937	.949	.966	.950	.870	.376	.373	.368
2.761	.900	.917	.945	.936	.948	.965	.949	.867	.339	.334	.329
3.012	.898	.916	.944	.936	.948	.965	.948	.865	.309	.303	.299

(b) Configuration V2

NPR	$p/p_{t,j}$ at -										
	PRB1	PRB2	PRB3	PRB4	PRB5	PRB6	PRB7	PRB8	PRLF1	PRLF2	PRLF3
	Blocker 1								Lower flap 2		
1.514	.936	.948	.965	.958	.966	.981	.970	.912	.900	.883	.845
1.759	.922	.937	.959	.949	.959	.975	.963	.894	.880	.860	.815
2.011	.913	.929	.953	.943	.955	.973	.958	.883	.868	.844	.795
2.245	.908	.925	.950	.940	.953	.971	.956	.877	.860	.835	.785
2.516	.904	.922	.948	.938	.950	.969	.954	.873	.855	.828	.777
2.755	.902	.920	.948	.937	.948	.967	.952	.870	.852	.824	.772
3.014	.900	.919	.947	.937	.948	.966	.951	.868	.849	.821	.769
3.212	.899	.919	.947	.937	.948	.965	.951	.867	.848	.820	.767

TABLE V.- Concluded

(c) Configuration V3

NPR	$p/p_{t,j}$ at -												
	PRB1	PRB2	PRB3	PRB4	PRB5	PRB6	PRB7	PRB8	PRB9	PRB10	PRLF1	PRLF2	PRLF3
	Blocker 2										Lower flap 1		
1.496	.931	.947	.959	.953	.958	.974	.971	.962	.930	.823	.660	.660	.654
1.755	.918	.937	.952	.944	.951	.966	.963	.952	.912	.782	.555	.555	.547
2.001	.911	.932	.949	.940	.948	.963	.959	.947	.902	.762	.480	.477	.468
2.254	.907	.929	.947	.938	.946	.963	.957	.945	.897	.752	.424	.420	.411
2.512	.903	.926	.945	.936	.944	.962	.956	.942	.893	.746	.378	.372	.364
2.757	.902	.925	.944	.935	.944	.961	.955	.941	.890	.743	.341	.334	.328
3.018	.900	.924	.943	.935	.943	.961	.954	.940	.888	.740	.307	.300	.296

(d) Configuration V4

NPR	$p/p_{t,j}$ at -												
	PRB1	PRB2	PRB3	PRB4	PRB5	PRB6	PRB7	PRB8	PRB9	PRB10	PRLF1	PRLF2	PRLF3
	Blocker 2										Lower flap 2		
1.494	.938	.952	.965	.957	.962	.978	.975	.966	.934	.824	.908	.893	.855
1.755	.924	.942	.957	.948	.955	.972	.969	.958	.918	.785	.889	.870	.823
2.013	.915	.935	.952	.942	.949	.970	.965	.953	.908	.764	.876	.855	.804
2.258	.910	.931	.949	.939	.946	.968	.963	.950	.902	.754	.869	.847	.794
2.506	.907	.929	.947	.937	.945	.965	.960	.947	.898	.748	.865	.841	.787
2.763	.905	.928	.946	.936	.944	.962	.959	.946	.895	.745	.862	.838	.783
3.019	.903	.927	.946	.936	.944	.962	.958	.945	.893	.739	.859	.835	.780
3.187	.903	.927	.945	.936	.944	.961	.958	.944	.893	.739	.858	.833	.778

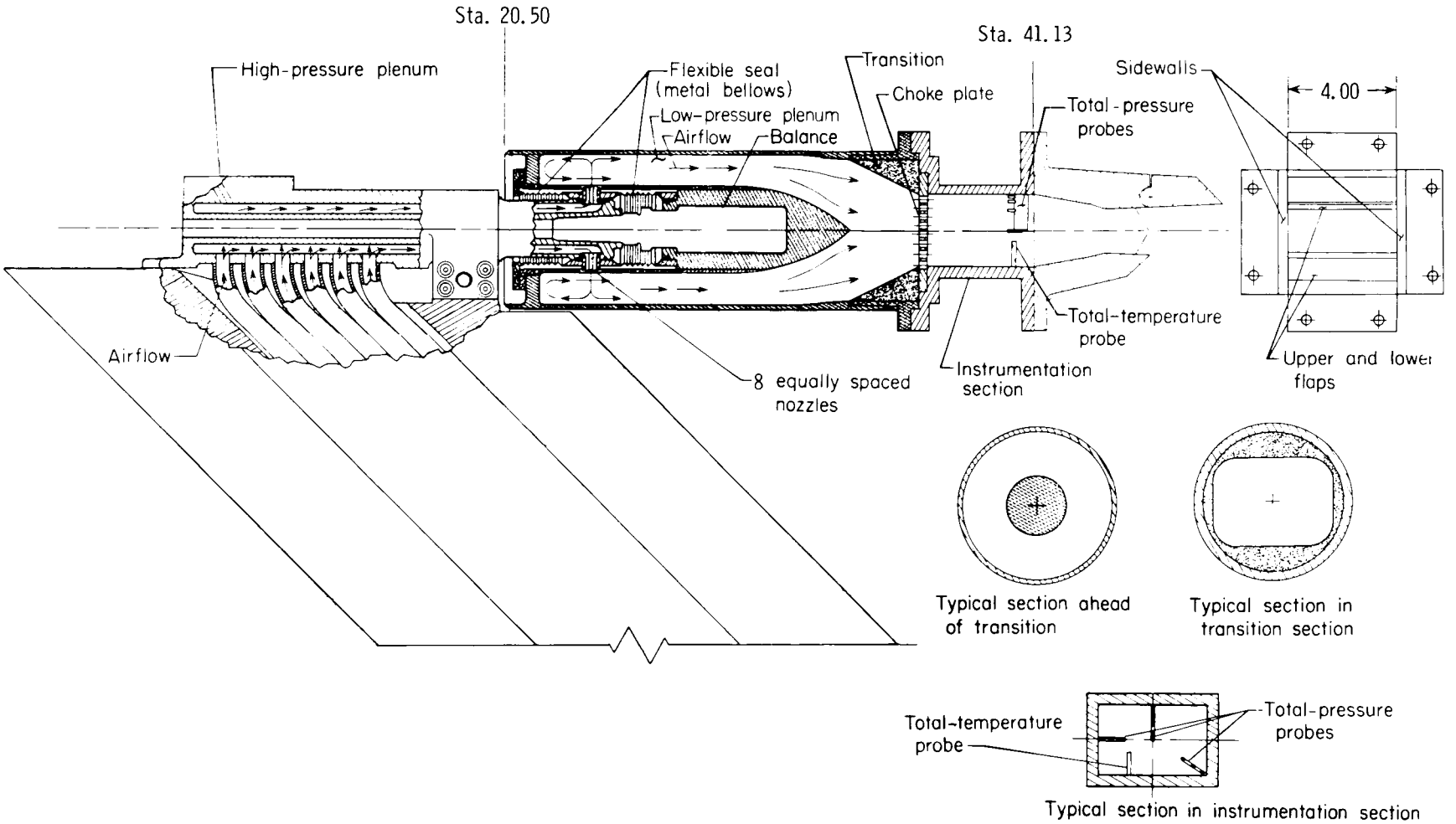

(a) Air-powered nacelle test apparatus.

Figure 1.- Sketch of air-powered nacelle model with typical nozzle configuration installed. Linear dimensions are in inches.

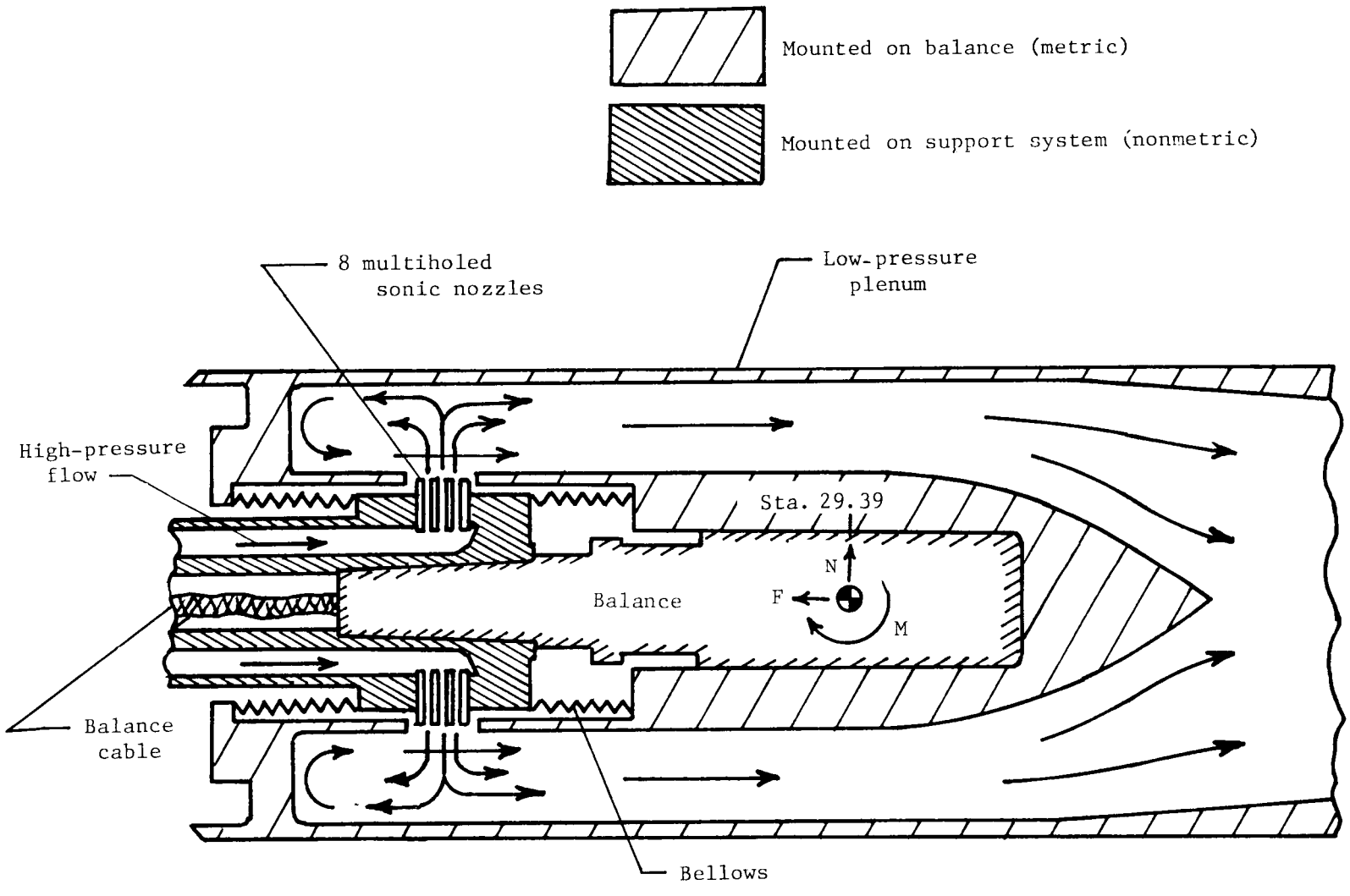

(b) Schematic cross section of flow transfer system.

Figure 1.- Concluded.

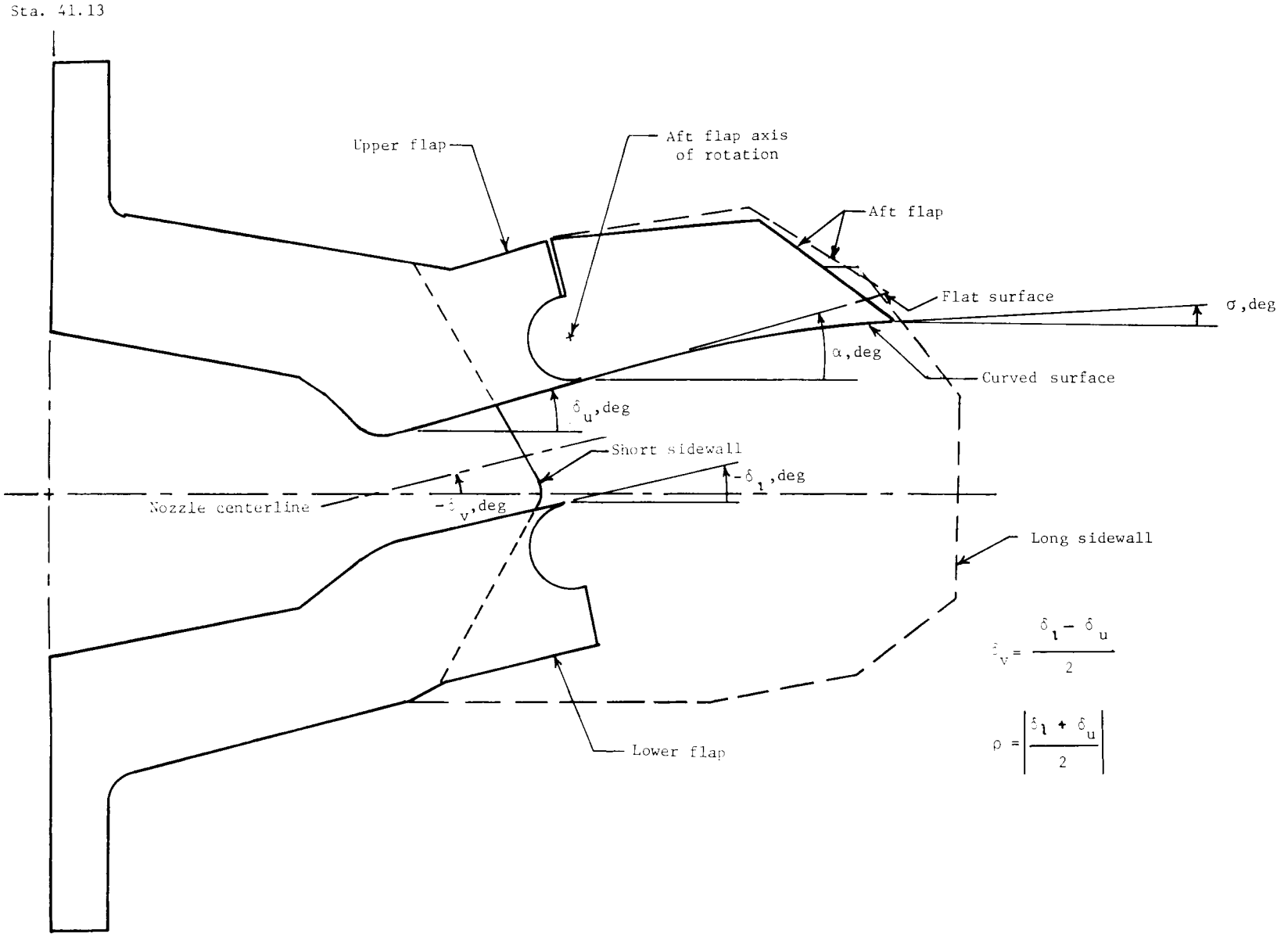

Figure 2.- Sketch of typical nozzle configurations showing nozzle components and angular sign conventions.

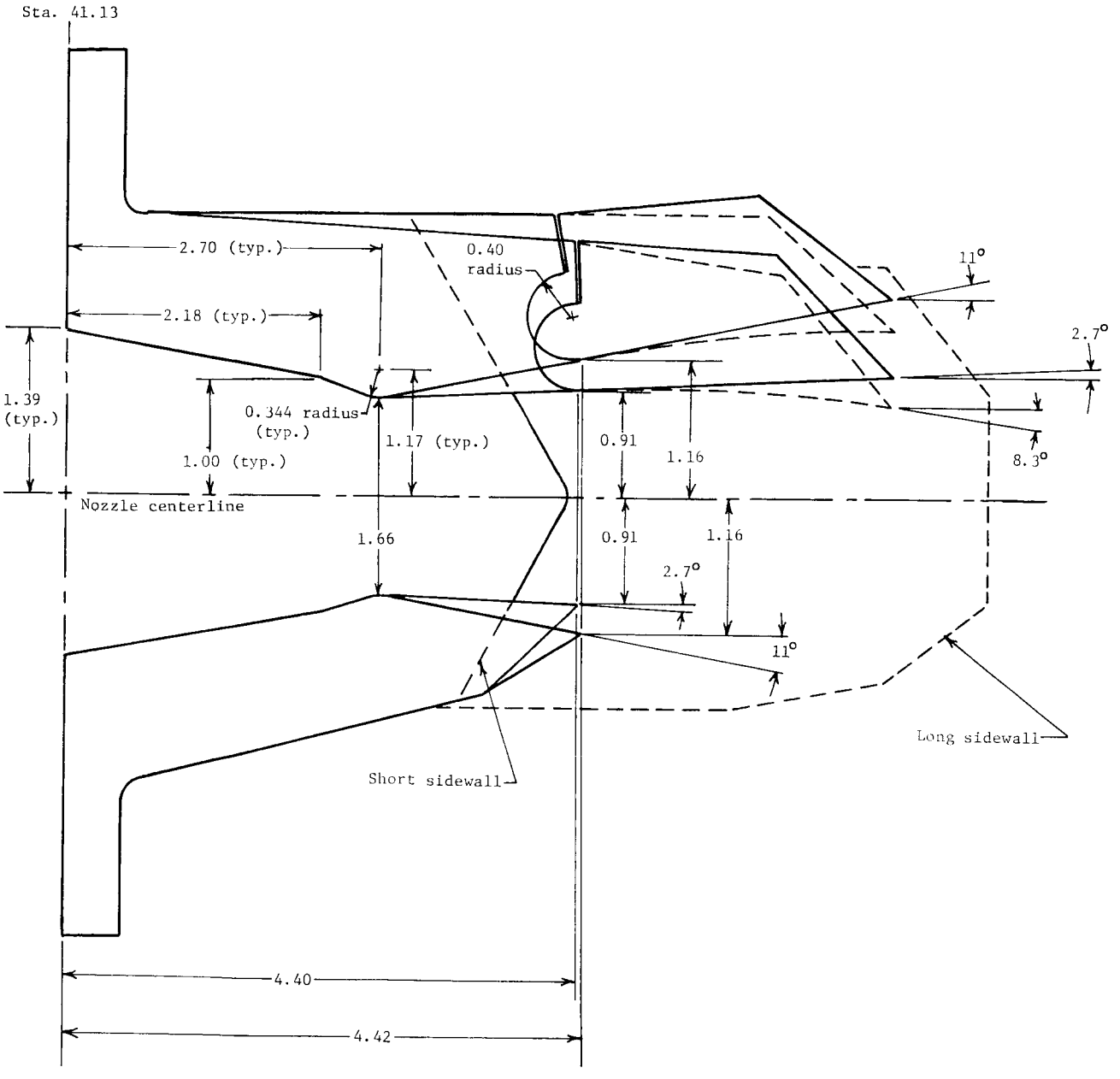

(a) Unvectored nozzles with 2.7° and 11.0° divergence angles, and nozzles (δ_v = ±4.15°) with 6.85° divergence angle.

Figure 3.- Afterburning power nozzle geometry. Linear dimensions are in inches.

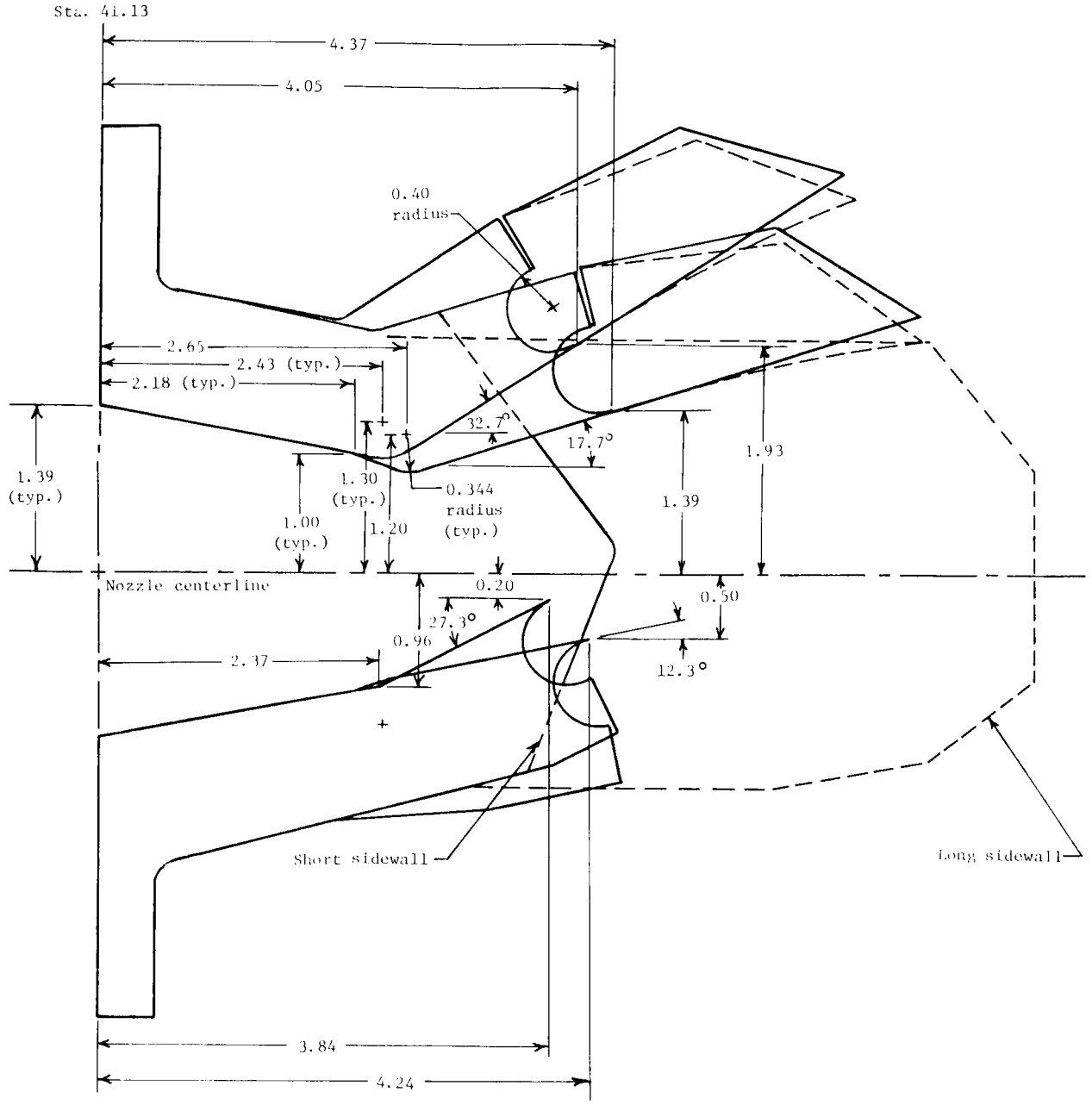

(b) Nozzles vectored -15° and -30° with 2.7° divergence angle.

Figure 3.- Continued.

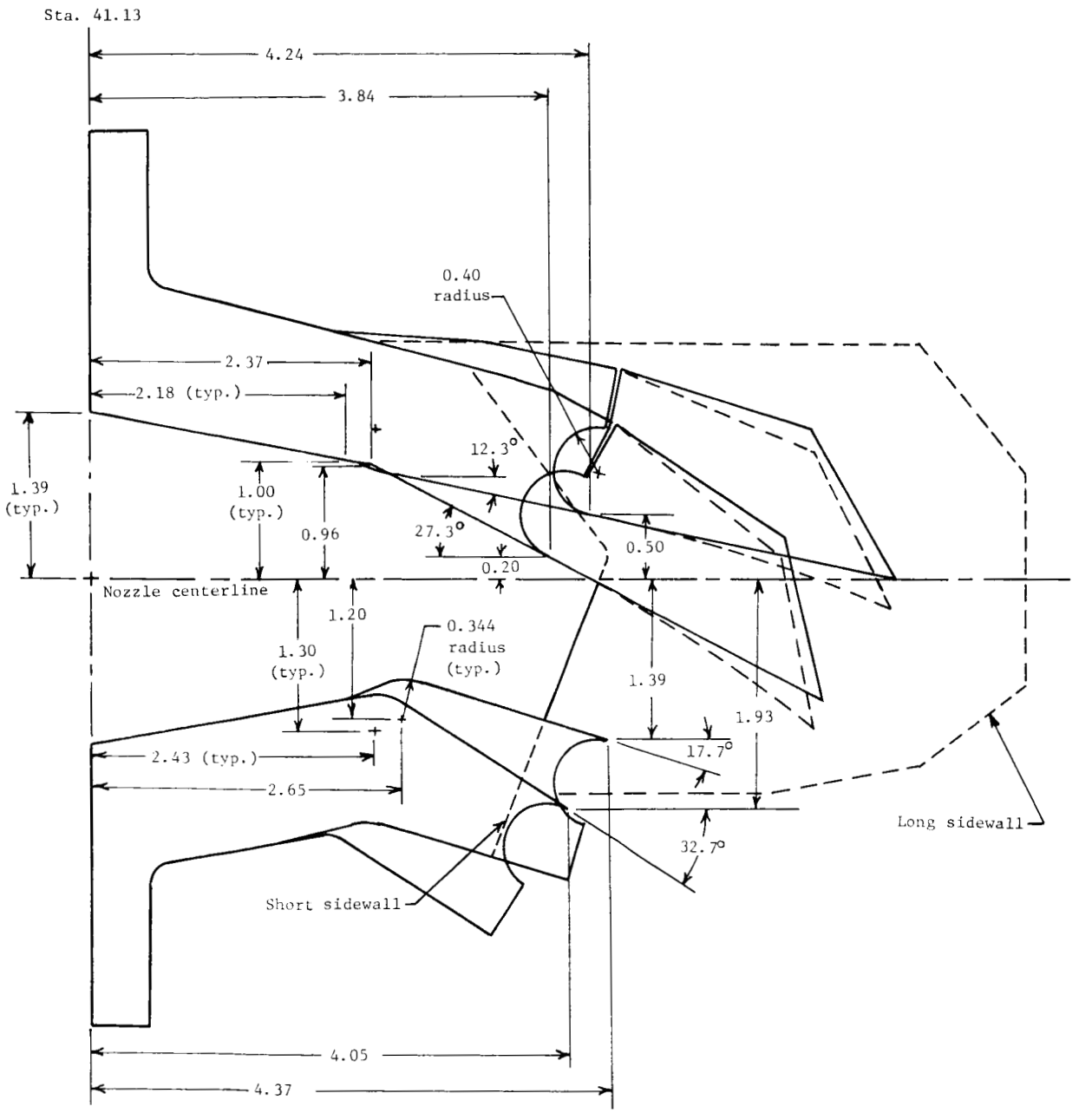

(c) Nozzles vectored 15° and 30° with 2.7° divergence angle.

Figure 3.- Concluded.

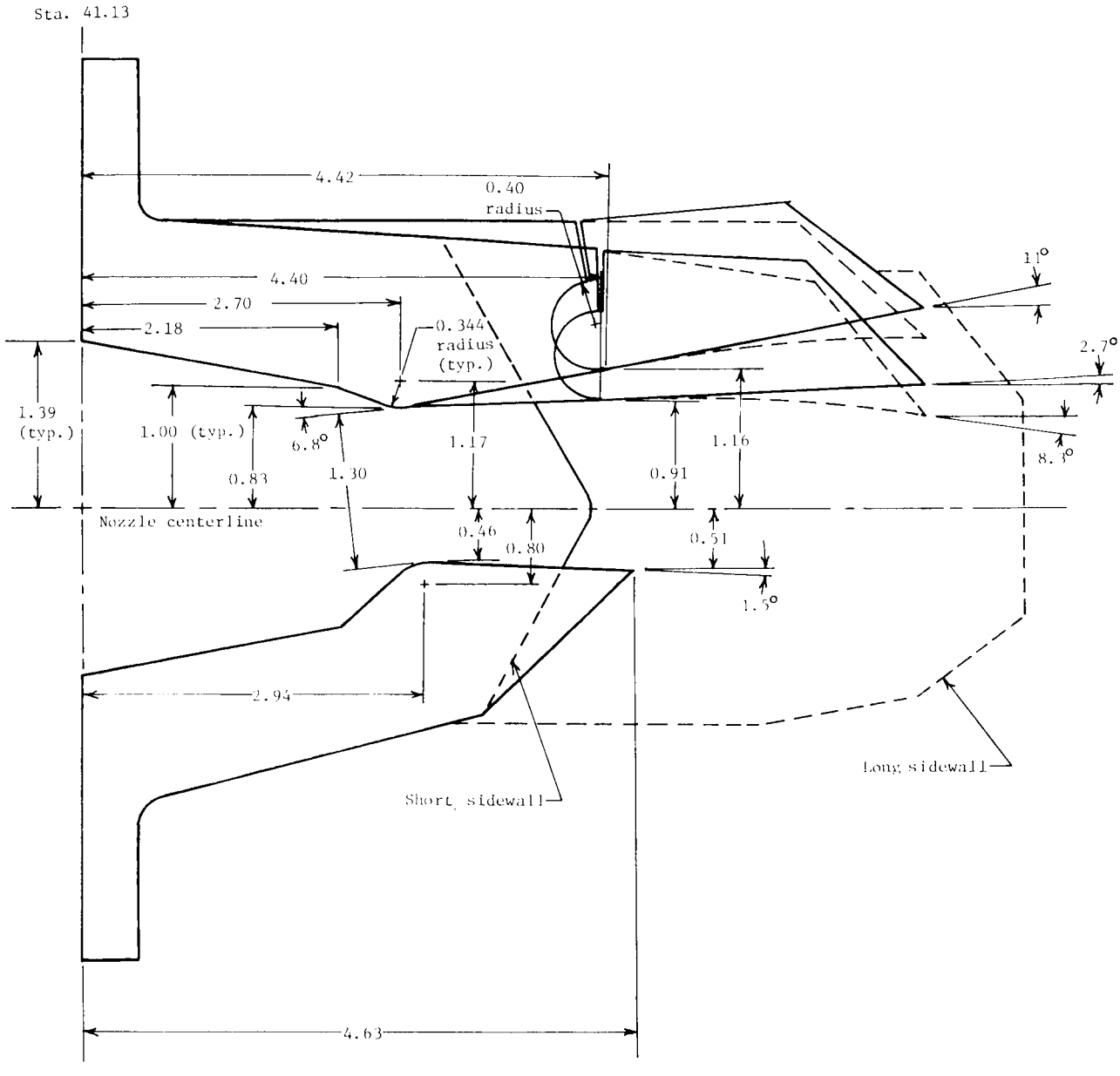

Figure 4.- Partial afterburning power nozzle geometry. Linear dimensions are in inches.

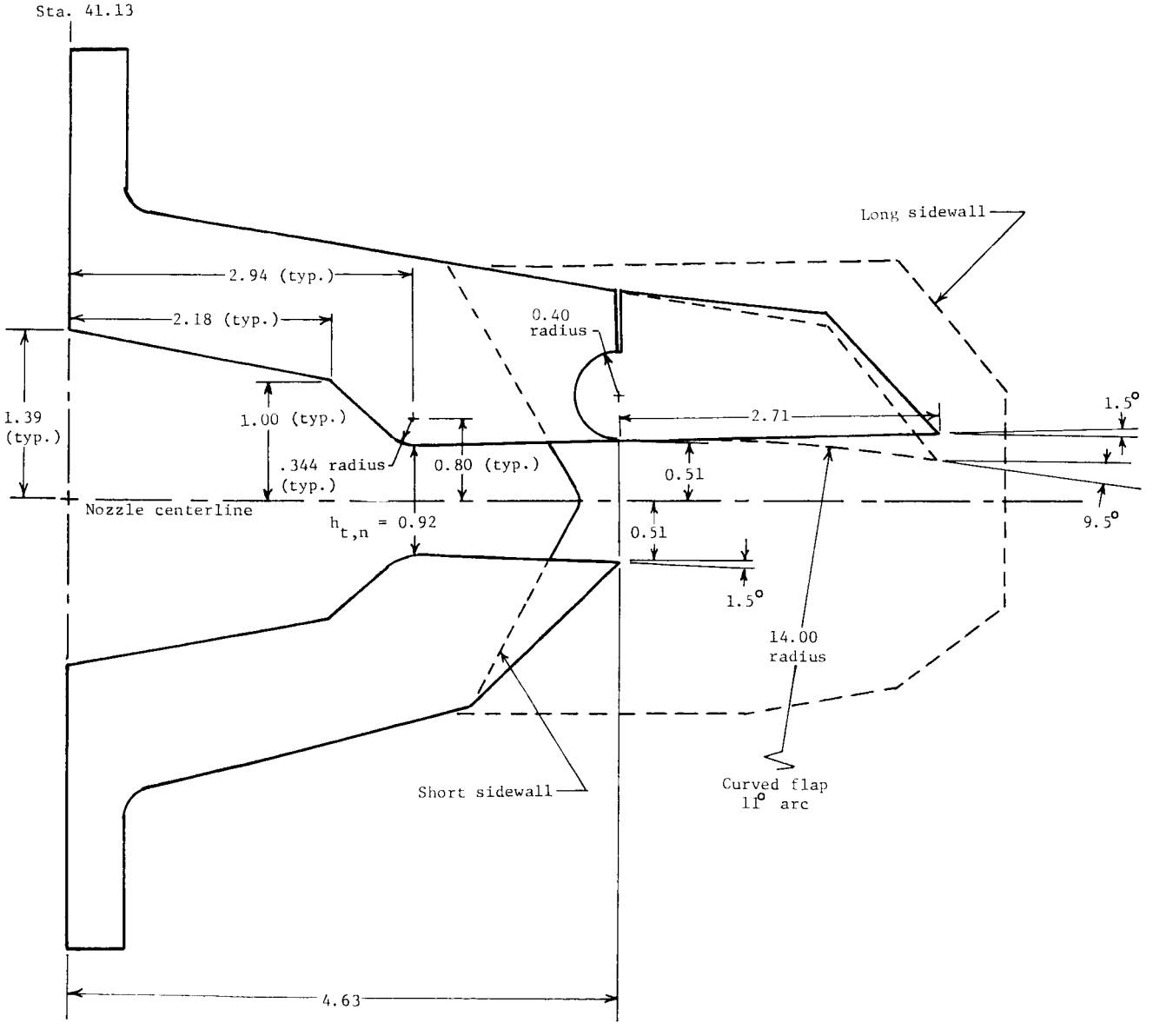

(a) Unvectored nozzles.

Figure 5.- Dry power nozzle geometry. Linear dimensions are in inches.

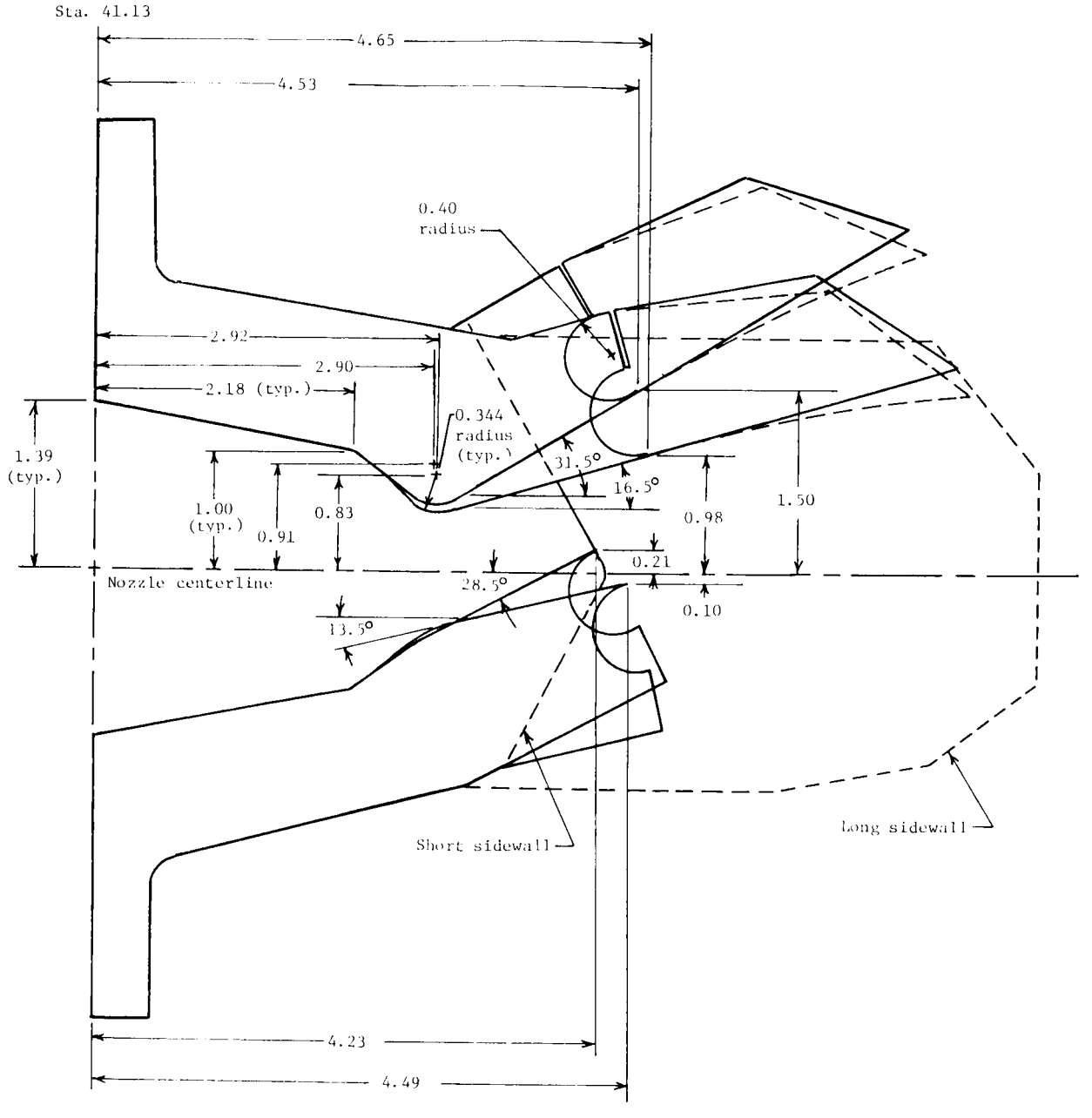

(b) Nozzles vectored -15° and -30°.

Figure 5.- Continued.

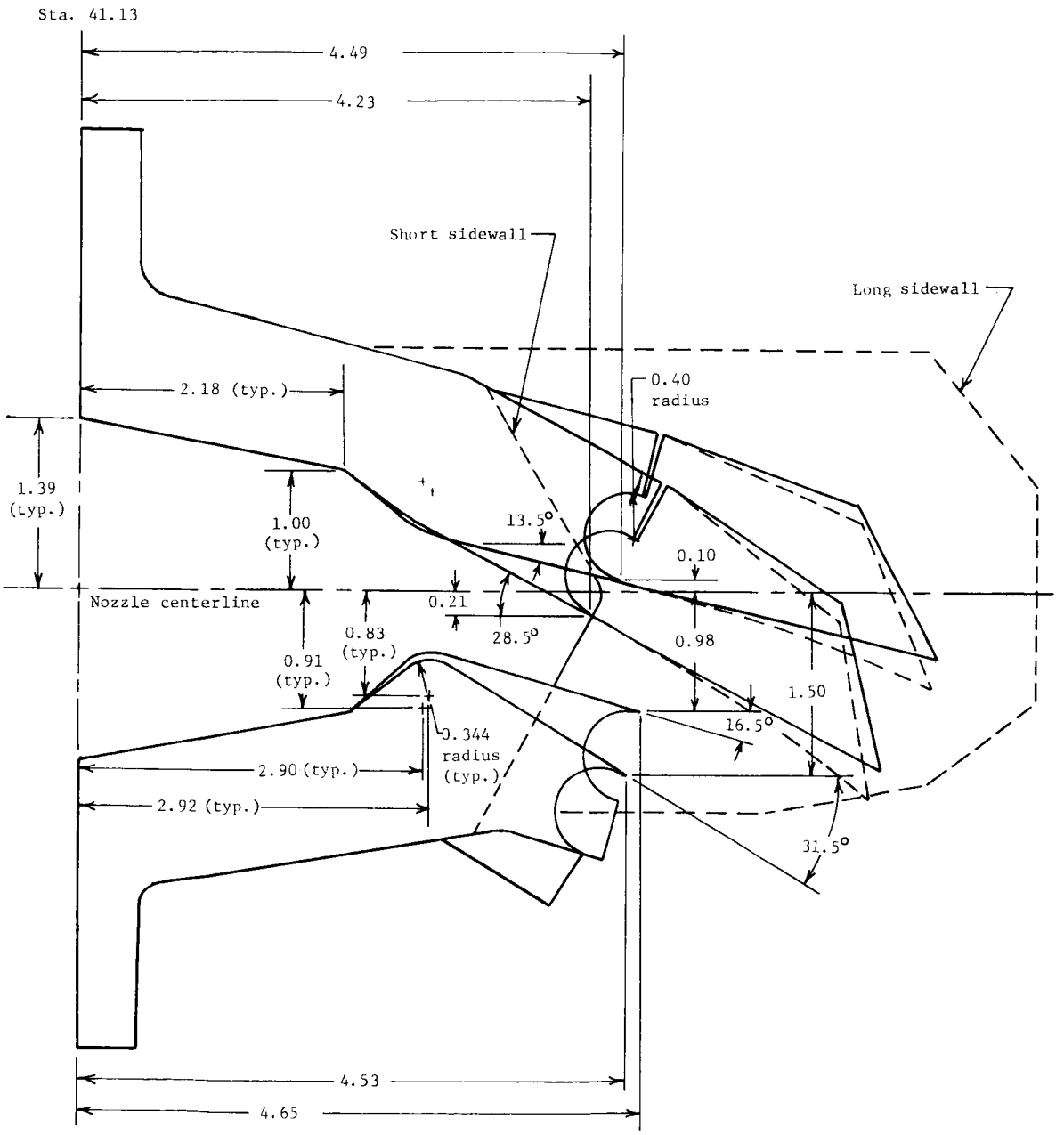

(c) Nozzles vectored 15° and 30°.

Figure 5.- Concluded.

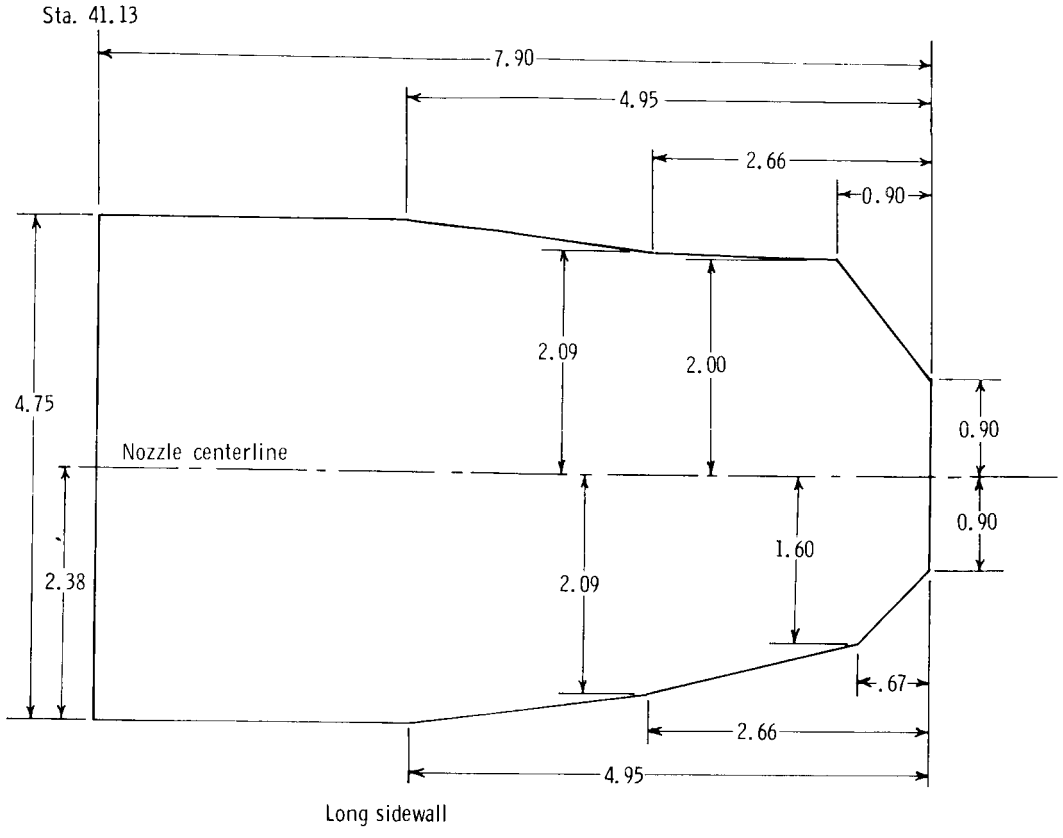

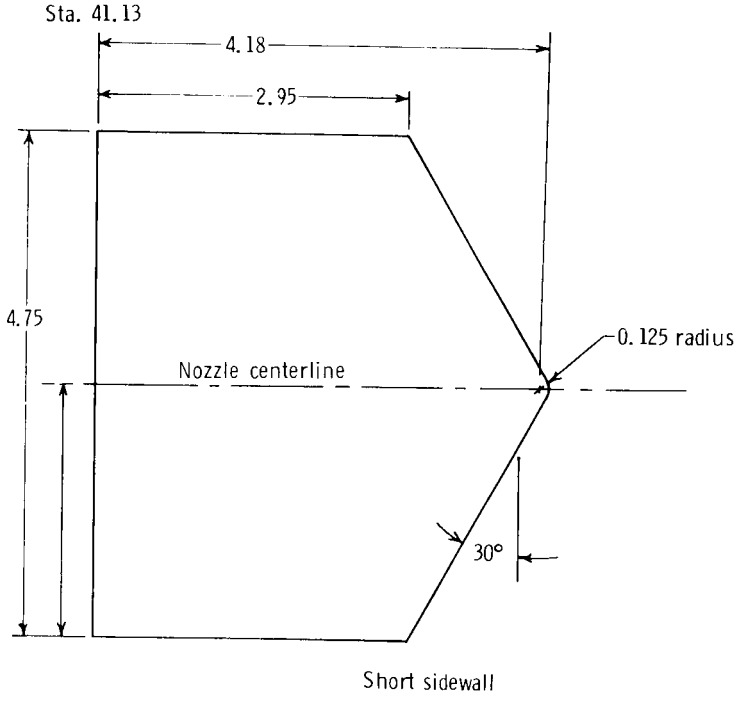

Figure 6.- Nozzle sidewall geometry. Linear dimensions are in inches.

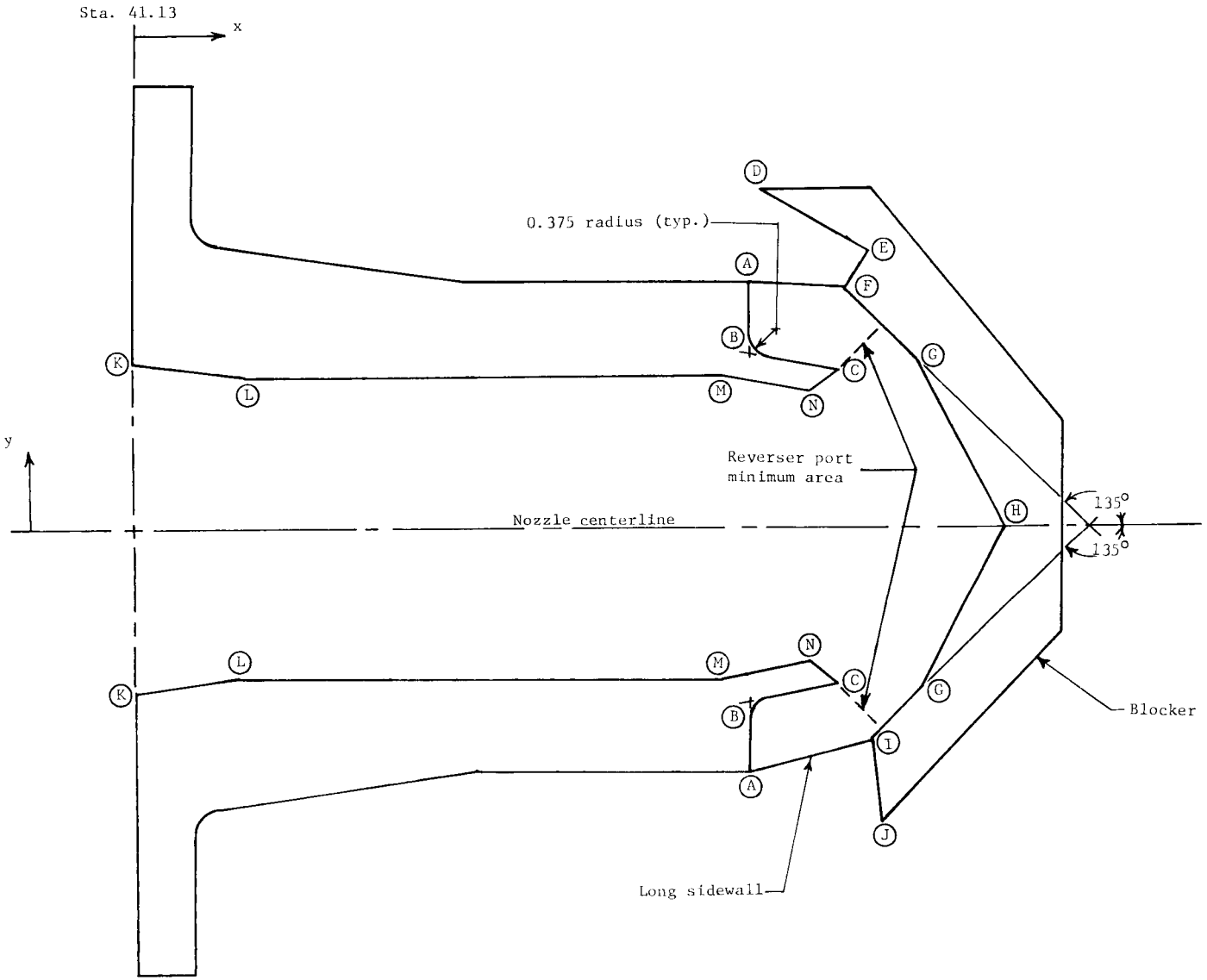

Point	x	y
A	5.24	±2.09
B	5.24	±1.47
C	6.00	±1.33
D	5.34	2.86
E	6.25	2.33
F	6.07	2.02
G	6.69	±1.40
H	7.40	0.00
I	6.29	-1.80
J	6.37	-2.50
K	0.00	±1.39
L	0.90	±1.30
M	5.00	±1.30
N	5.75	±1.16

Figure 7.- Thrust-reverser nozzle geometry. Linear dimensions are in inches.

Configuration	Blocker	Lower flap
V1	1	1
V2	1	2
V3	2	1
V4	2	2

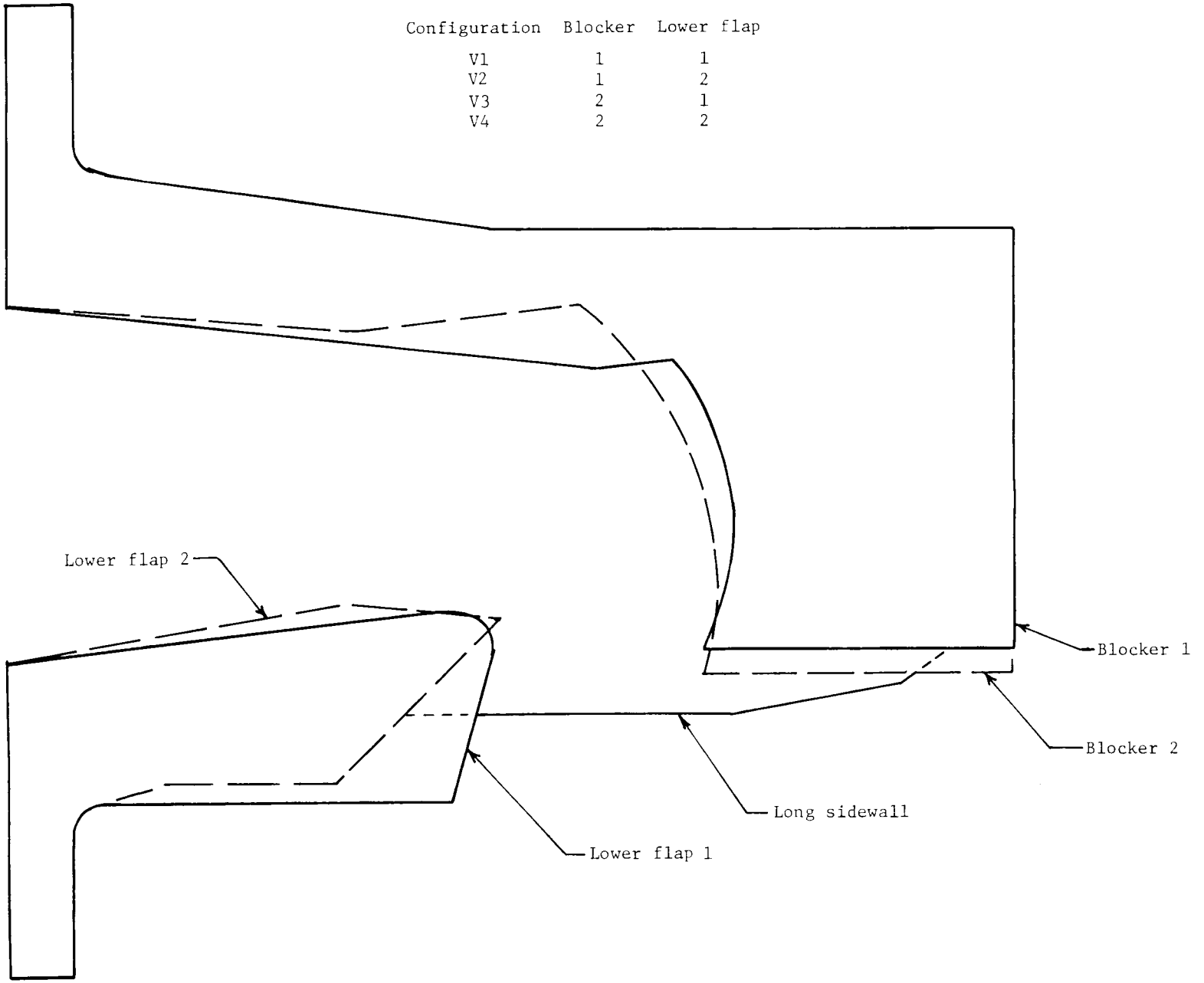

Figure 8.- Sketch of vertical takeoff or landing nozzle configurations.

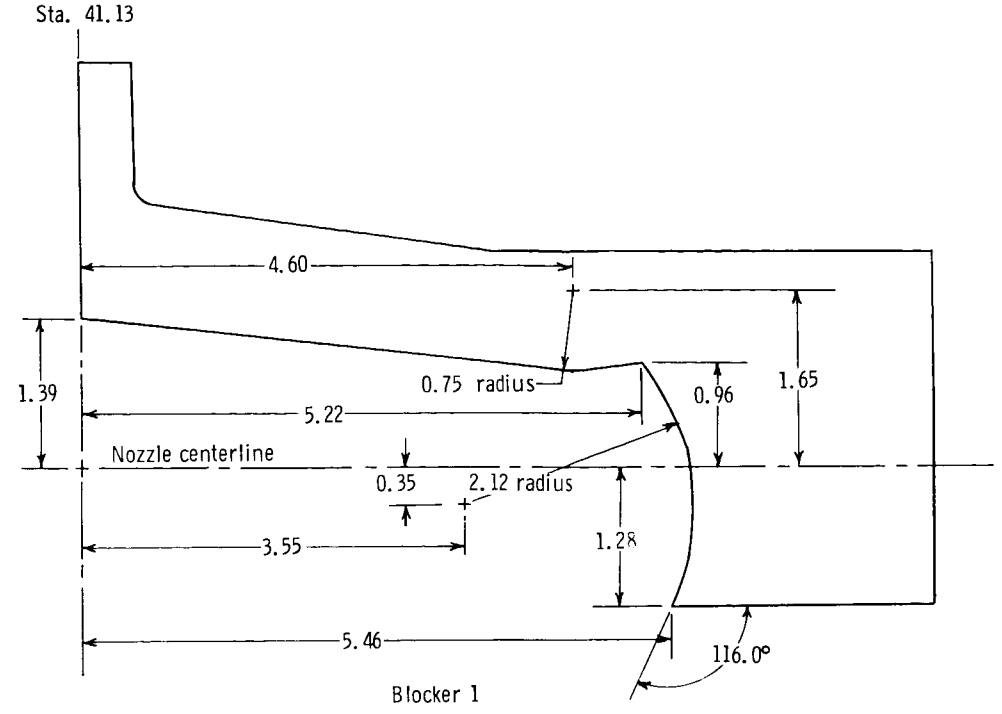

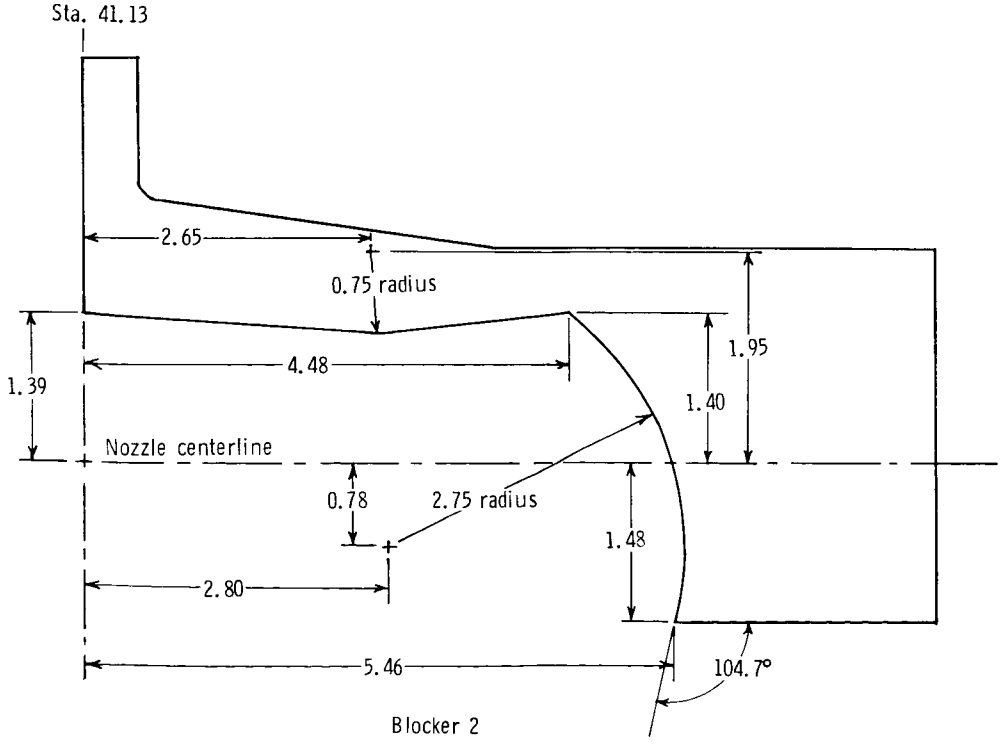

(a) Vertical takeoff or landing nozzle blockers.

Figure 9.- Vertical takeoff or landing nozzle components. Linear dimensions are in inches.

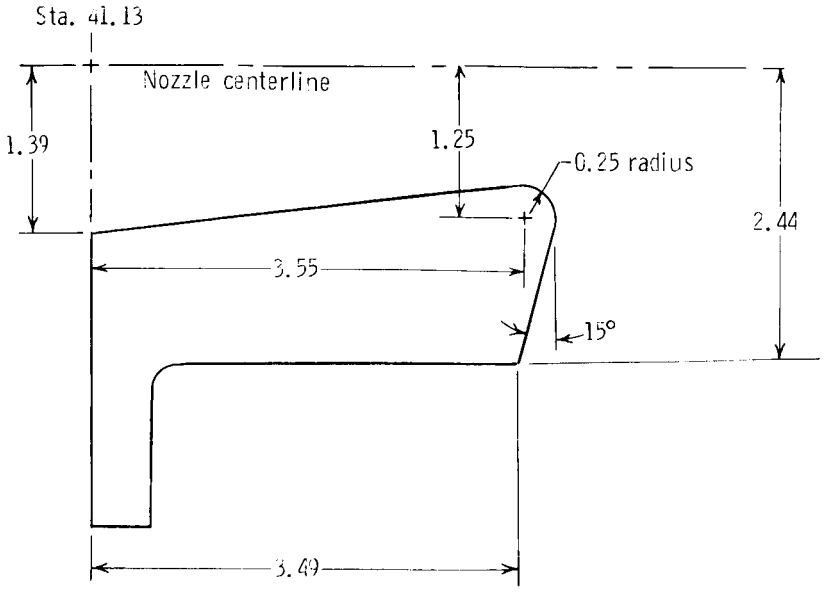

Lower flap 1

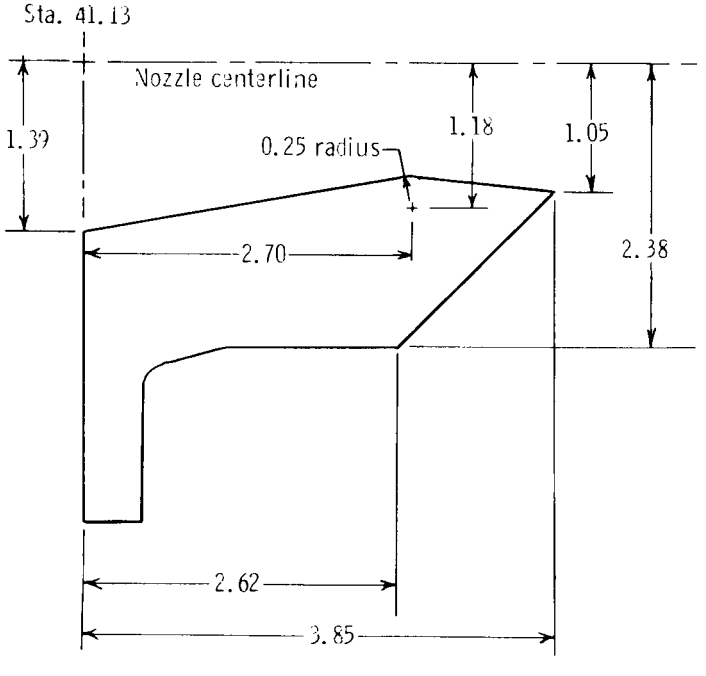

Lower flap 2

(b) Vertical takeoff or landing nozzle lower flaps.

Figure 9.- Concluded.

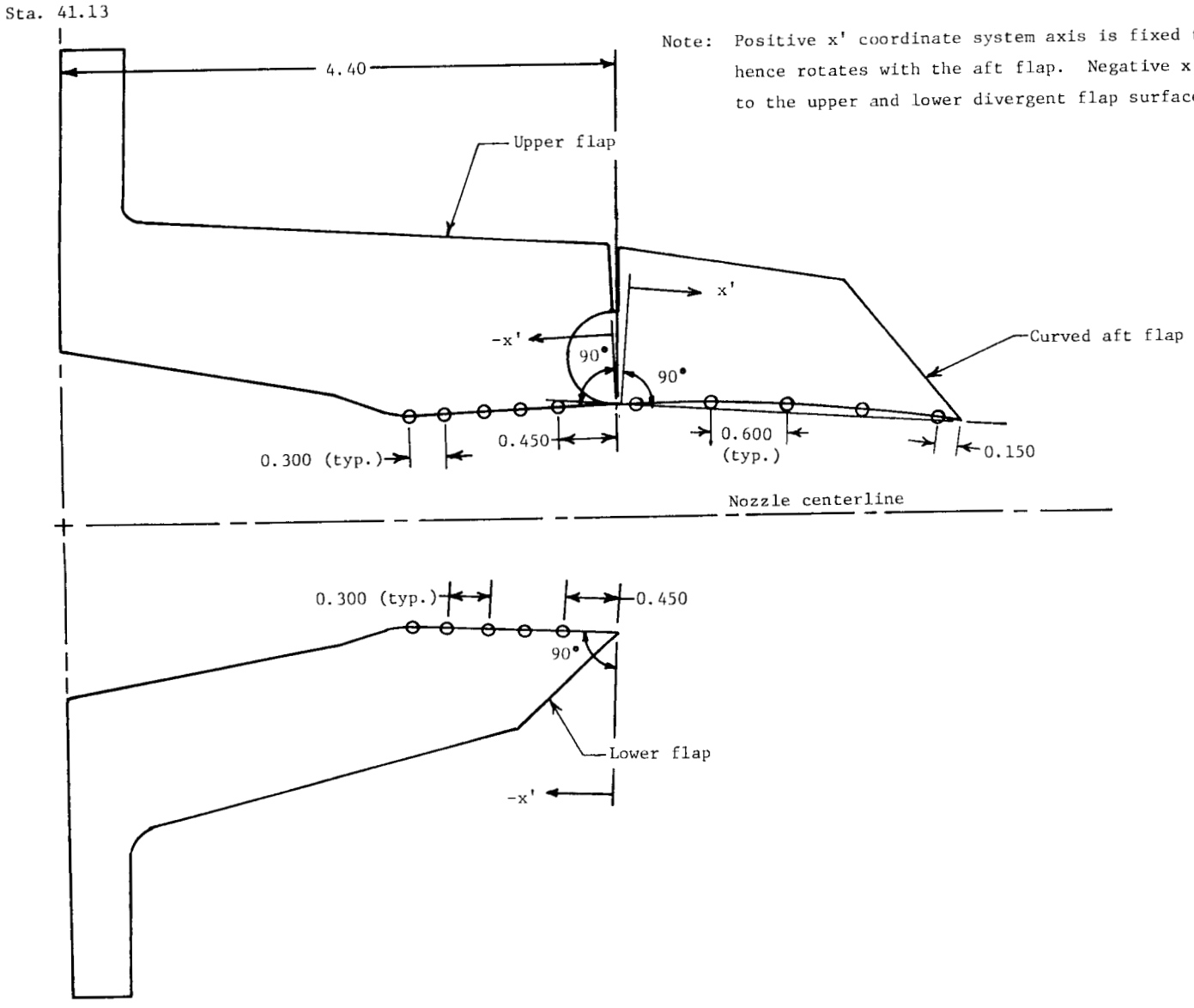

(a) Unvectored afterburning power nozzle with curved aft flap.

Figure 10.- Definition of pressure orifice coordinate system and location of pressure orifices on internal surfaces of flaps for two typical nozzle configurations. Linear dimensions are in inches.

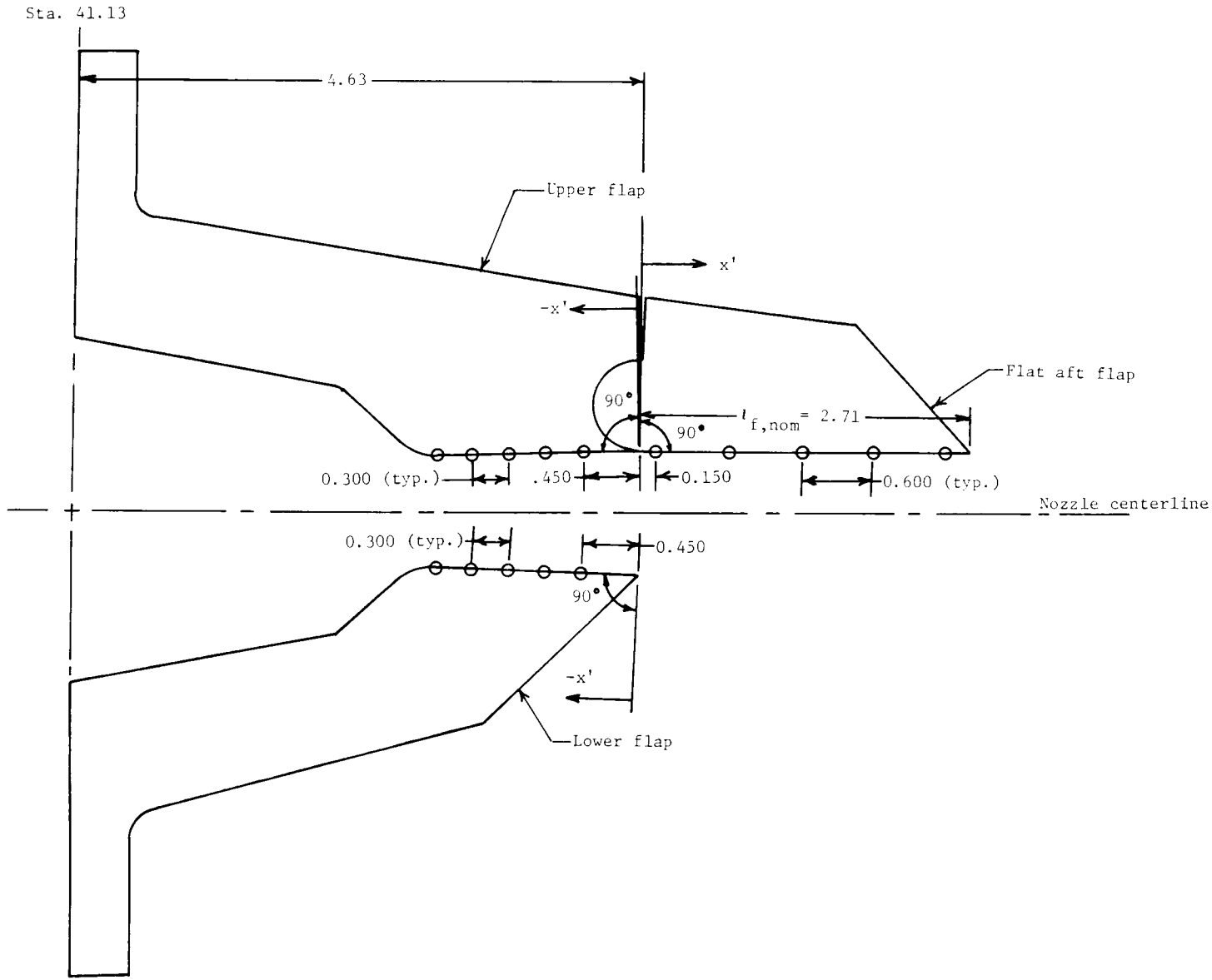

(b) Unvectored dry power nozzle with flat aft flap.

Figure 10.- Concluded.

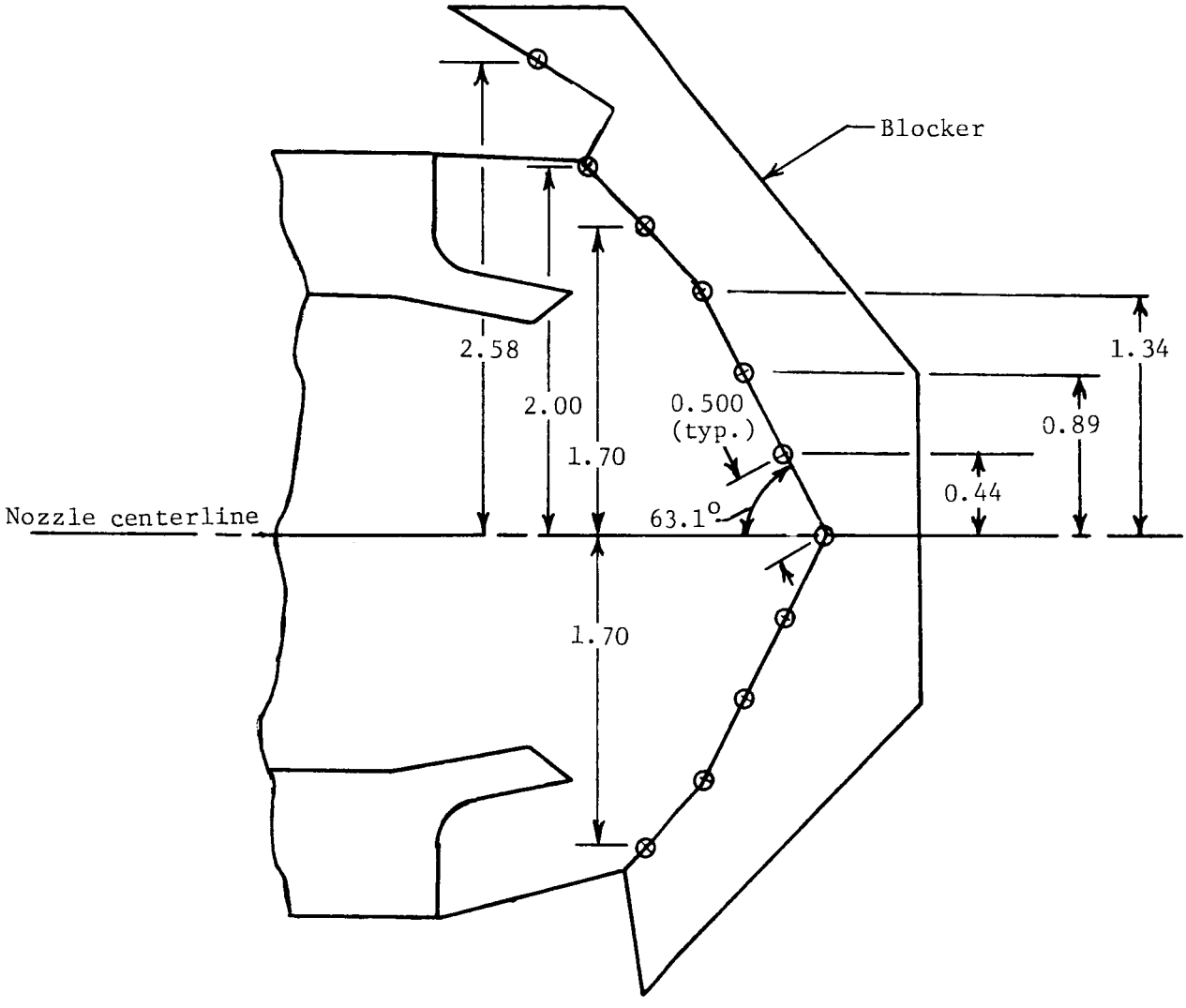

Figure 11.- Location of pressure orifices on thrust-reverser blocker. Linear dimensions are in inches.

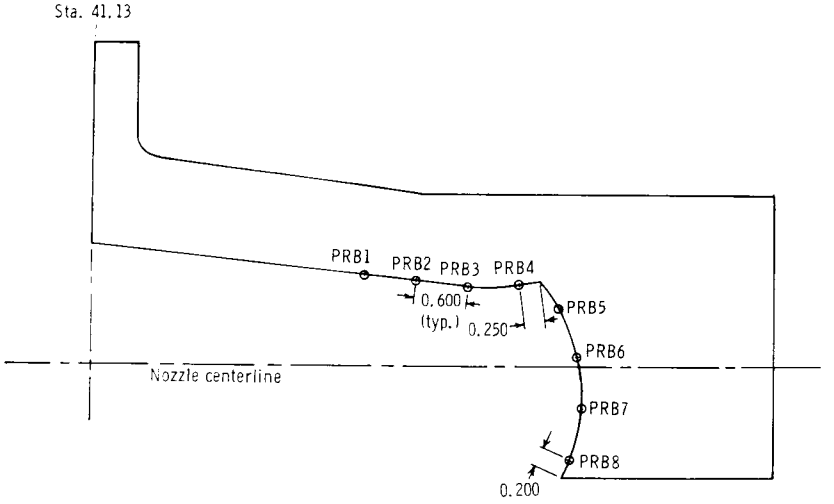

Blocker 1

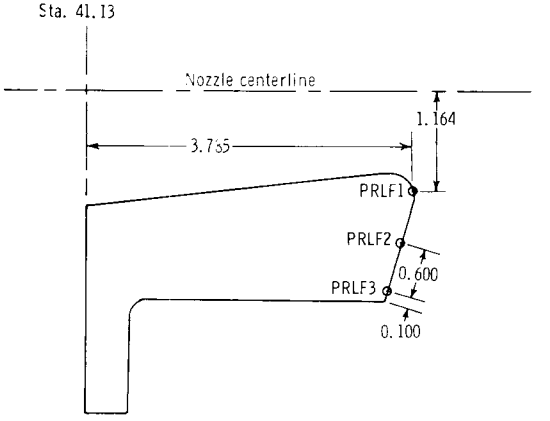

Lower flap 1

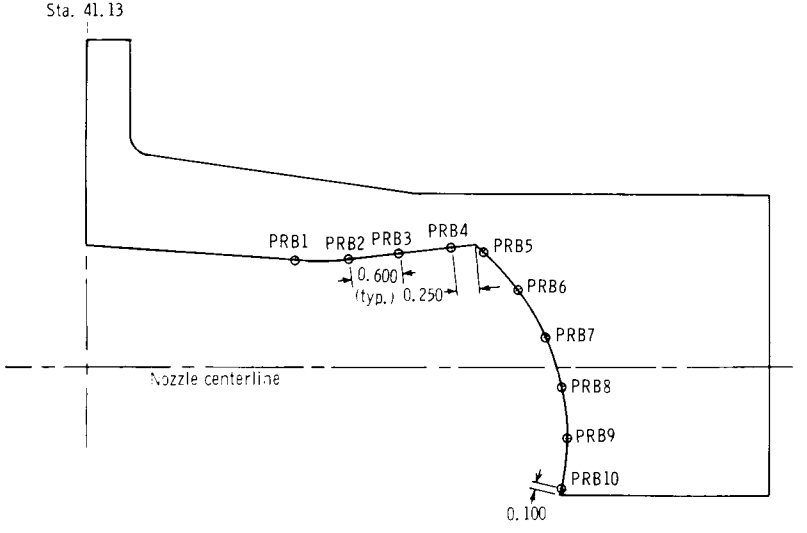

Blocker 2

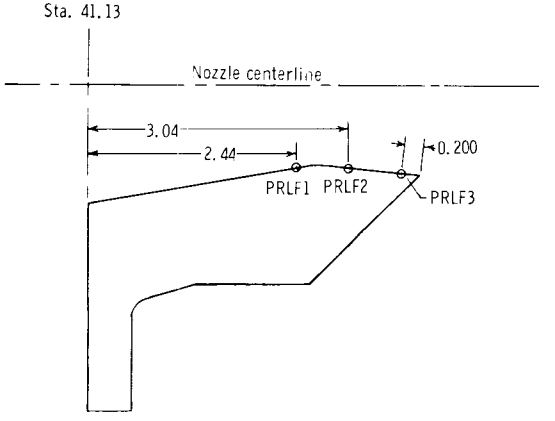

Lower flap 2

Figure 12.- Location of pressure orifices on vertical takeoff or landing nozzle components. Linear dimensions are in inches.

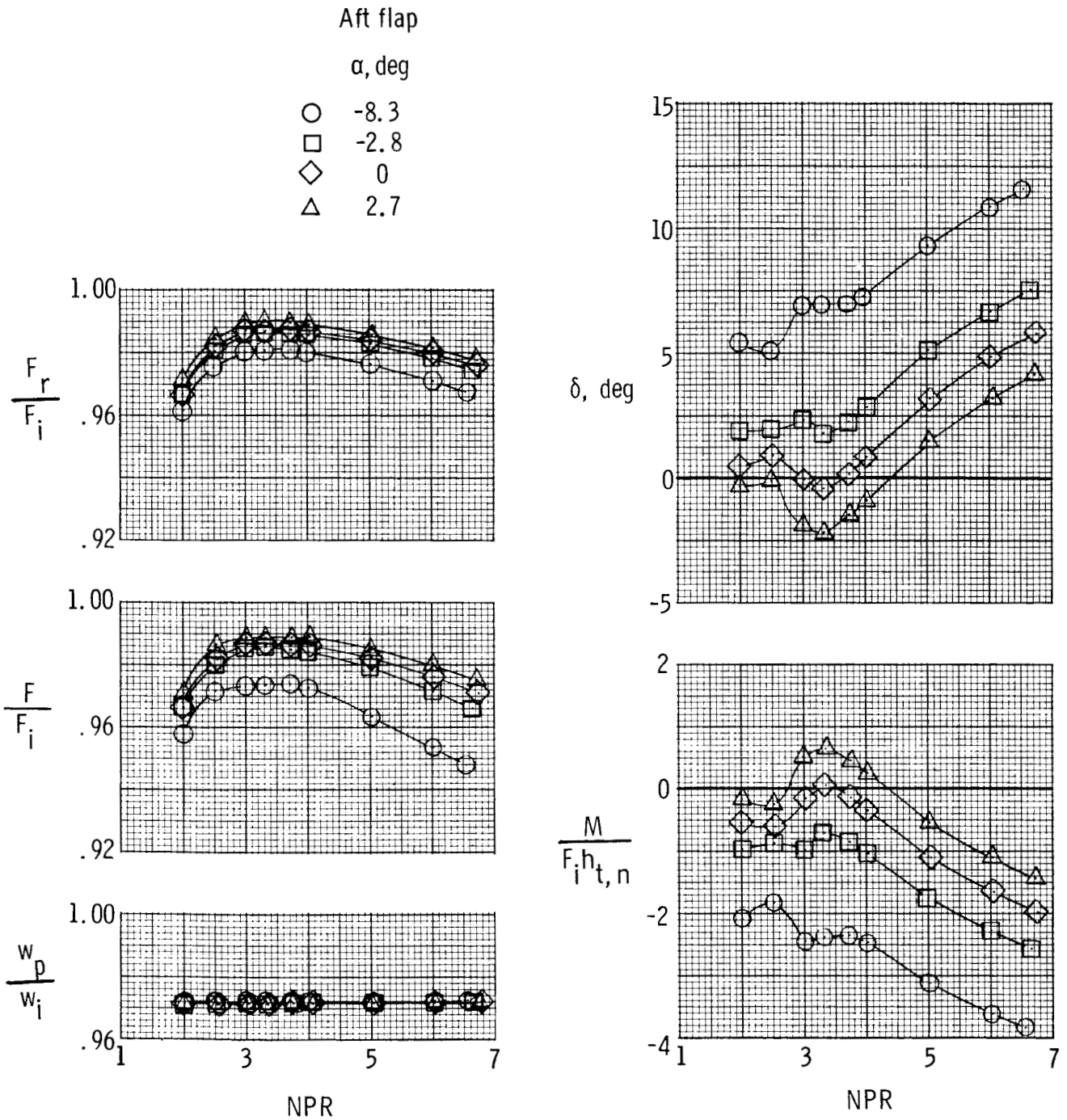

(a) Configuration A1FS, $\delta_v = 0°$.

Figure 13.- Variation of nozzle performance parameters with nozzle pressure ratio for three afterburning configurations with several aft flap (flat) angles.

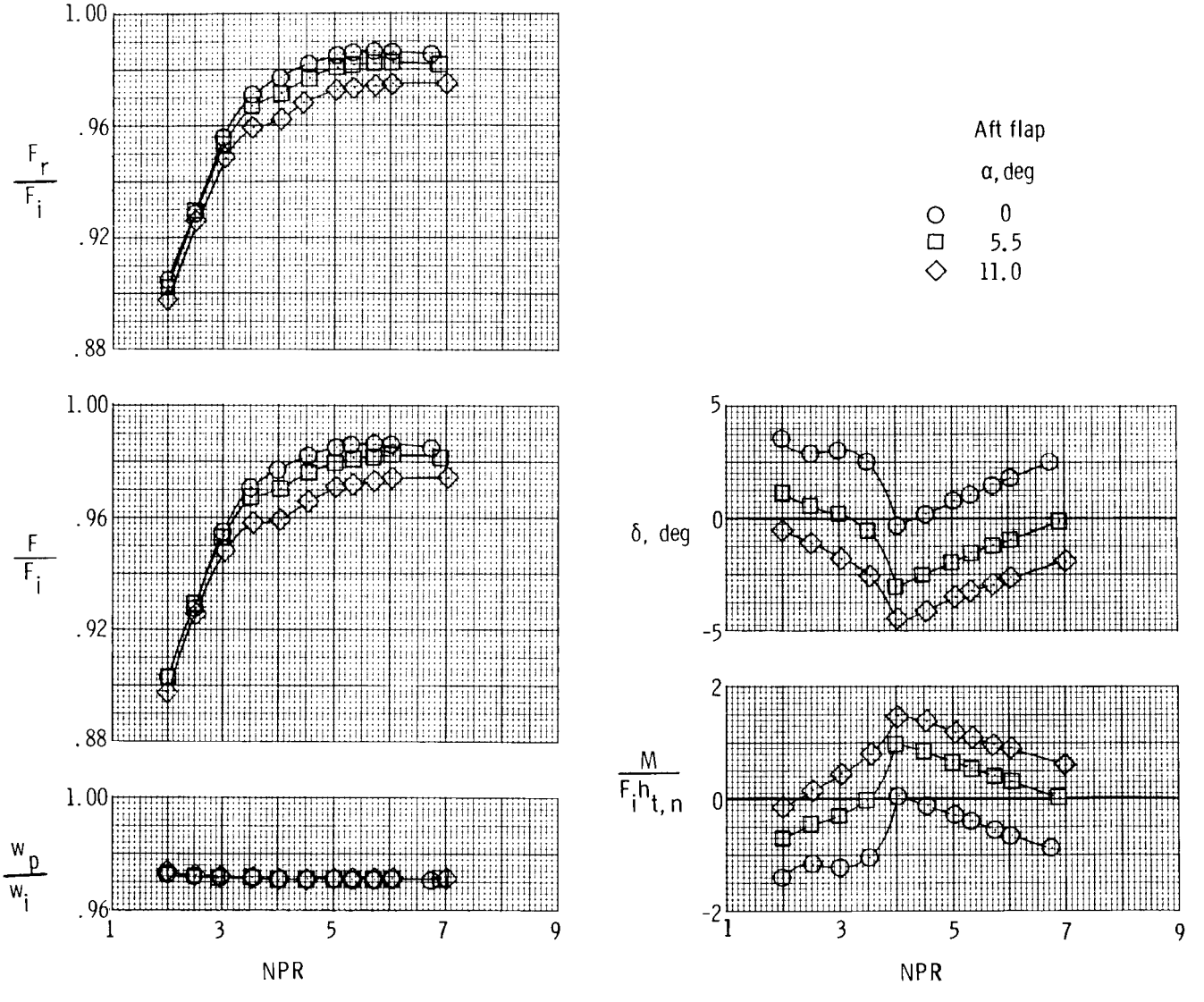

(b) Configuration A2FS, $\delta_v = 0°$.

Figure 13.- Continued.

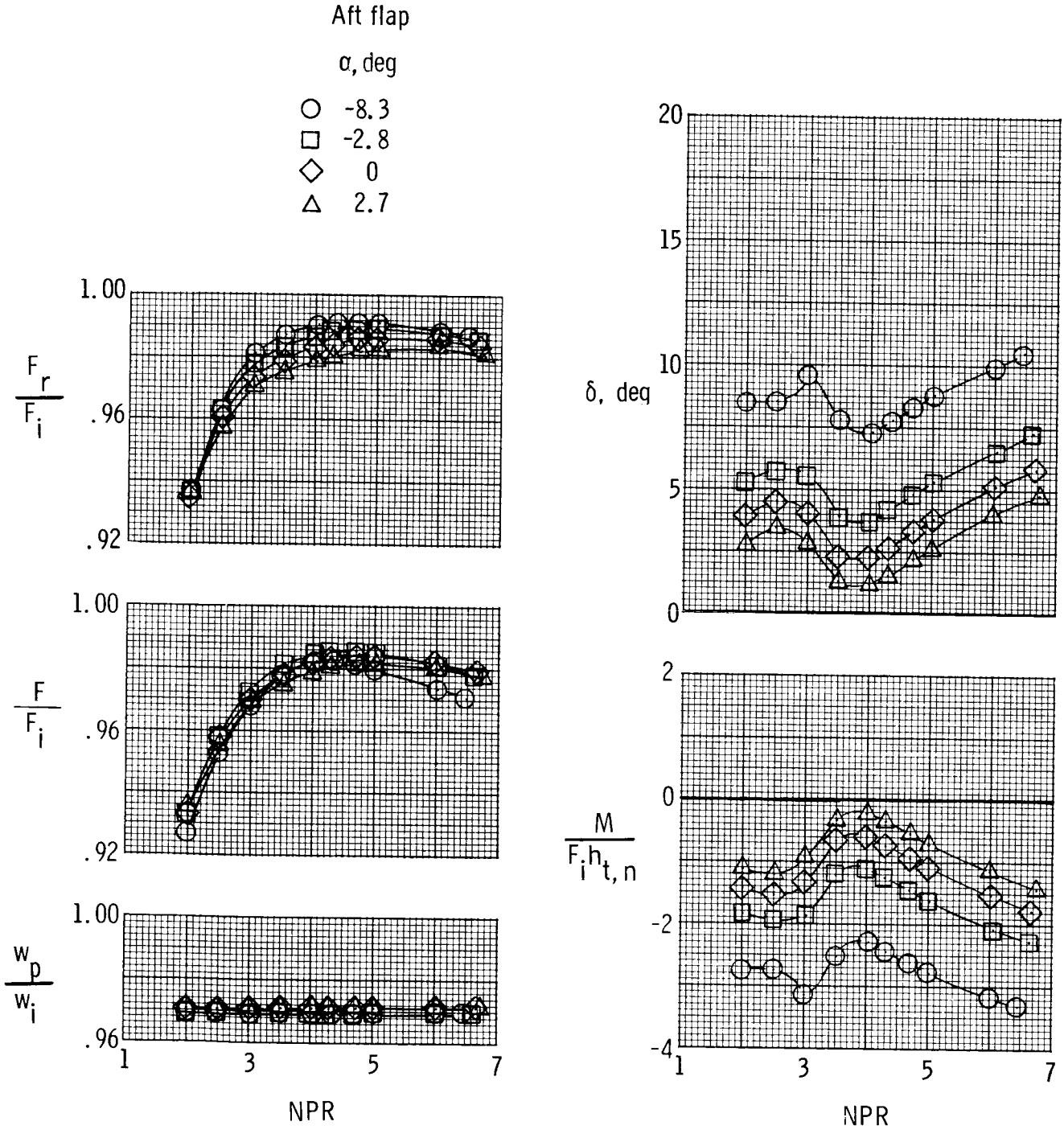

(c) Configuration A3FS, δ_v = 4.15°.

Figure 13.- Continued.

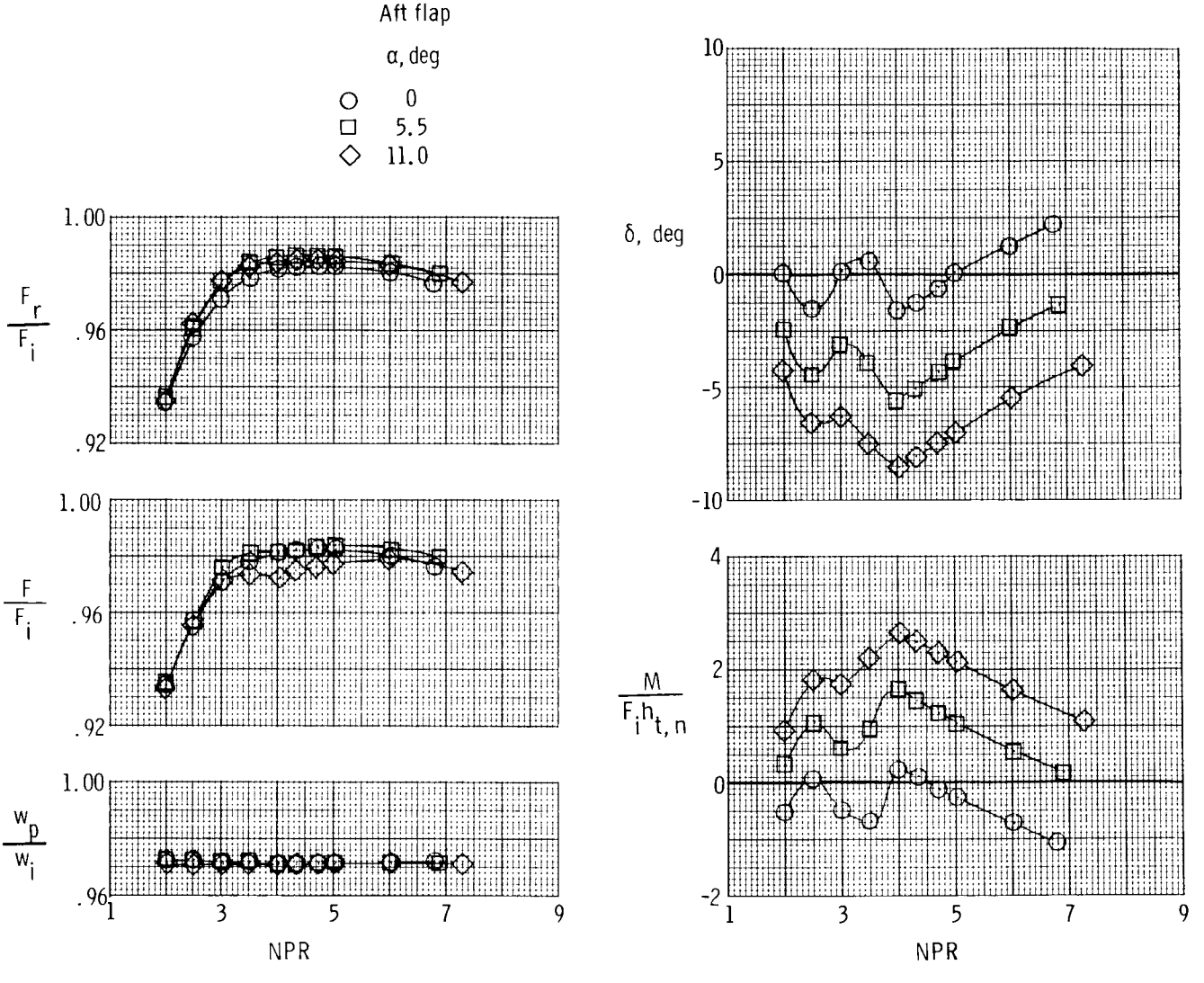

(d) Configuration A3FS, δ_v = -4.15°.

Figure 13.- Concluded.

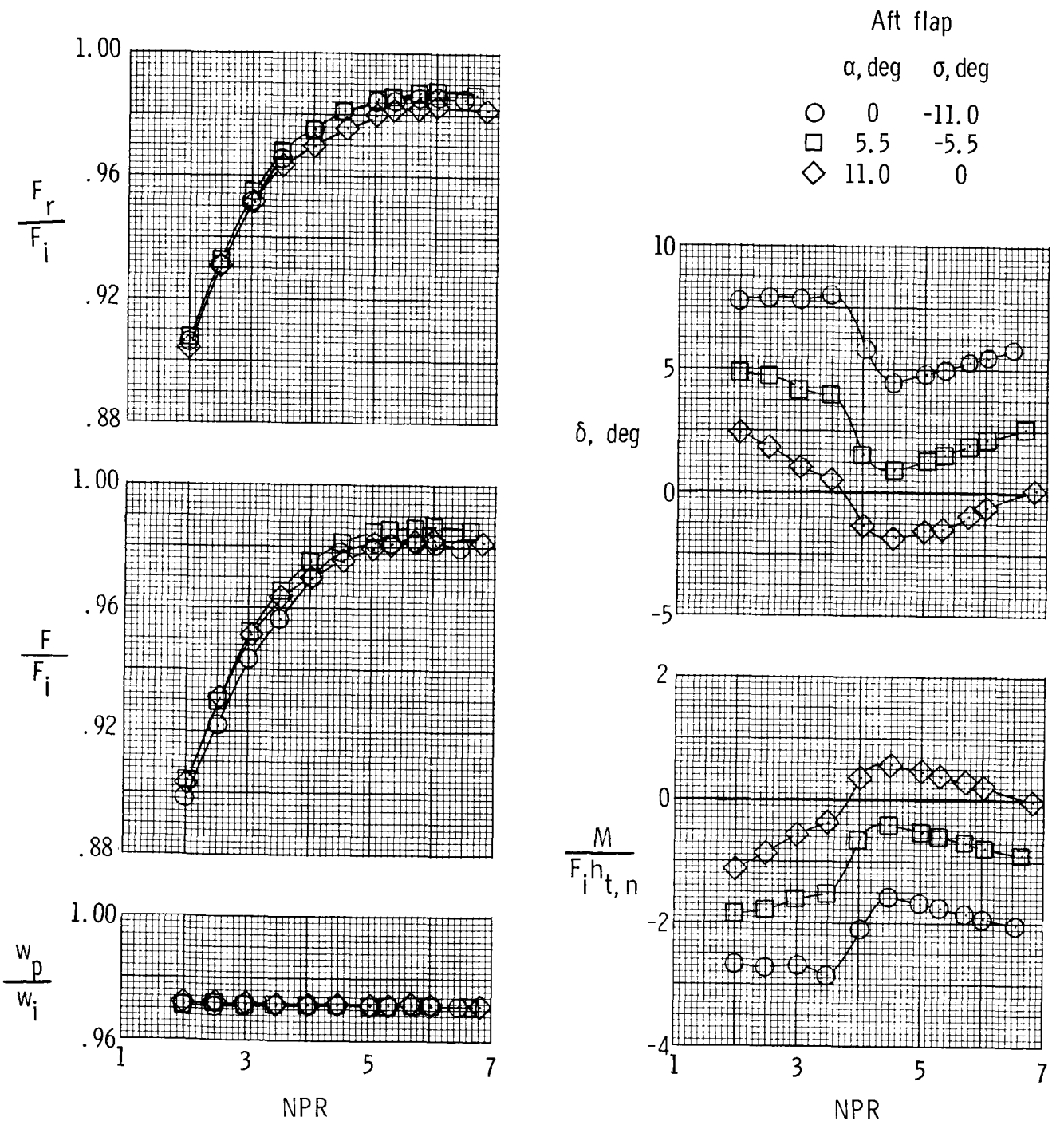

(a) Configuration A2CS, $\delta_v = 0°$.

Figure 14.- Variation of nozzle performance parameters with nozzle pressure ratio for two afterburning configurations with several aft flap (curved) angles.

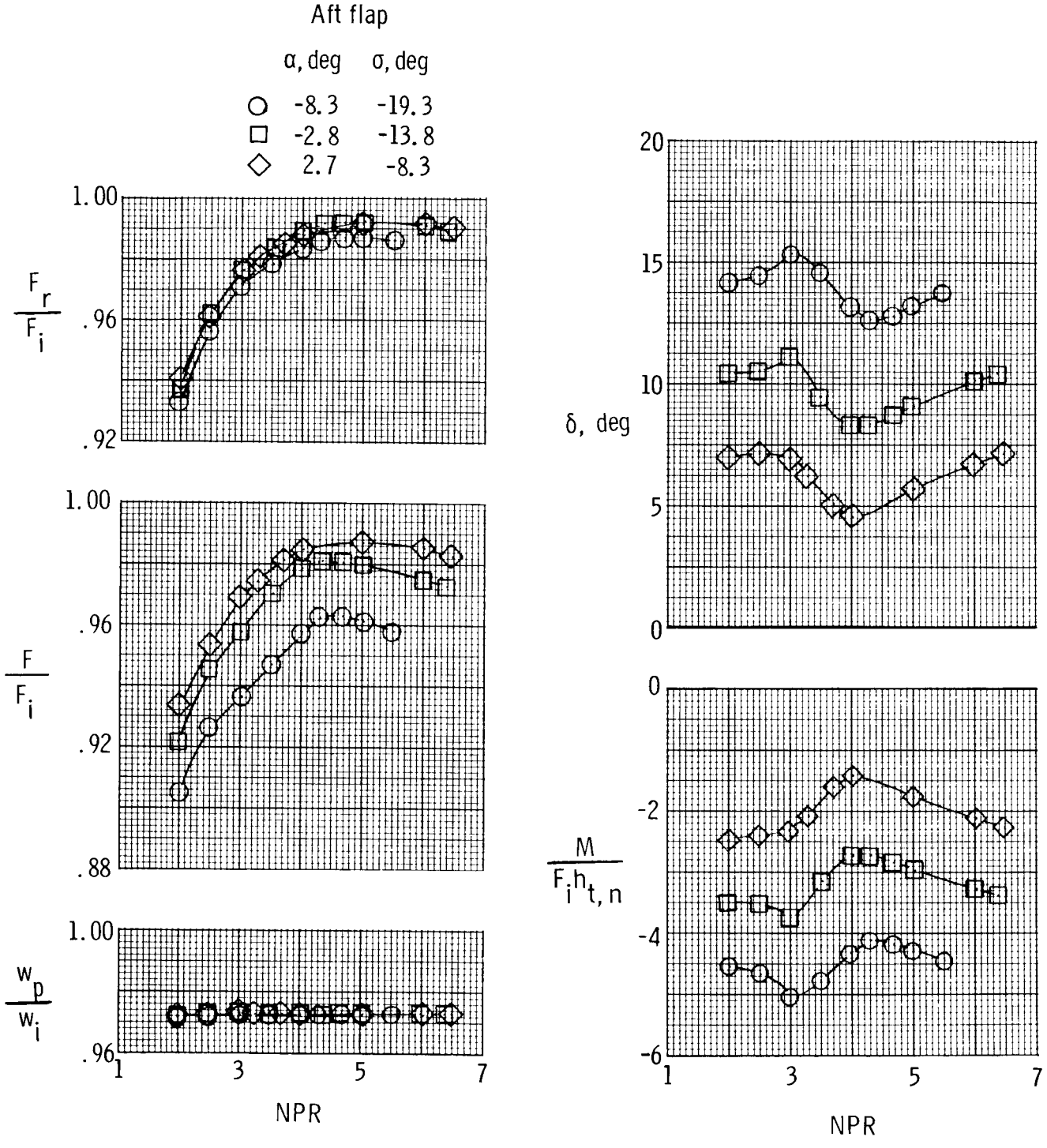

(b) Configuration A3CS, $\delta_v = 4.15°$.

Figure 14.- Concluded.

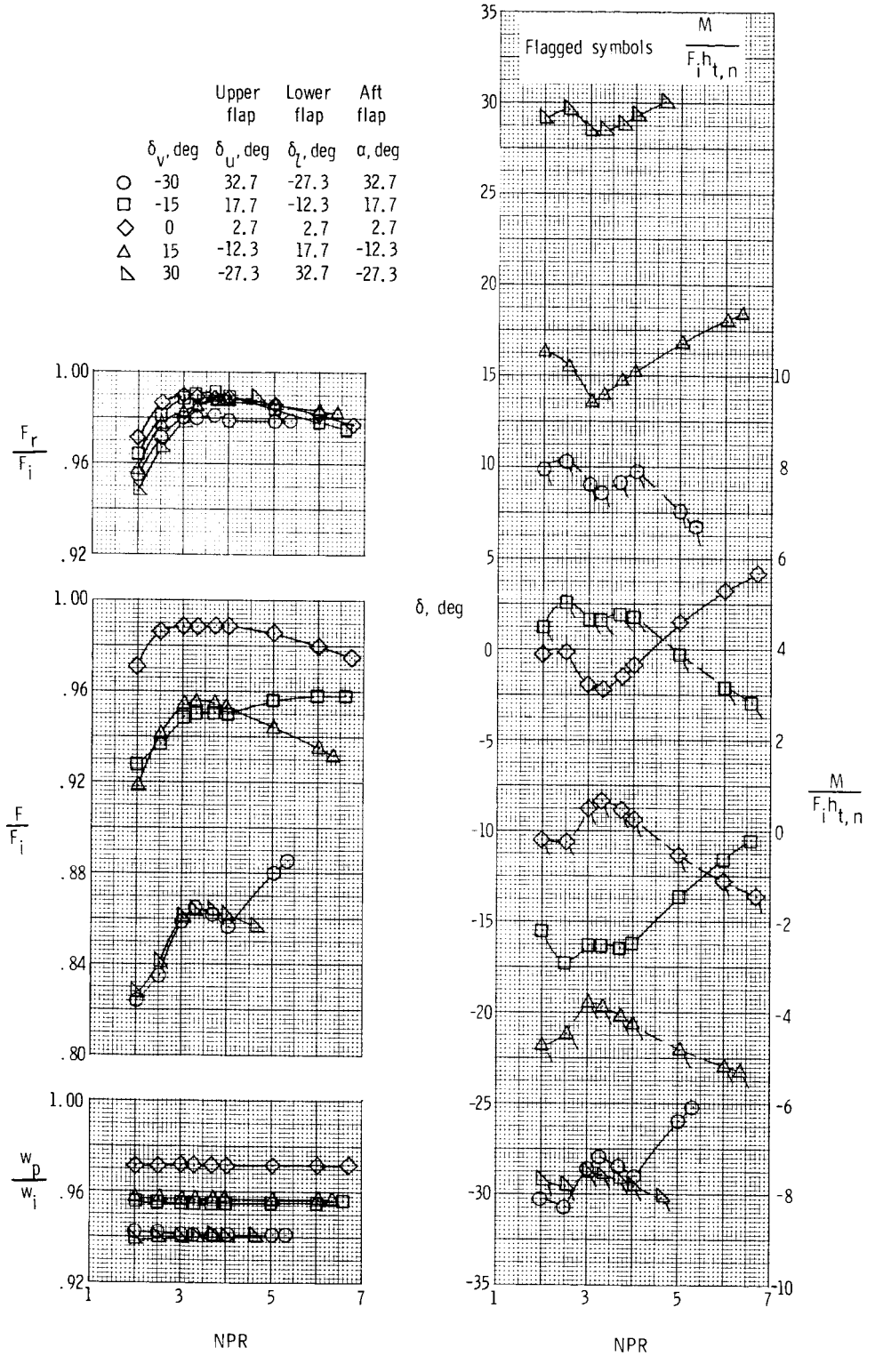

(a) Configuration A1FS.

Figure 15.- Variation of nozzle performance parameters with nozzle pressure ratio for three afterburning configurations at several geometric vector angles.

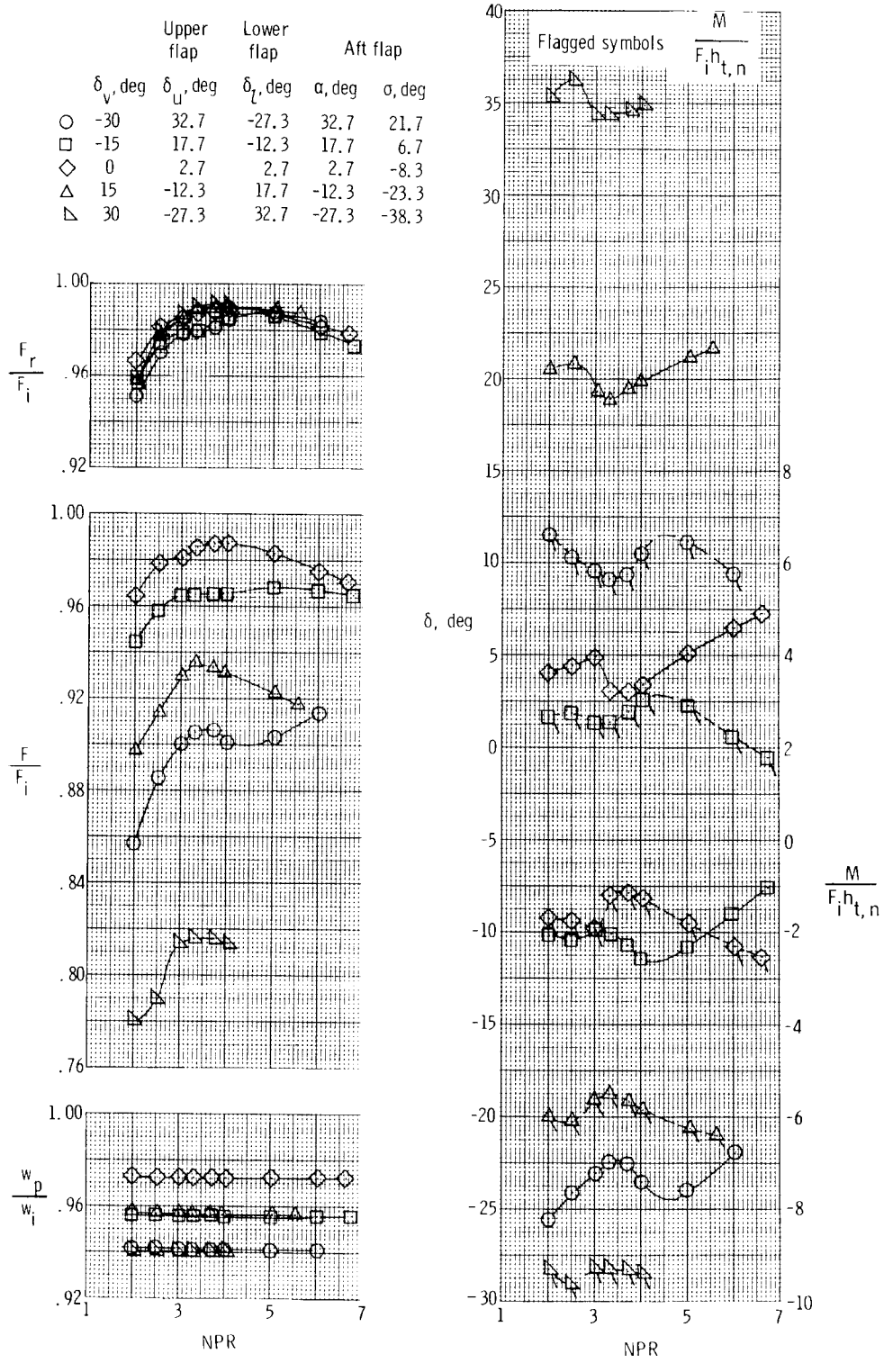

(b) Configuration A1CS.

Figure 15.- Continued.

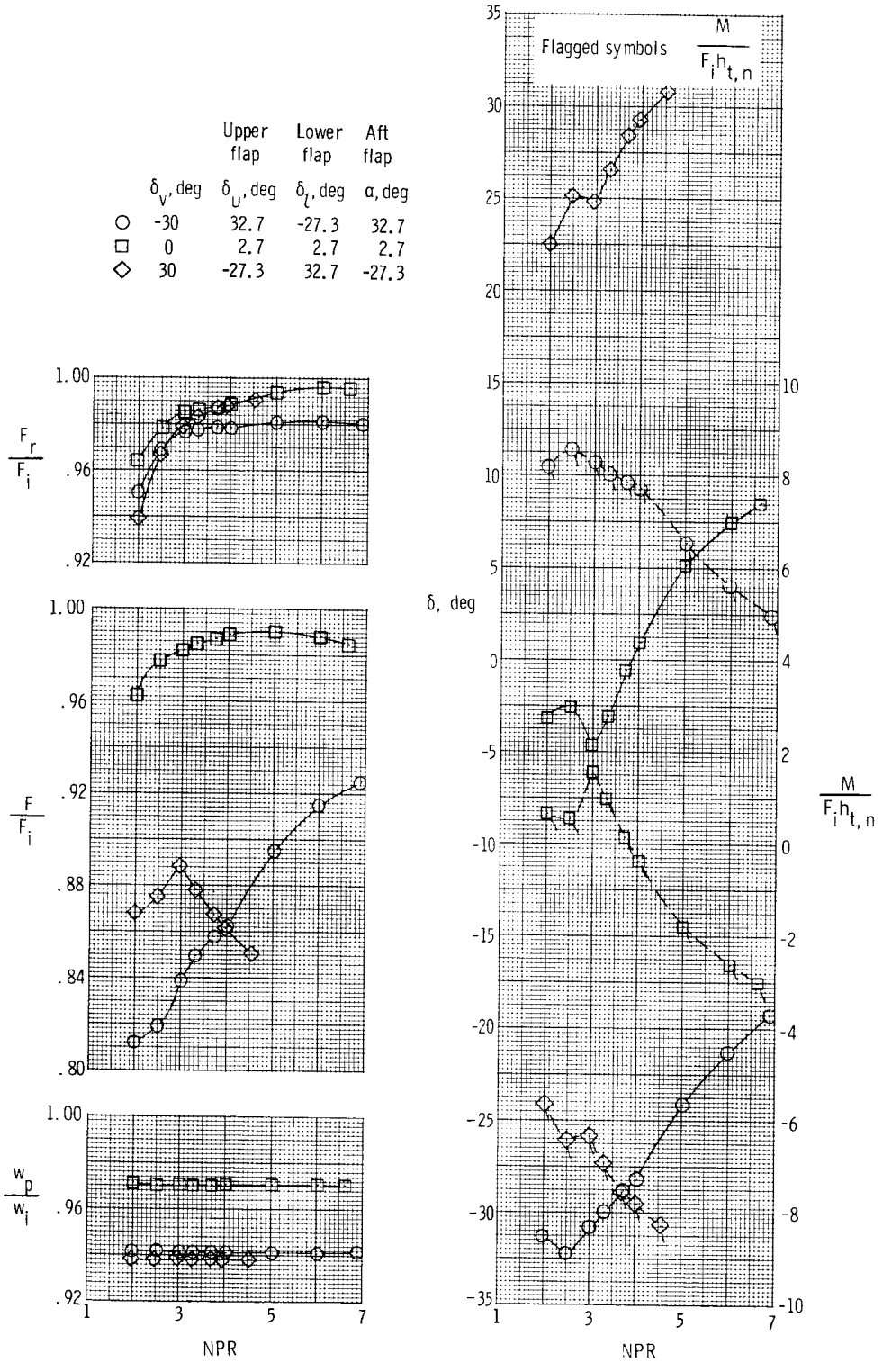

(c) Configuration A1FL.

Figure 15.- Concluded.

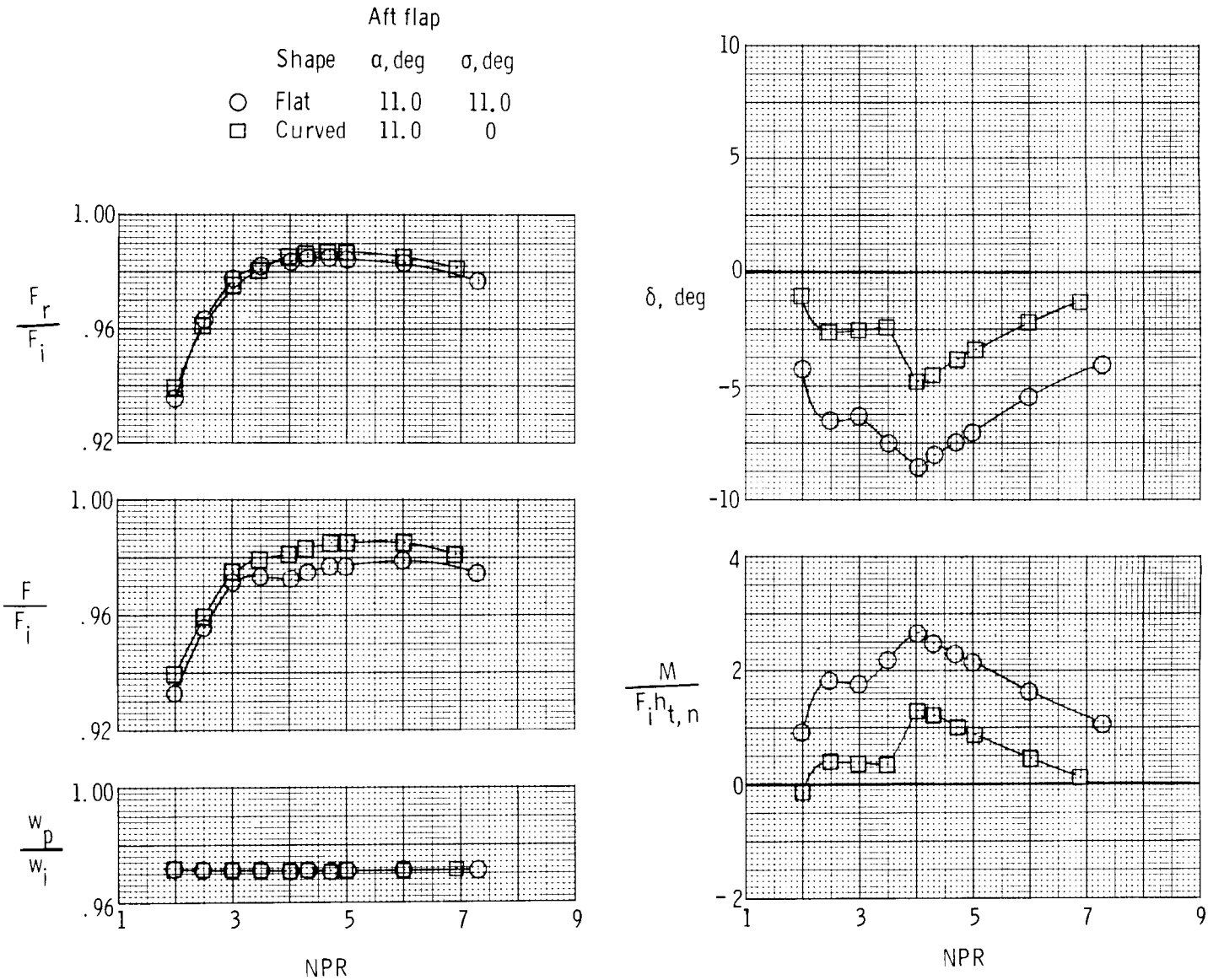

Figure 16.- Variation of nozzle performance parameters with nozzle pressure ratio for afterburning configurations with flat (configuration A3FS) and curved (configuration A3CS) aft flaps. δ_v = -4.15°.

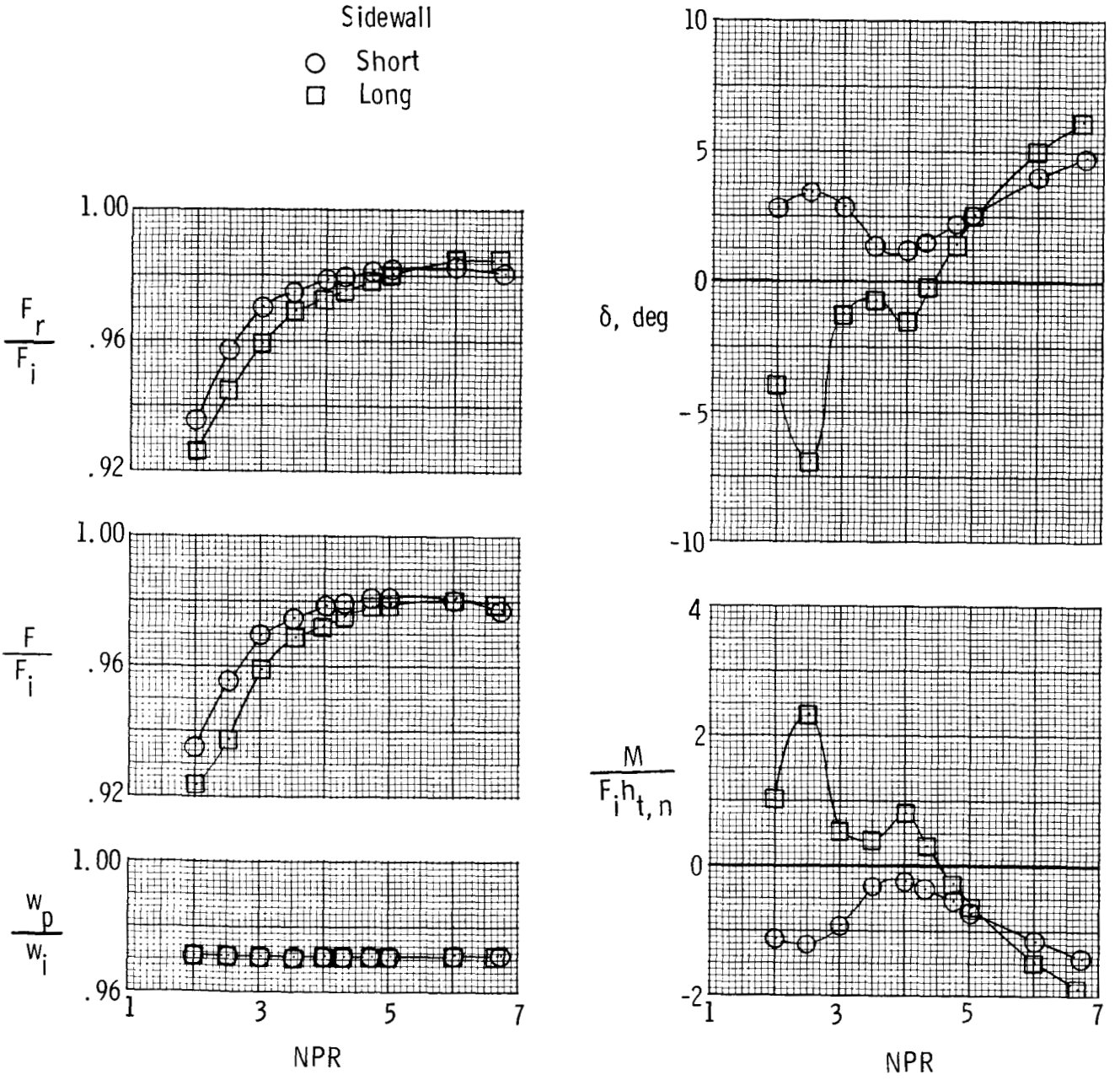

Figure 17.- Variation of nozzle performance parameters with nozzle pressure ratio for afterburning configurations with short (configuration A3FS) and long (configuration A3FL) sidewalls. $\delta_v = 4.15°$ and $\alpha = 2.7°$.

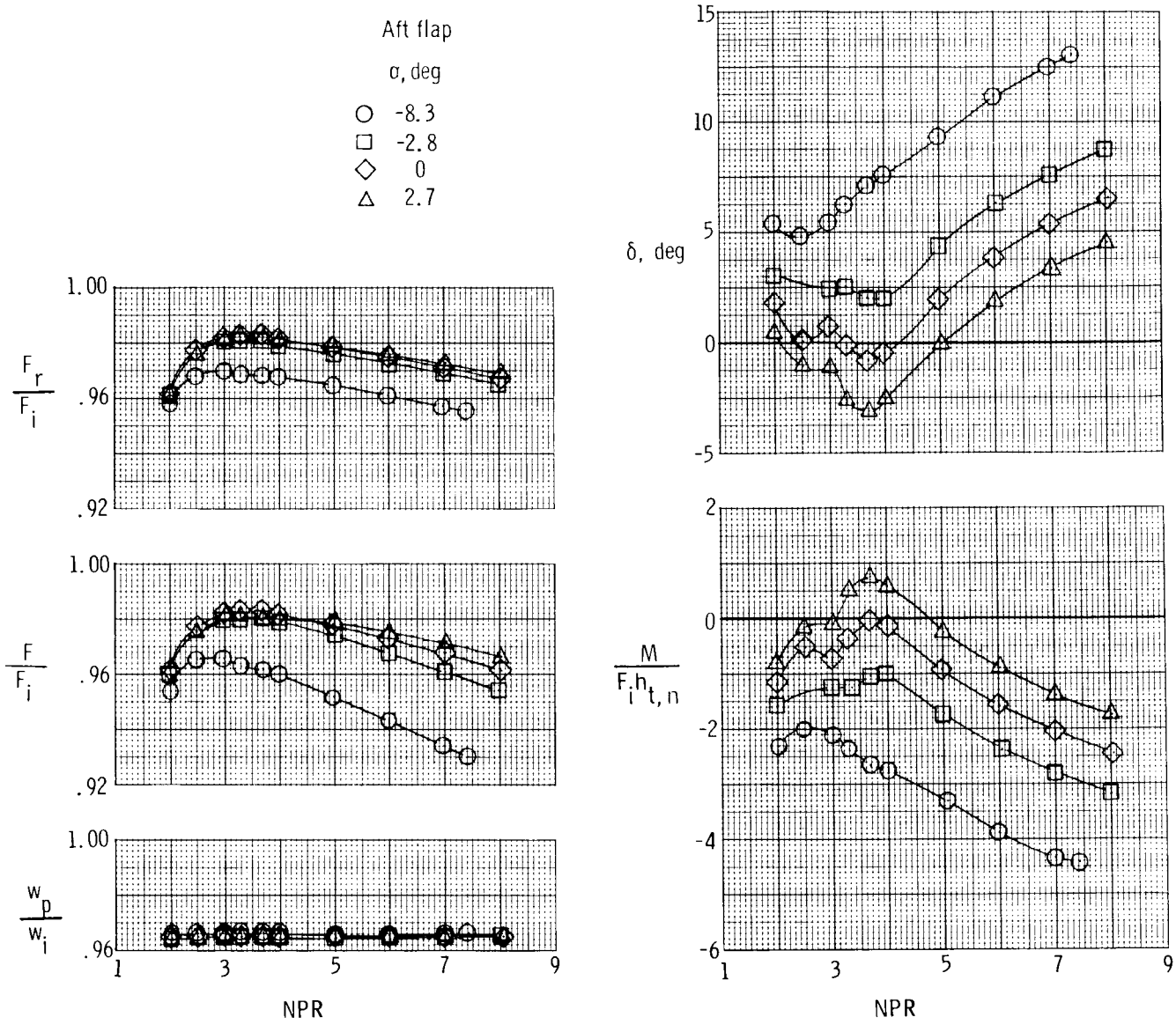

(a) Configuration P1FS, $\delta_v = -0.60°$.

Figure 18.- Variation of nozzle performance parameters with nozzle pressure ratio for two partial afterburning configurations for several aft flap (flat) angles.

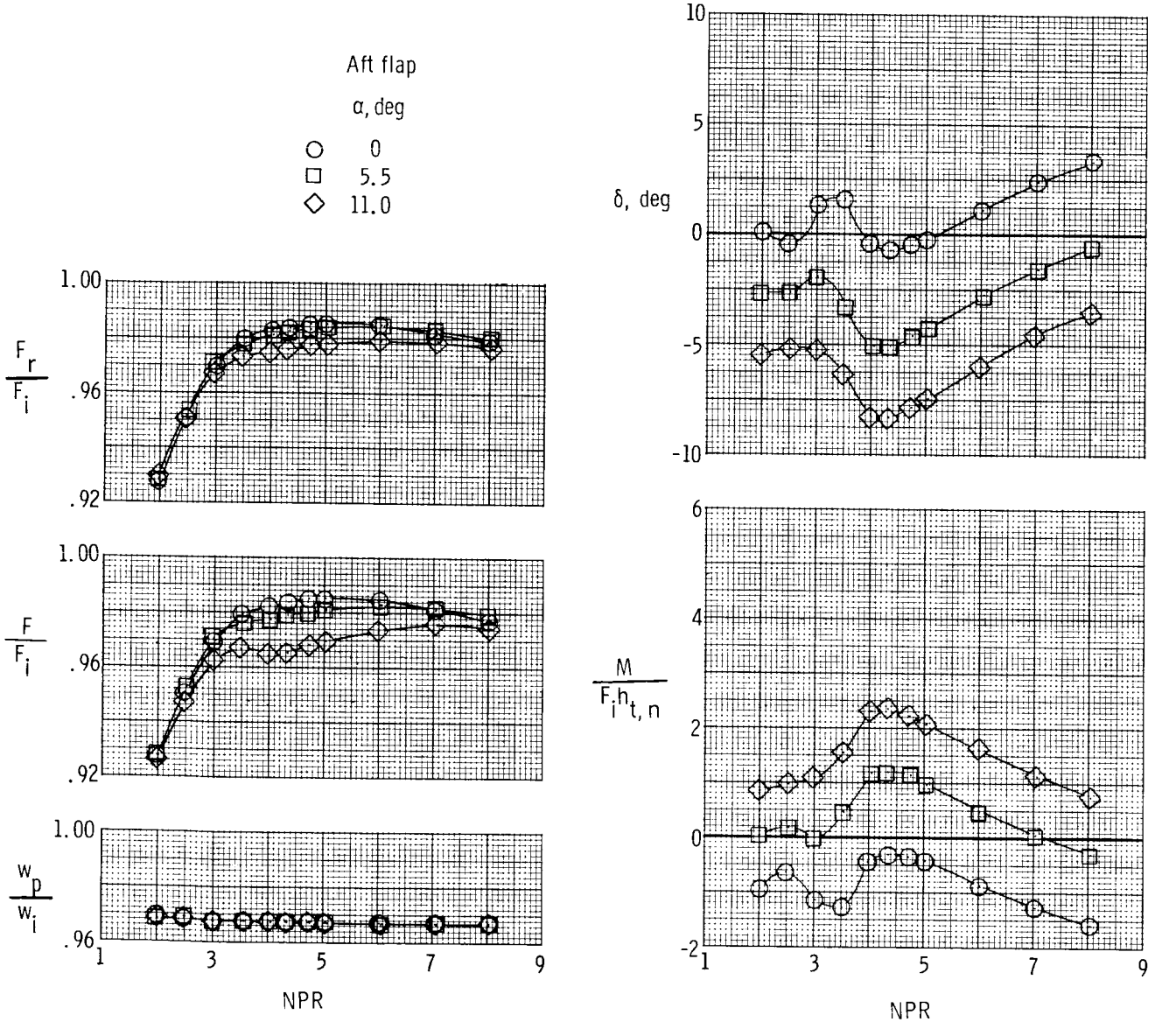

(b) Configuration P2FS, $\delta_v = -4.75°$.

Figure 18.- Concluded.

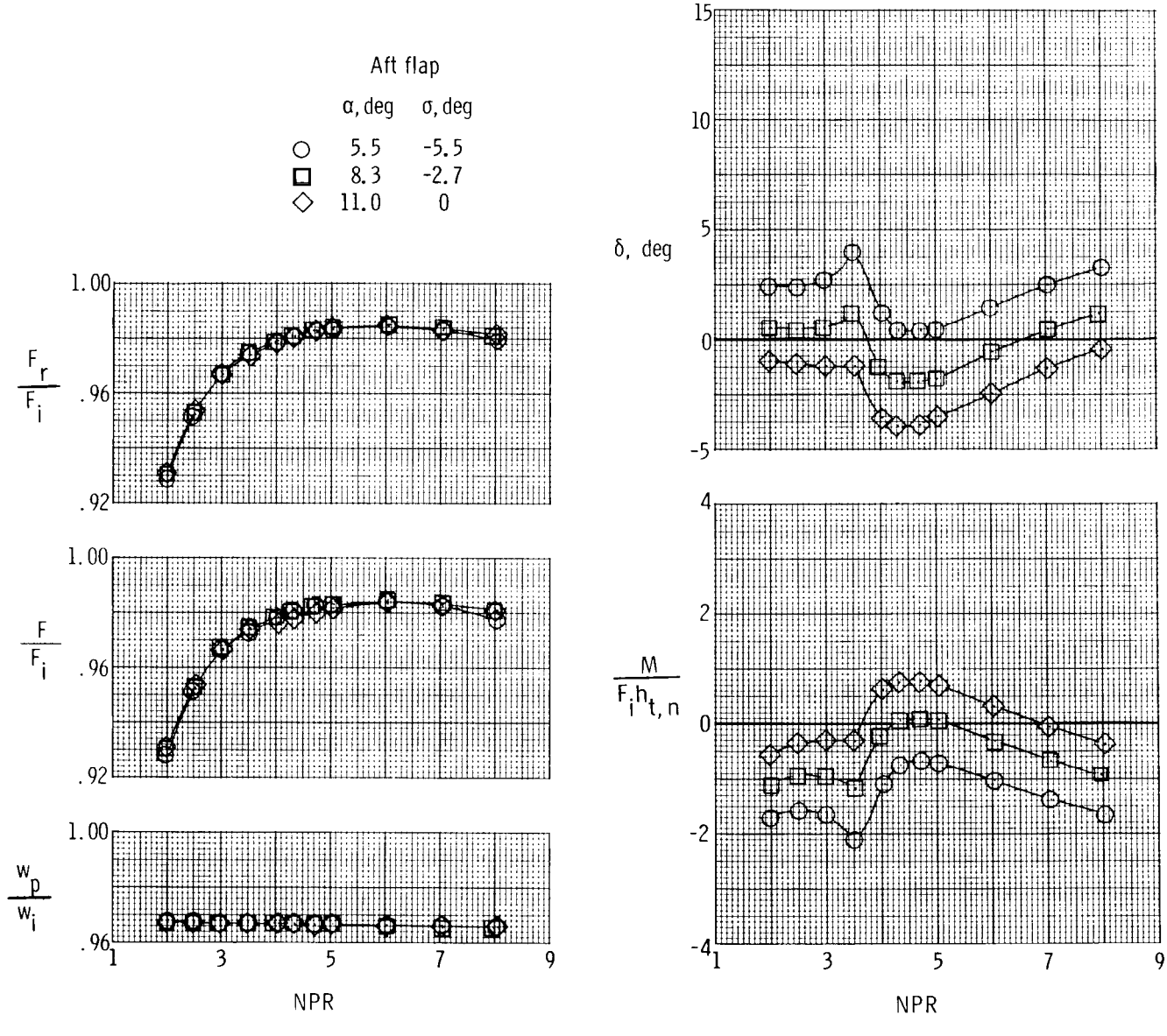

Figure 19.- Variation of nozzle performance parameters with nozzle pressure ratio for partial afterburning configuration P2CS for several aft flap (curved) angles.

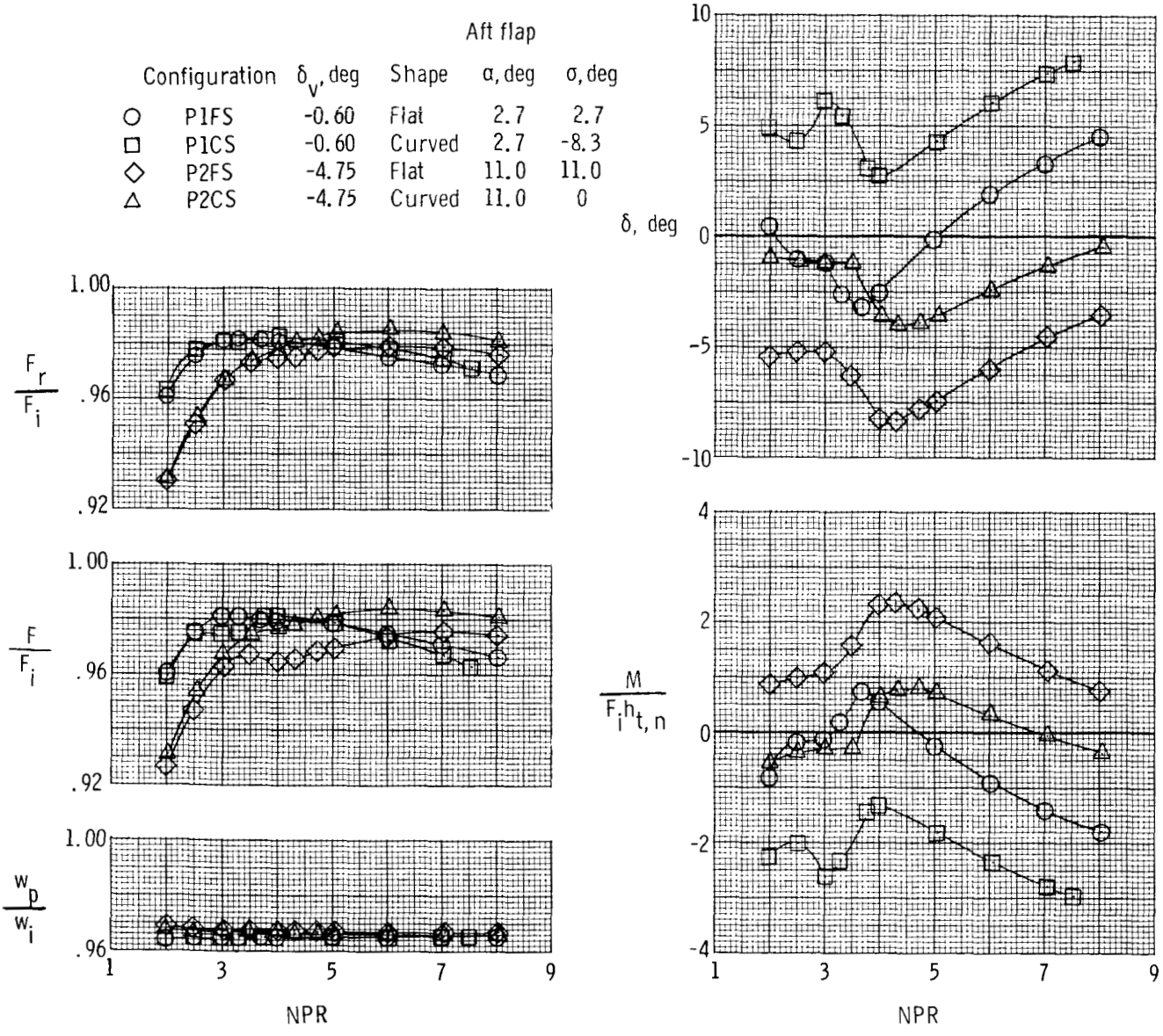

Figure 20.- Variation of nozzle performance parameters with nozzle pressure ratio for partial afterburning configurations with flat and curved aft flaps.

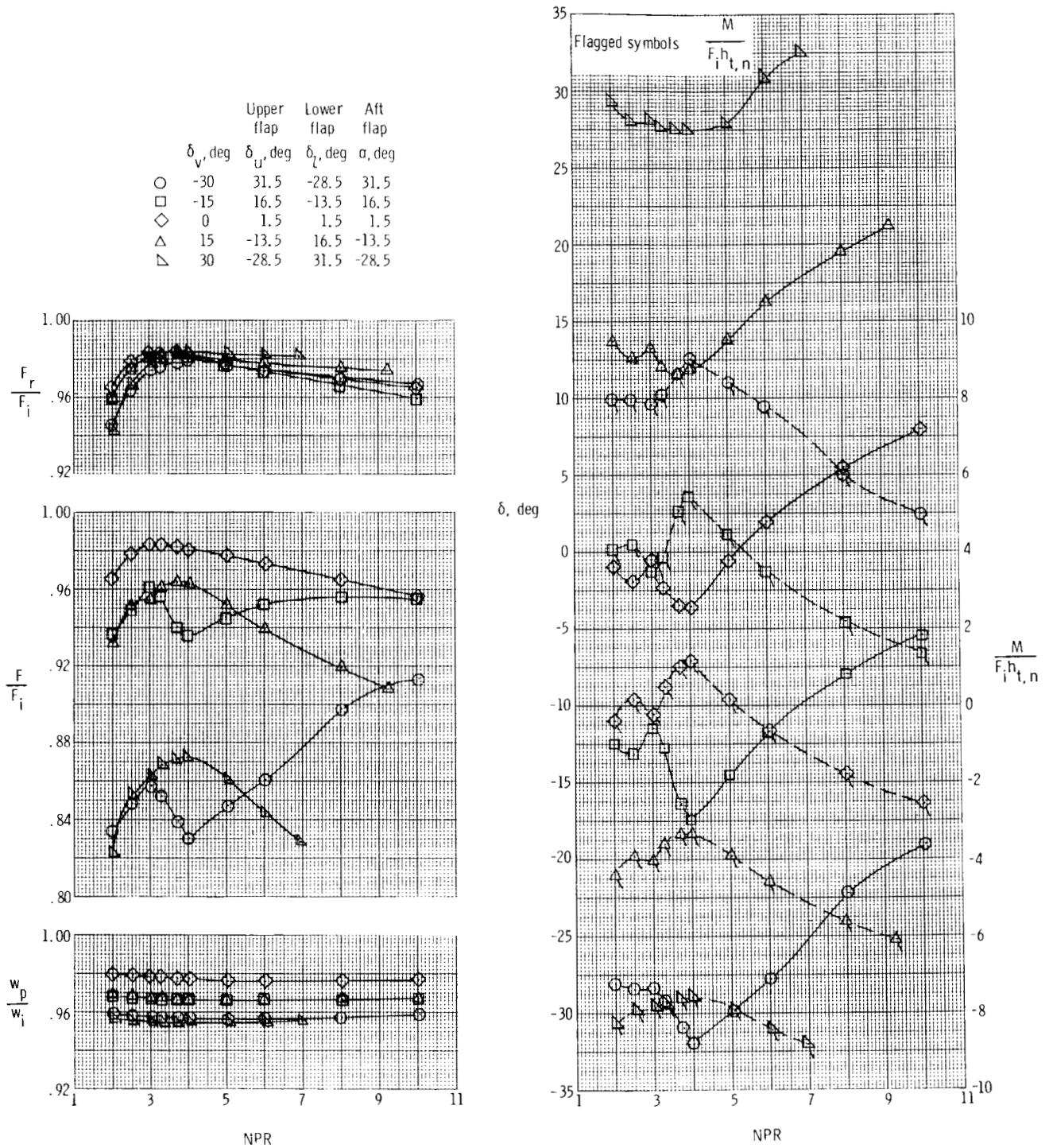

(a) Configuration D1FS.

Figure 21.- Variation of nozzle performance parameters with nozzle pressure ratio for three dry power configurations at several geometric vector angles.

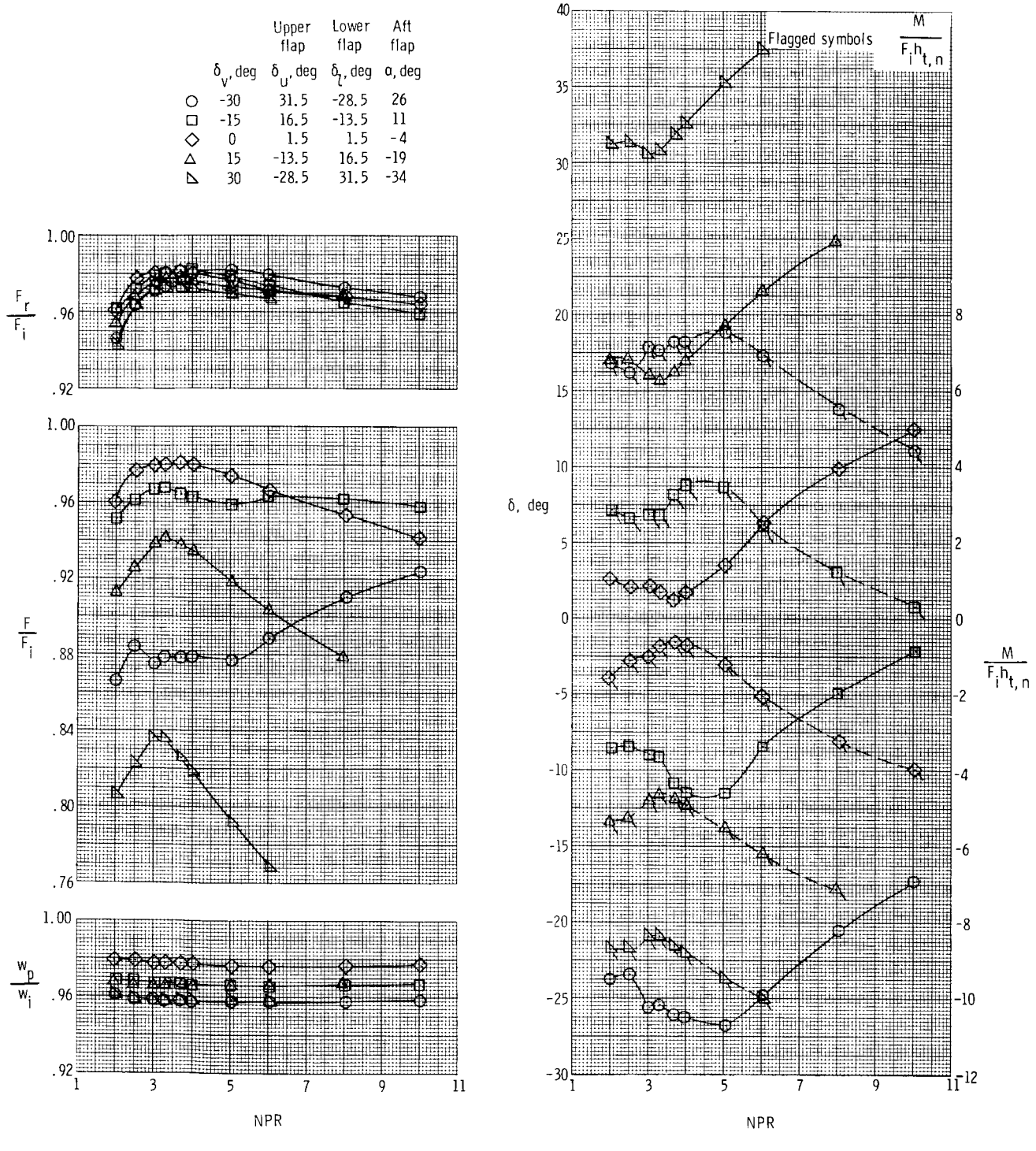

(a) Concluded.

Figure 21.- Continued.

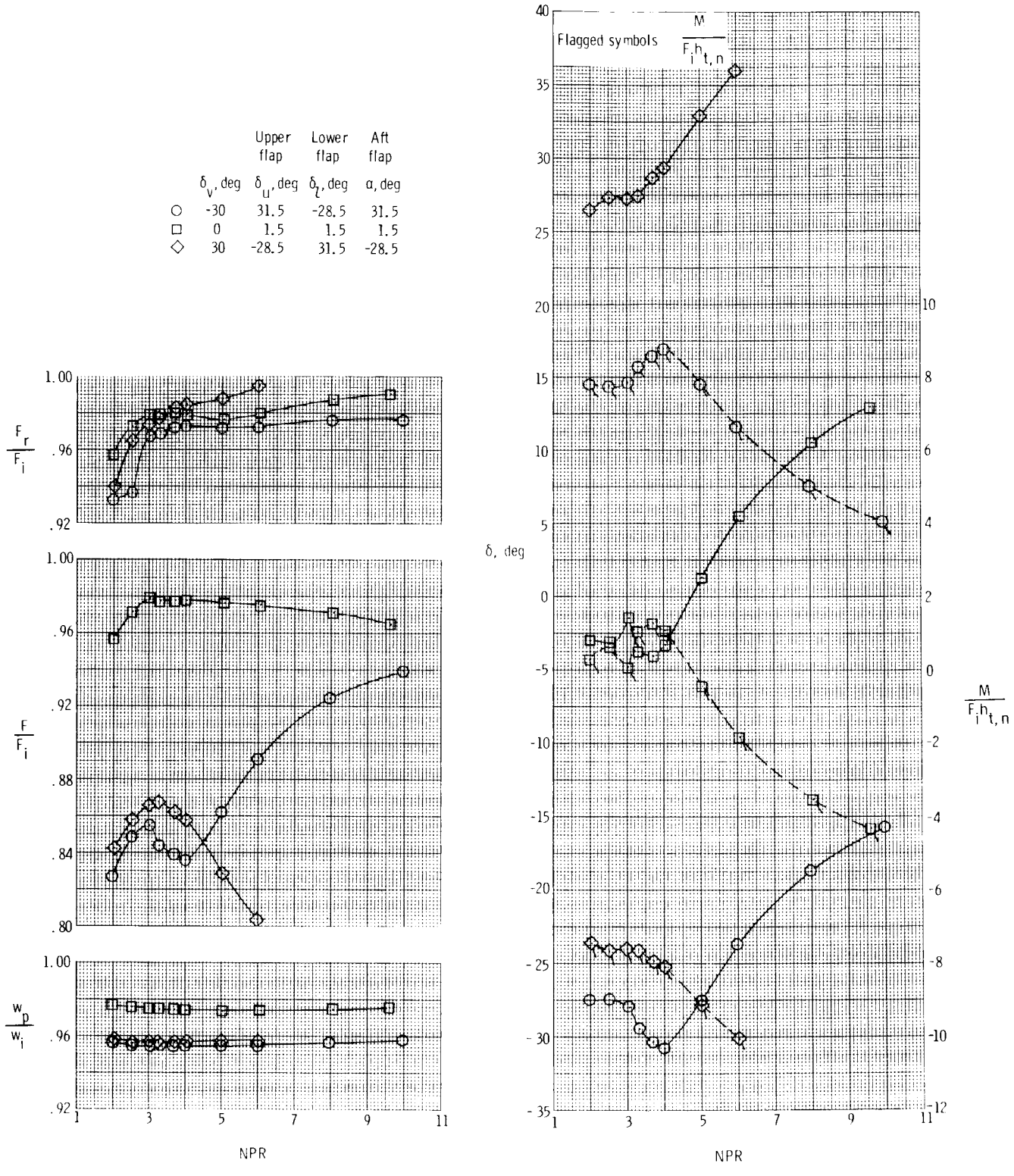

(b) Configuration D1FL.

Figure 21.- Concluded.

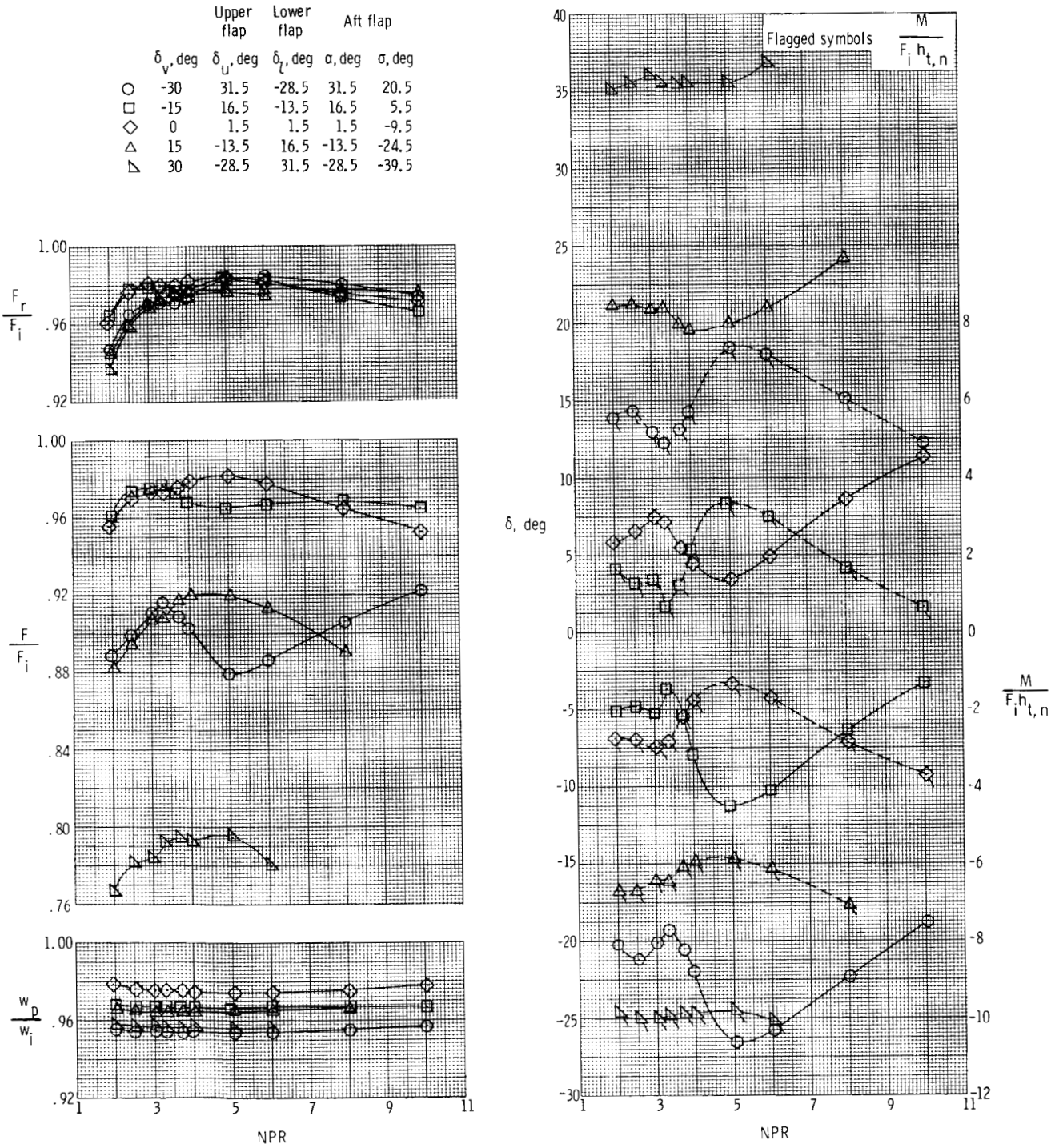

Figure 22.- Variation of nozzle performance parameters with nozzle pressure ratio for configuration D1CS at five geometric vector angles.

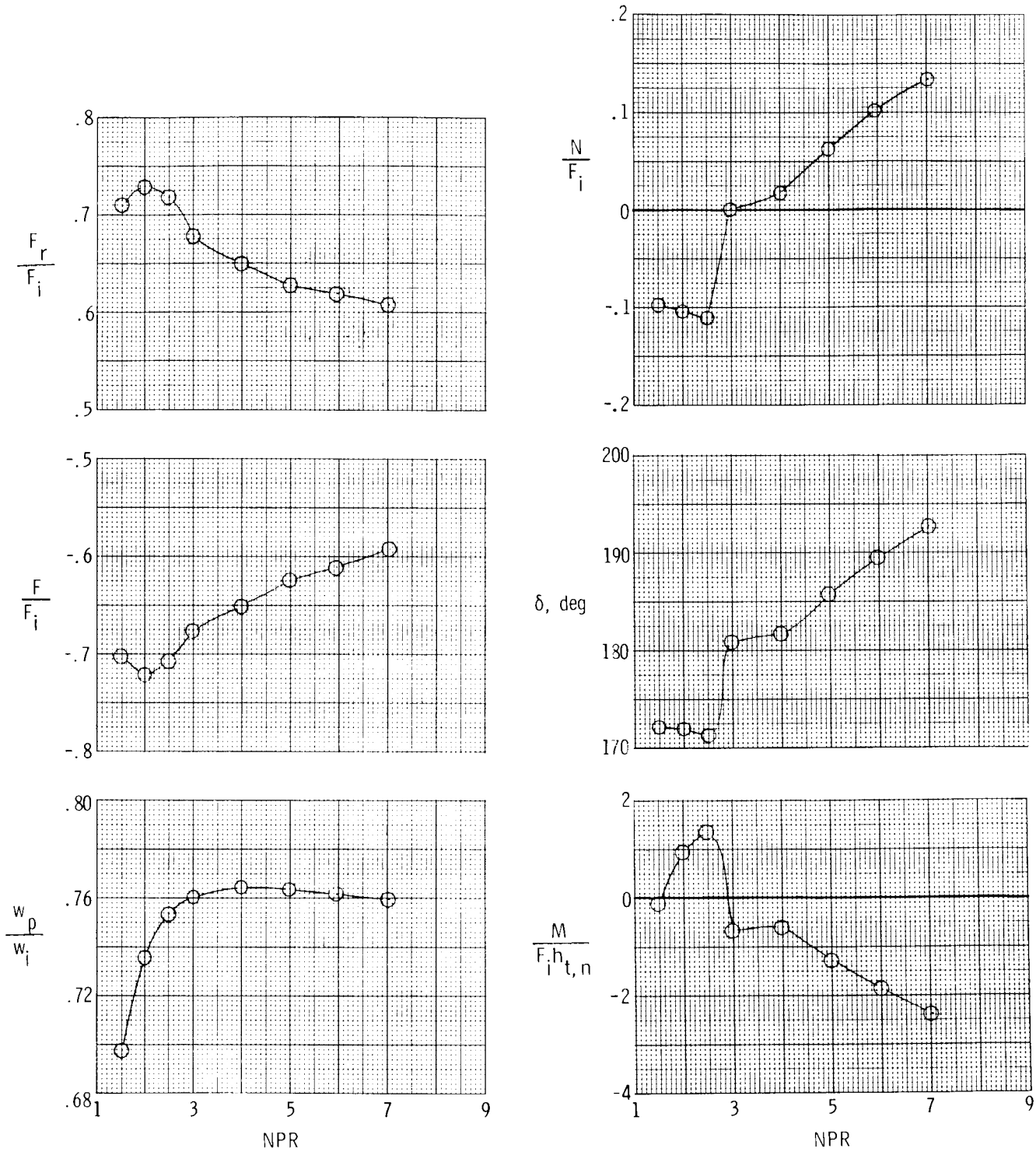

Figure 23.- Variation of nozzle performance parameters with nozzle pressure ratio for dry power thrust-reverser configuration.

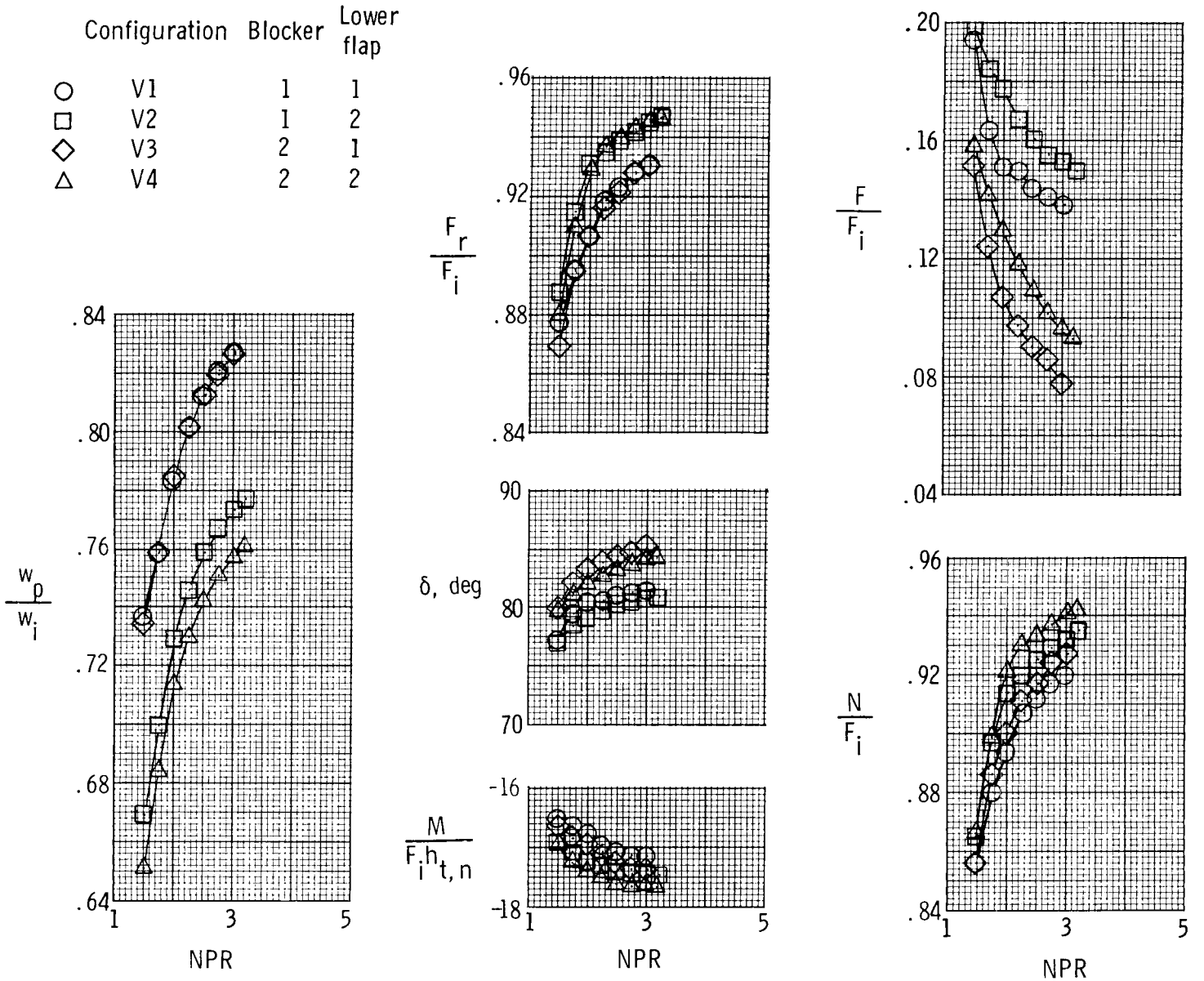

Figure 24.- Variation of nozzle performance parameters with nozzle pressure ratio for four vertical takeoff or landing configurations.

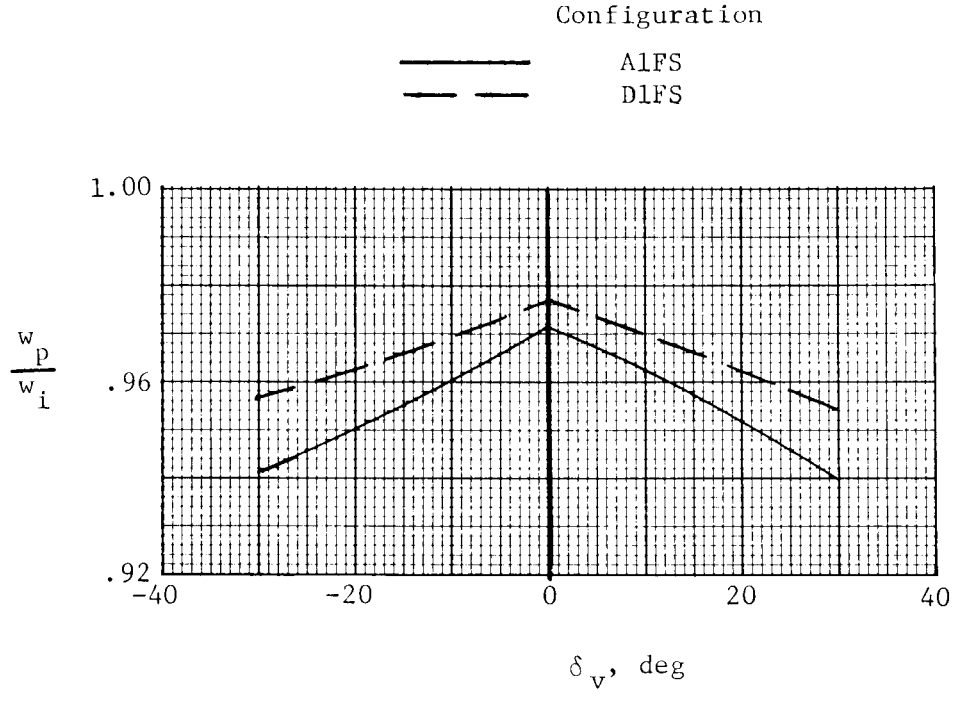

Figure 25.- Effect of nozzle geometric vector angle on discharge coefficient for afterburning and dry power nozzle configurations at nozzle pressure ratio of 4.0.

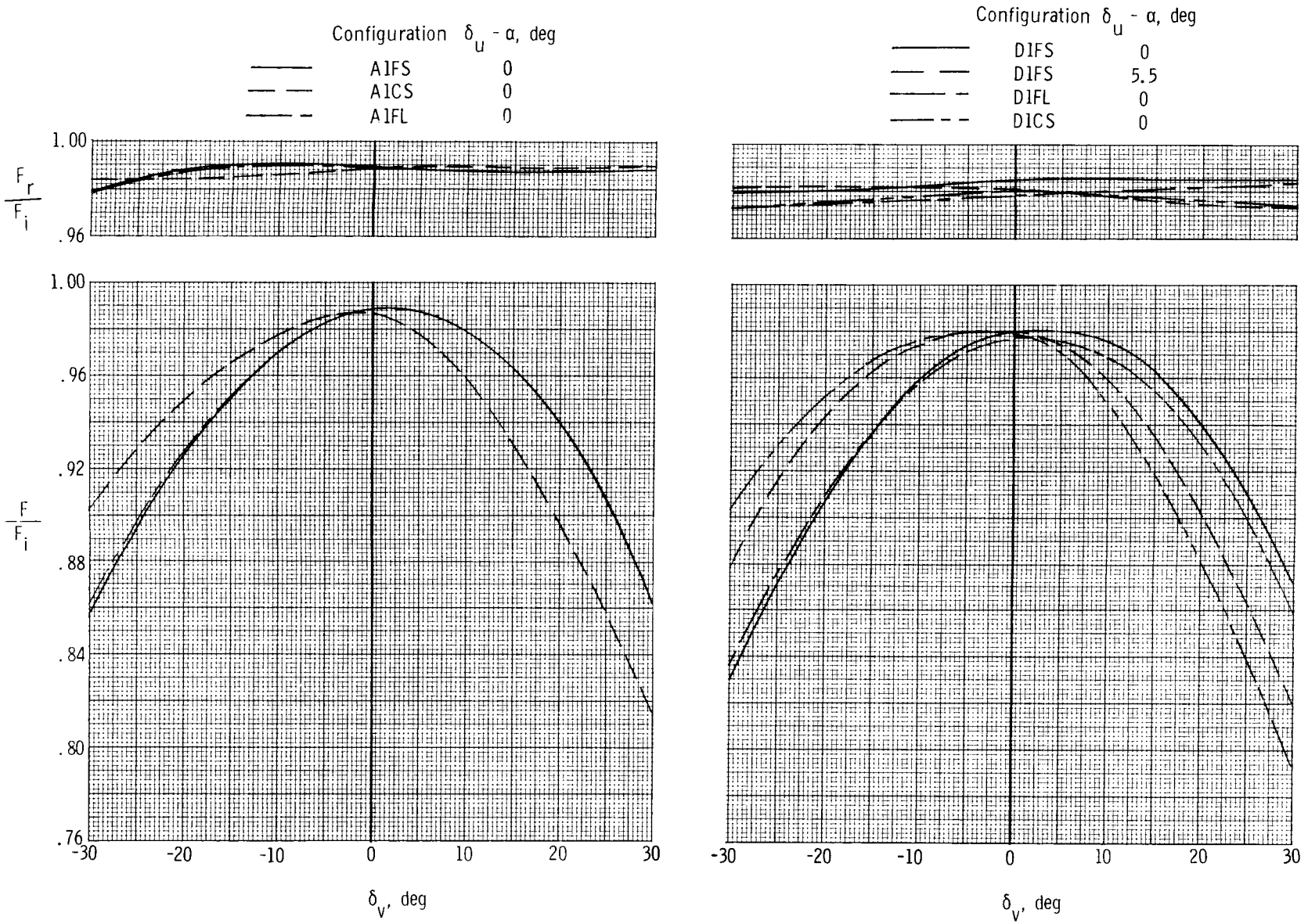

(a) F_r/F_i and F/F_i.

Figure 26.- Variation of internal performance parameters with nozzle geometric vector angle for afterburning and dry power nozzles at nozzle pressure ratio of 4.0.

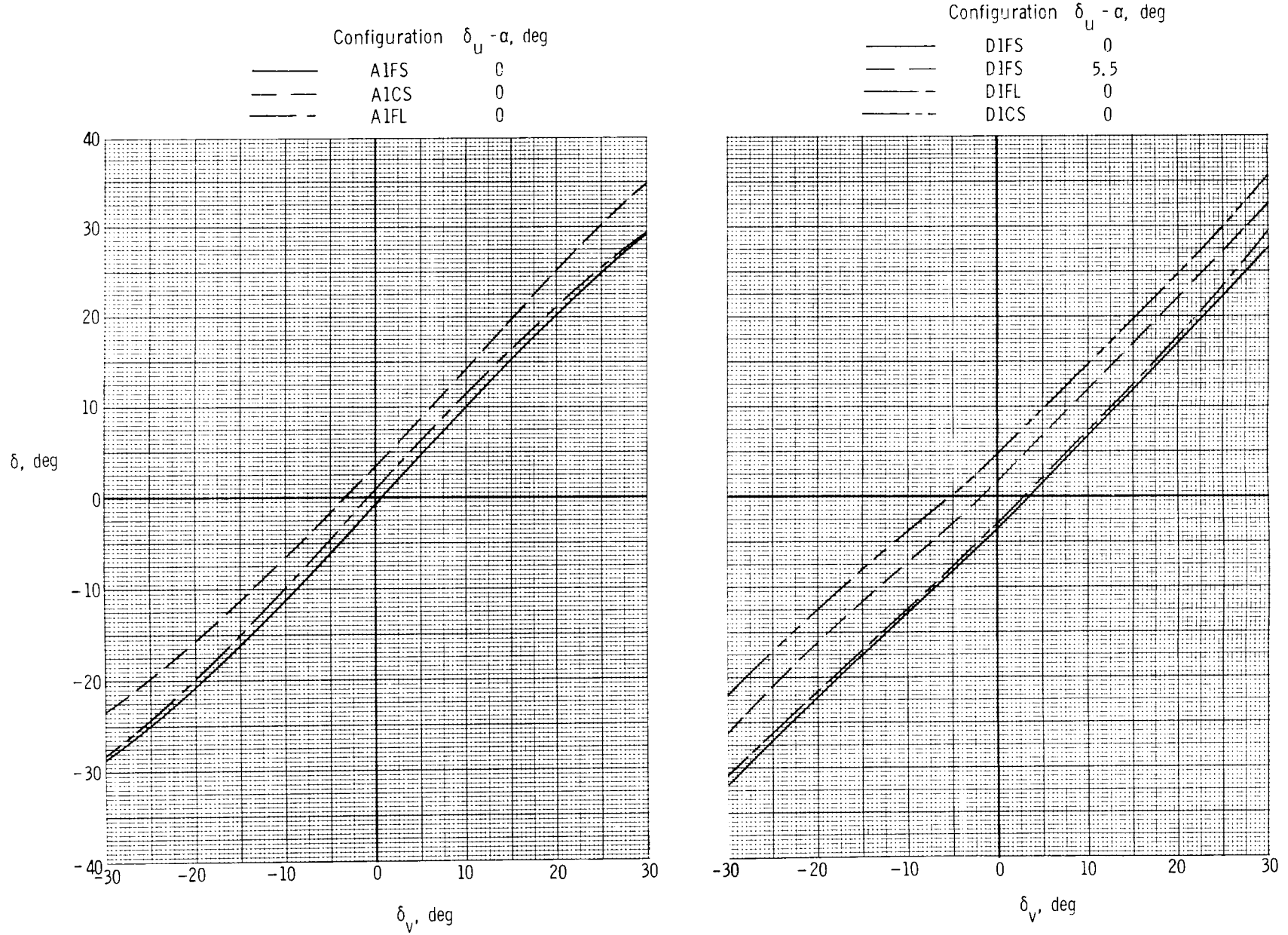

(b) δ.

Figure 26.- Continued.

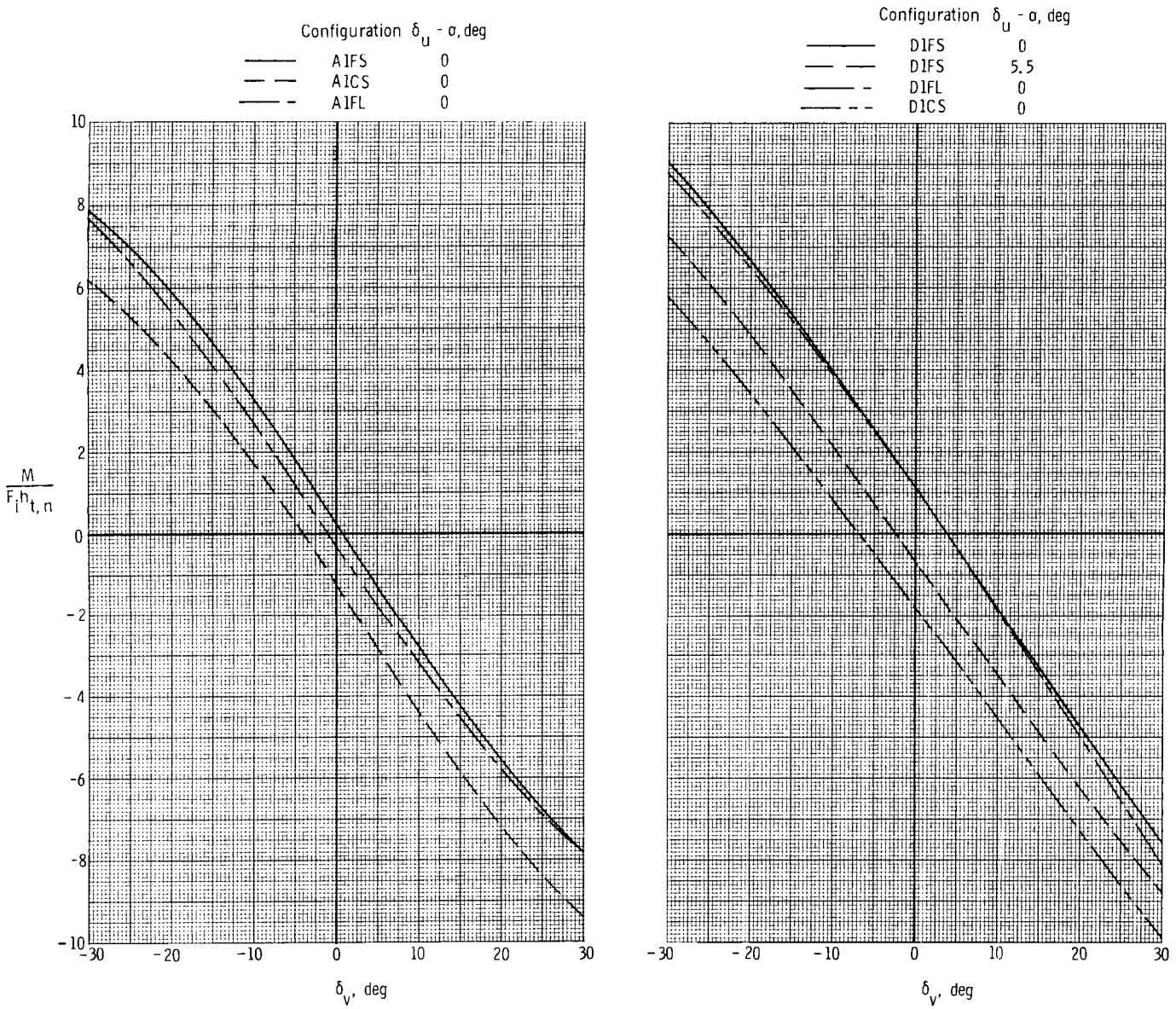

(c) $M/F_i h_{t,n}$.

Figure 26.- Concluded.

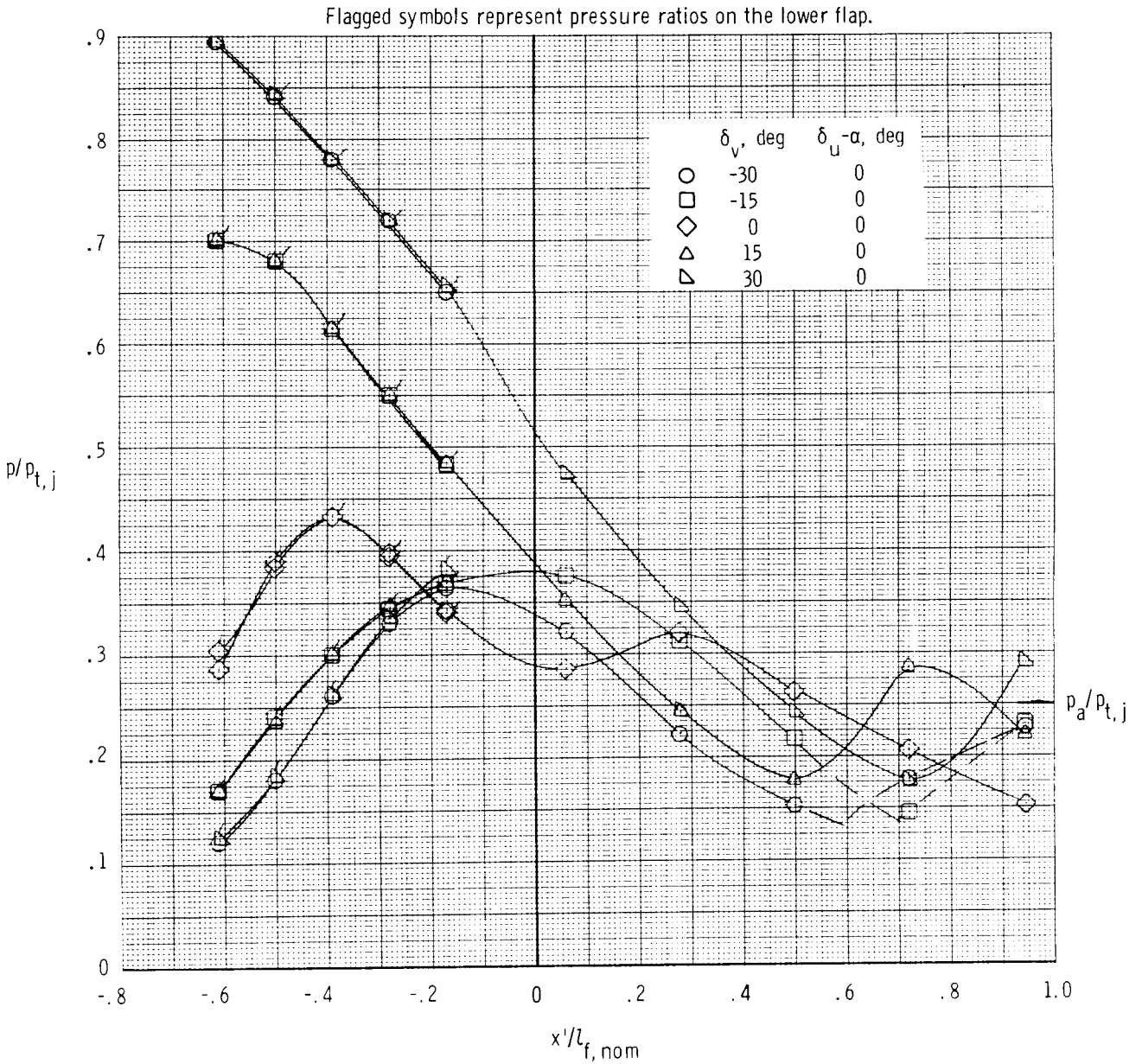

Figure 27.- Effect of nozzle geometric vector angle on internal static pressure distributions for afterburning nozzle configuration A1FS at nozzle pressure ratio of 4.0.

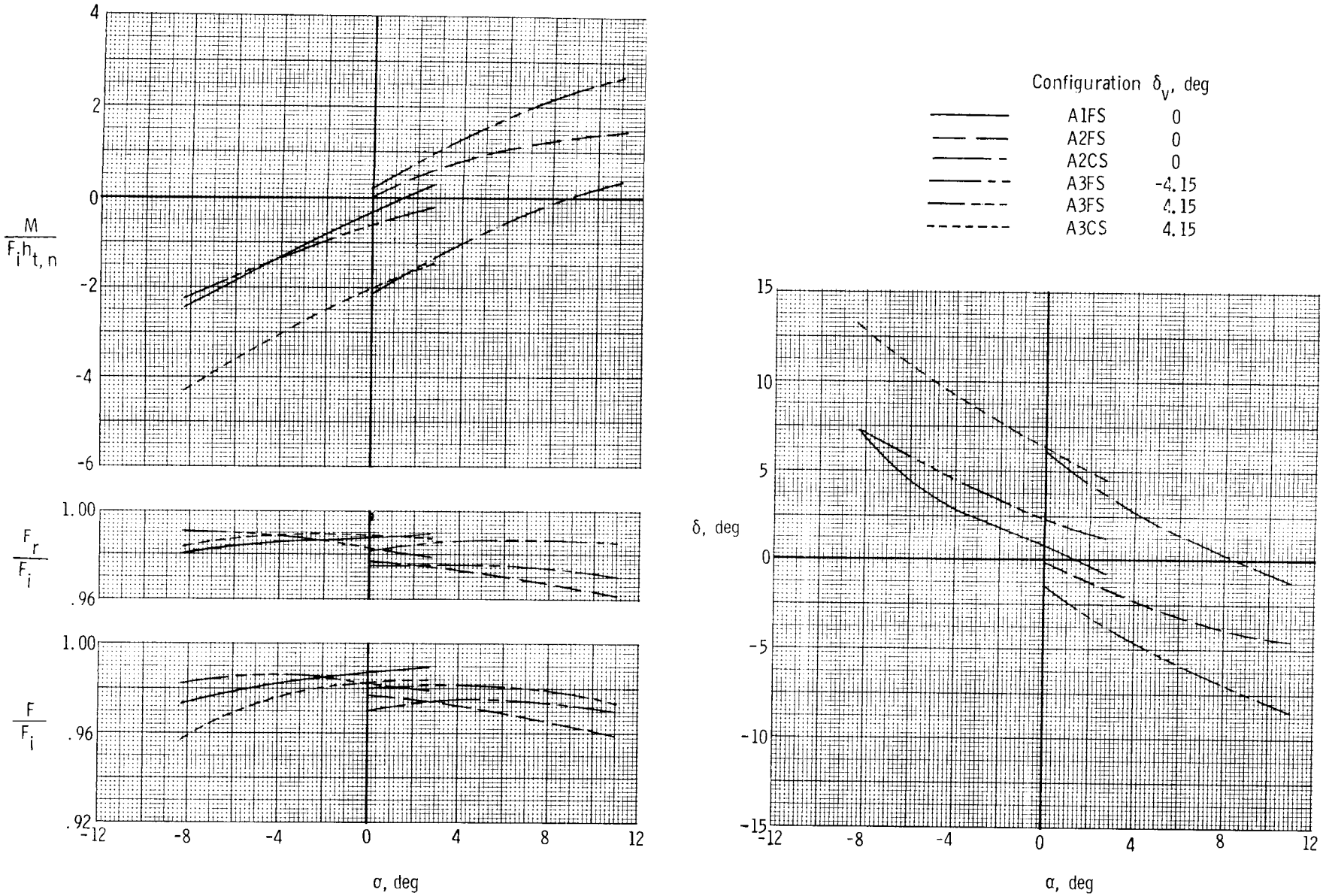

Figure 28.- Variation of internal performance parameters with aft flap initial angle for afterburning power nozzles at nozzle pressure ratio of 4.0.

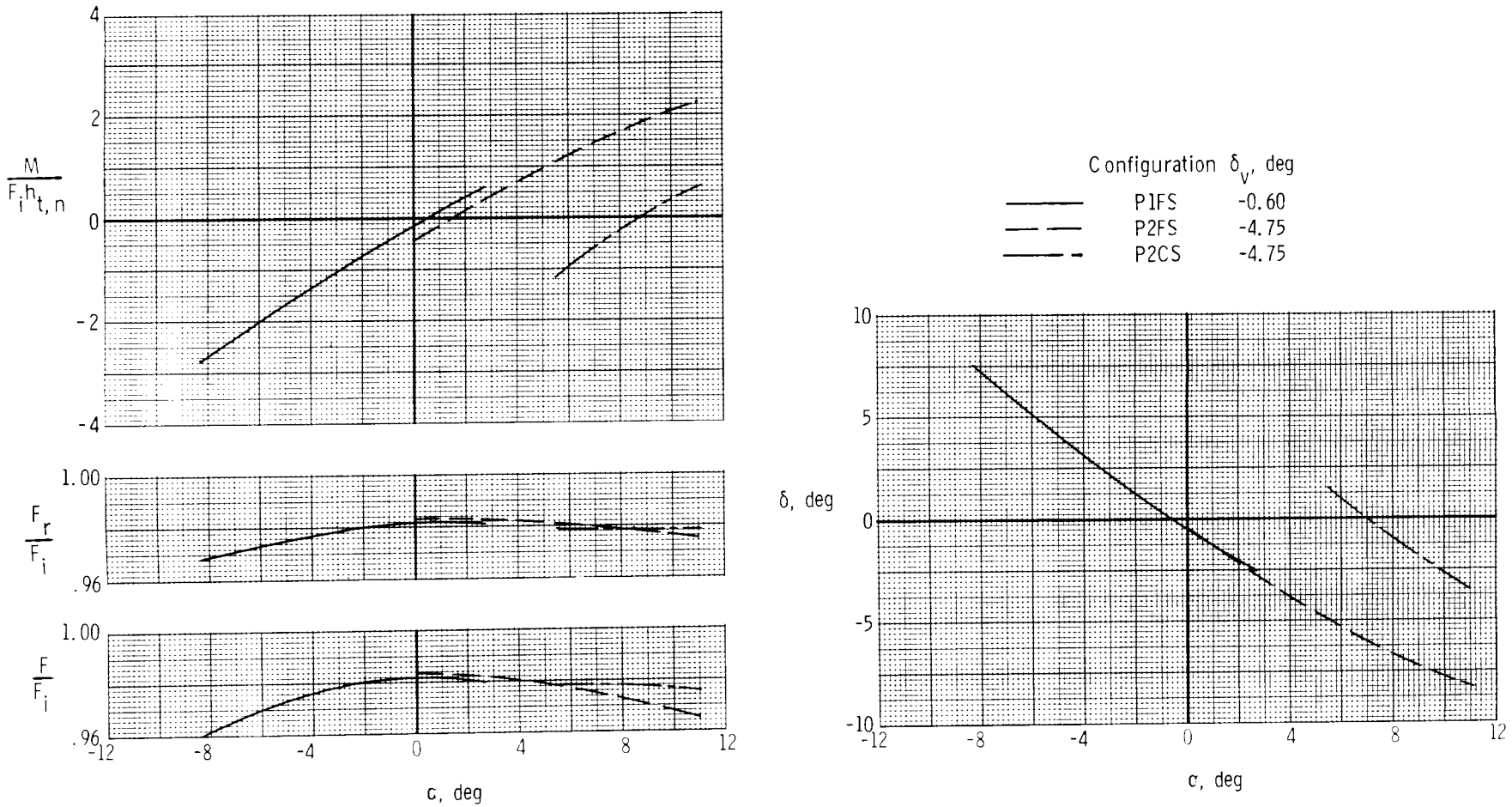

Figure 29.- Variation of internal performance parameters with aft flap initial angle for partial afterburning power nozzles at nozzle pressure ratio of 4.0.

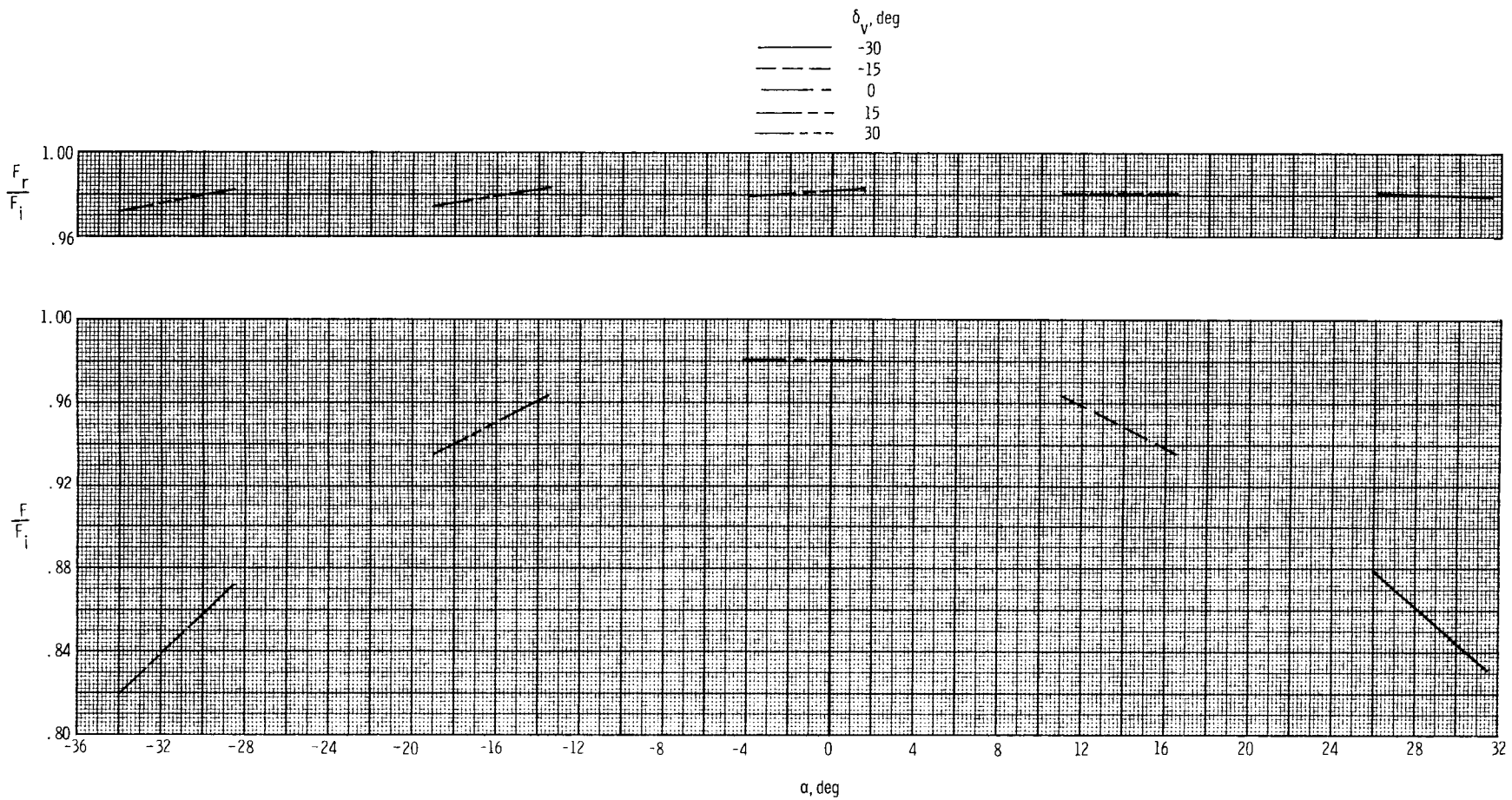

(a) F_r/F_i and F/F_i.

Figure 30.- Variation of internal performance parameters with aft flap initial angle for dry power nozzle configuration D1FS at nozzle pressure ratio of 4.0.

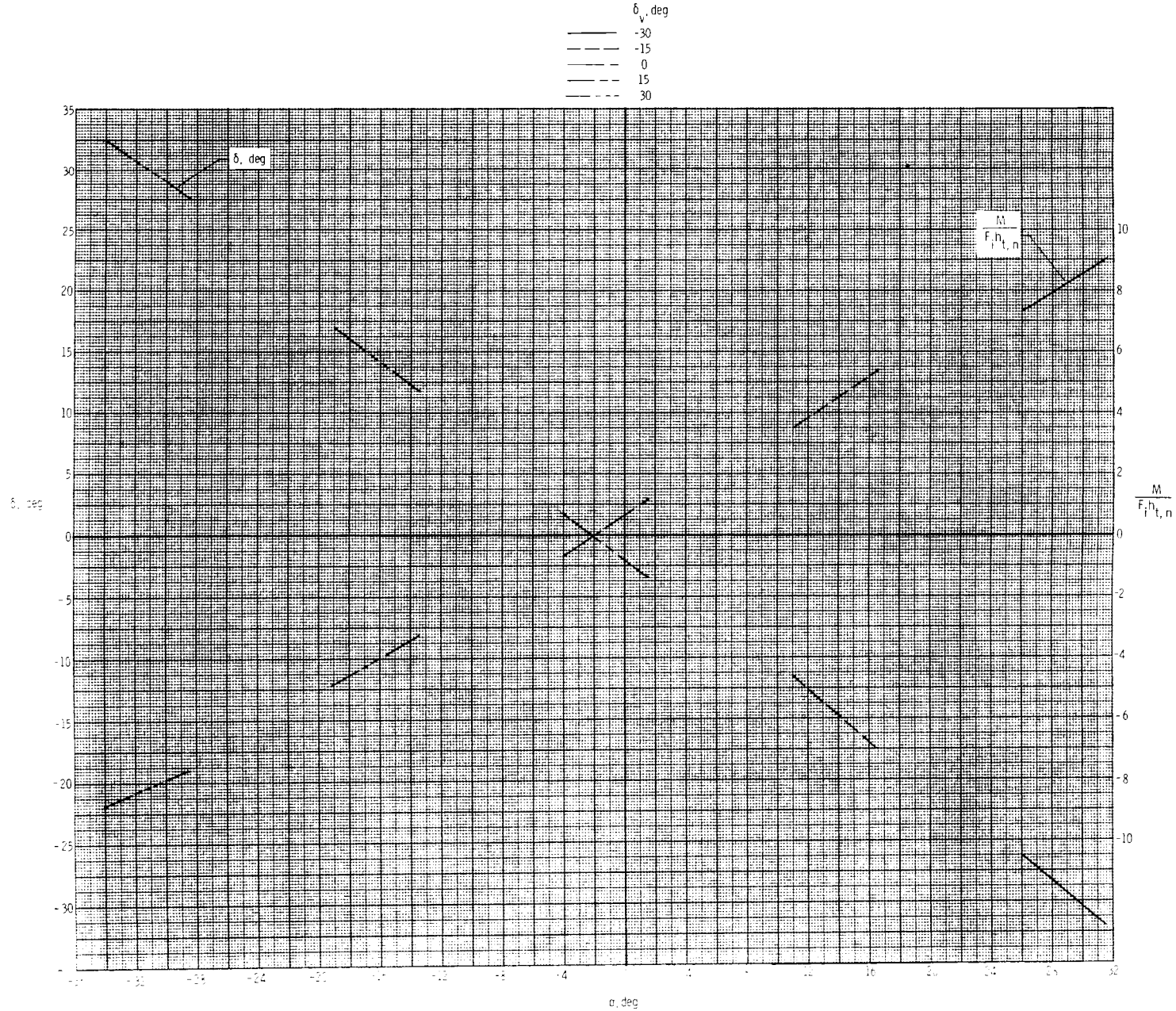

(b) δ and $M/F_i h_{t,n}$.

Figure 30.- Concluded.

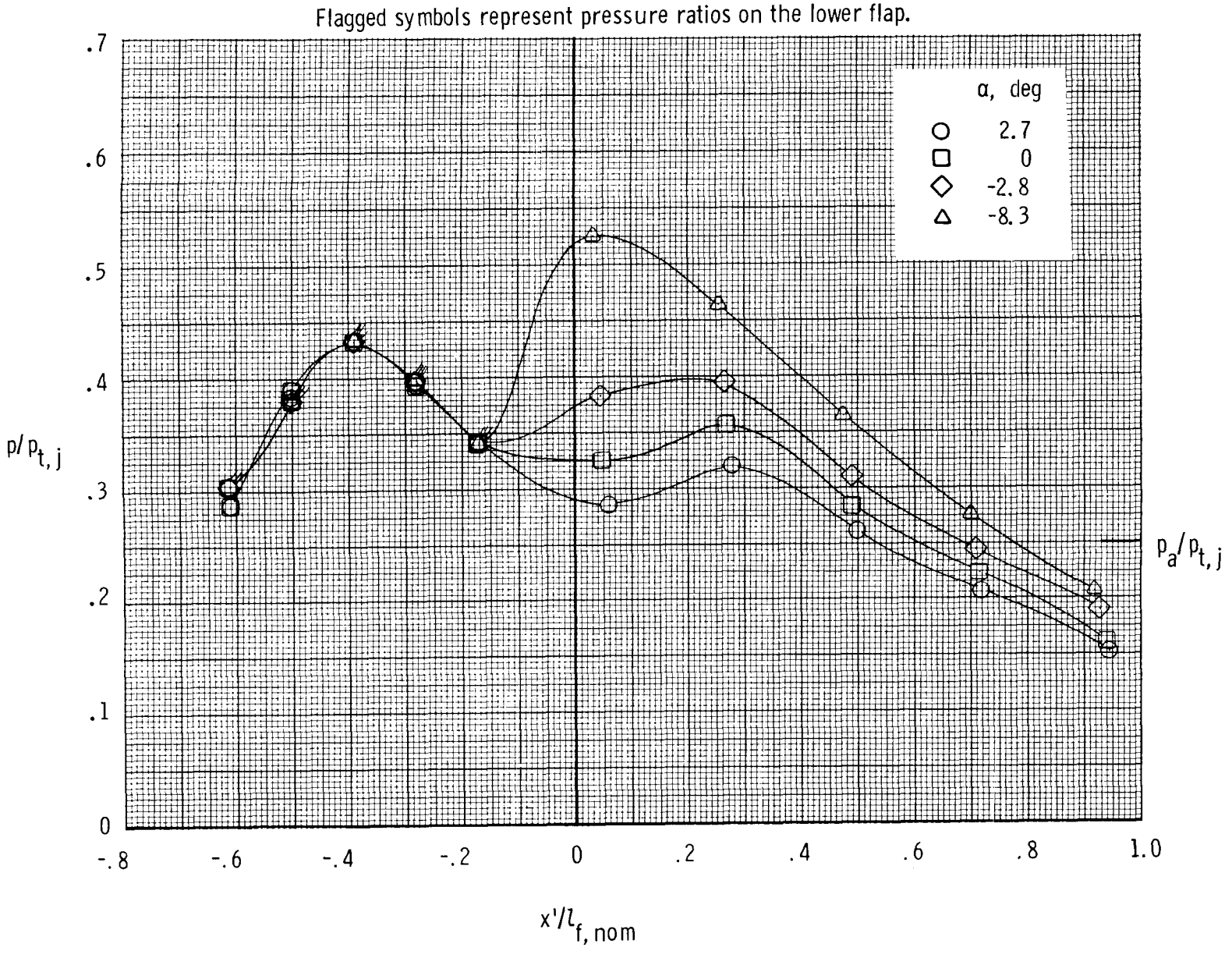

Figure 31.- Effect of aft flap initial angle on internal static pressure distributions for afterburning nozzle configuration A1FS, δ_v = 0°, at nozzle pressure ratio of 4.0.

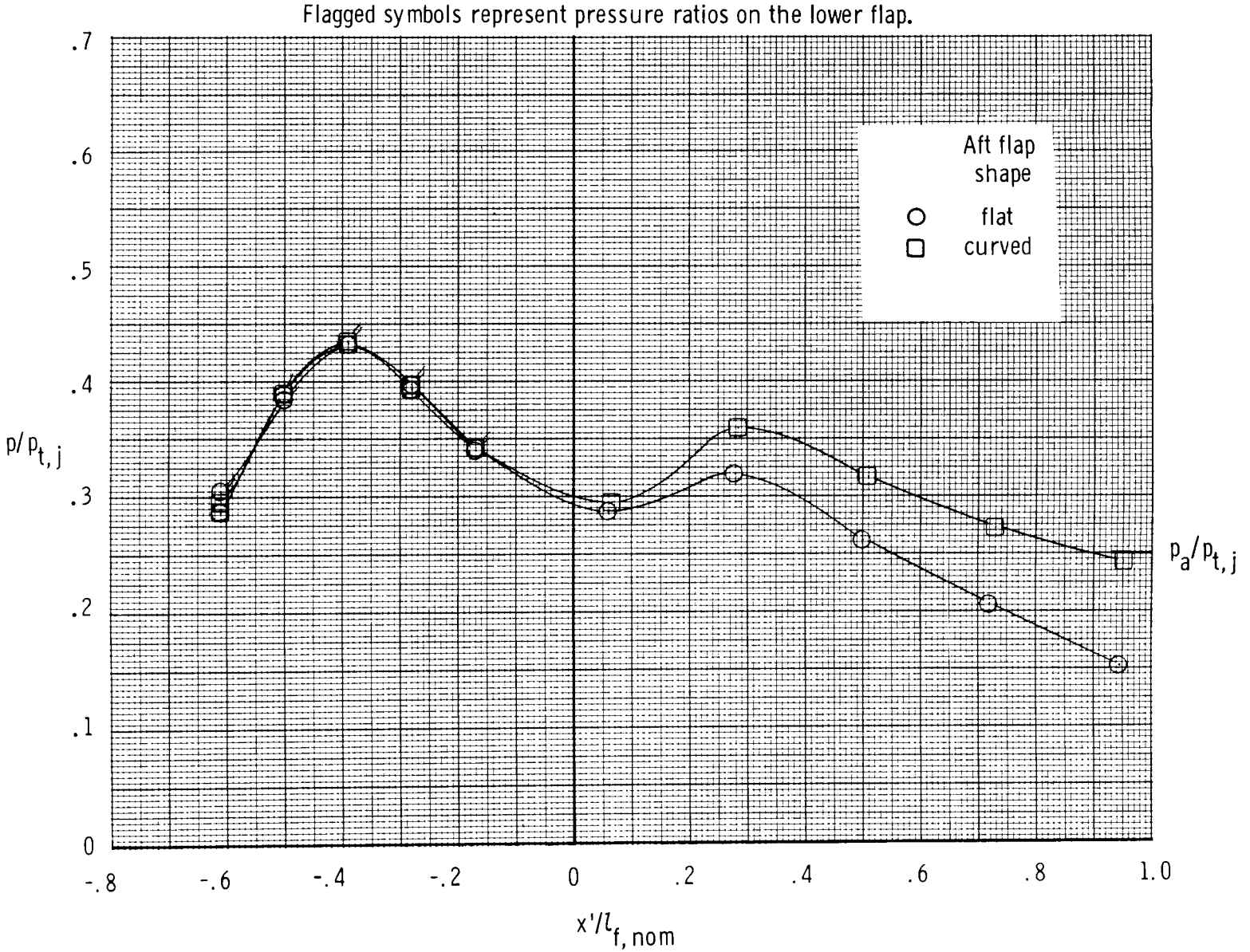

Figure 32.- Effect of aft flap shape on internal static pressure distributions for afterburning nozzle configuration having $A_e/A_t = 1.10$, $\delta_v = 0°$, $\alpha = 2.7°$, and short sidewall (configurations A1FS and A1CS) at nozzle pressure ratio of 4.0.

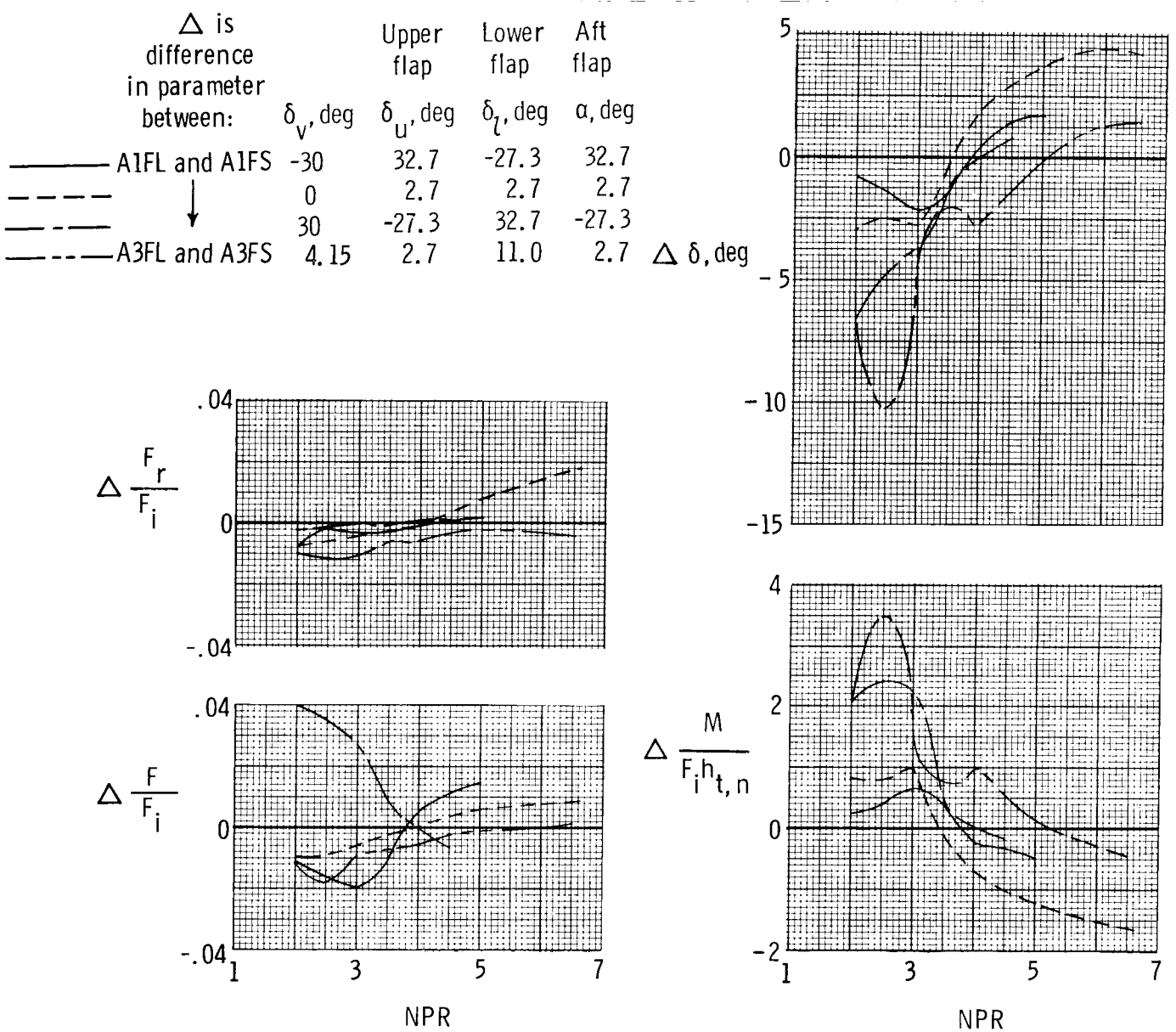

(a) Afterburning nozzle configurations.

Figure 33.- Incremental effect of nozzle sidewall length on nozzle performance for afterburning and dry power nozzle configurations.

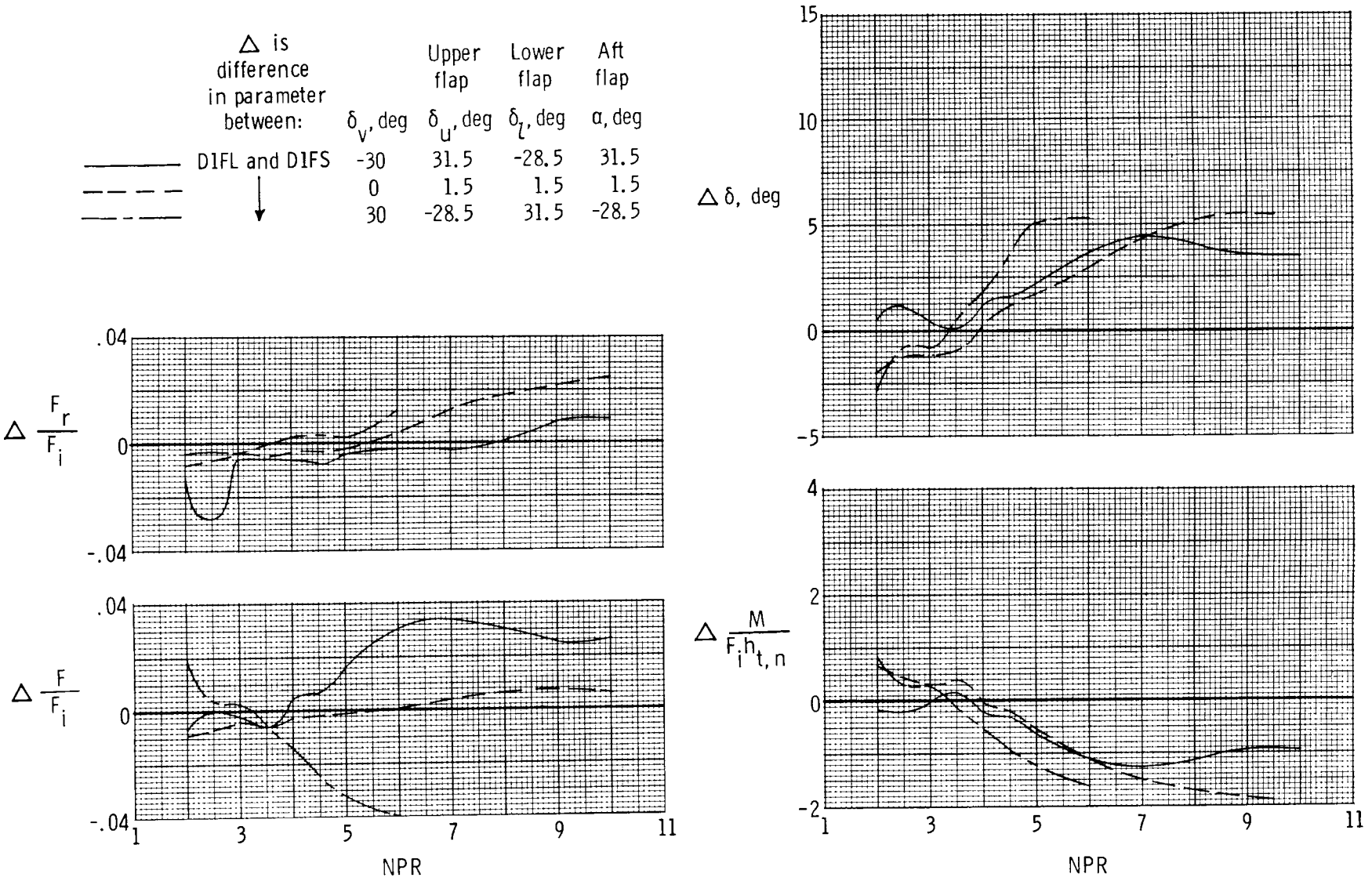

(b) Dry power nozzle configurations.

Figure 33.- Concluded.

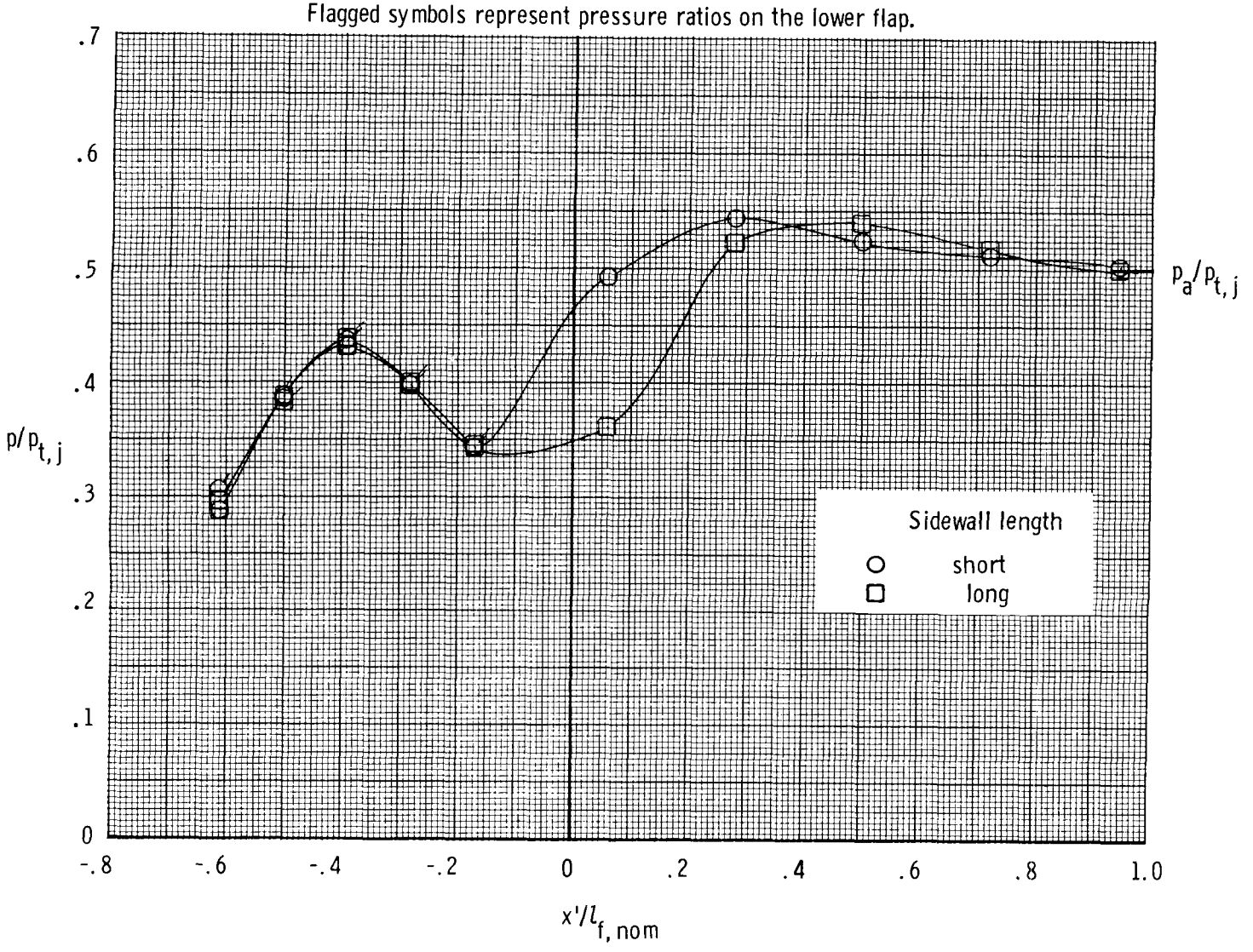

(a) NPR = 2.0.

Figure 34.- Effect of sidewall length on internal static pressure distributions for afterburning nozzle configuration having A_e/A_t = 1.10, δ_v = 0°, α = 2.7°, and flat aft flap shape (configurations A1FS and A1FL).

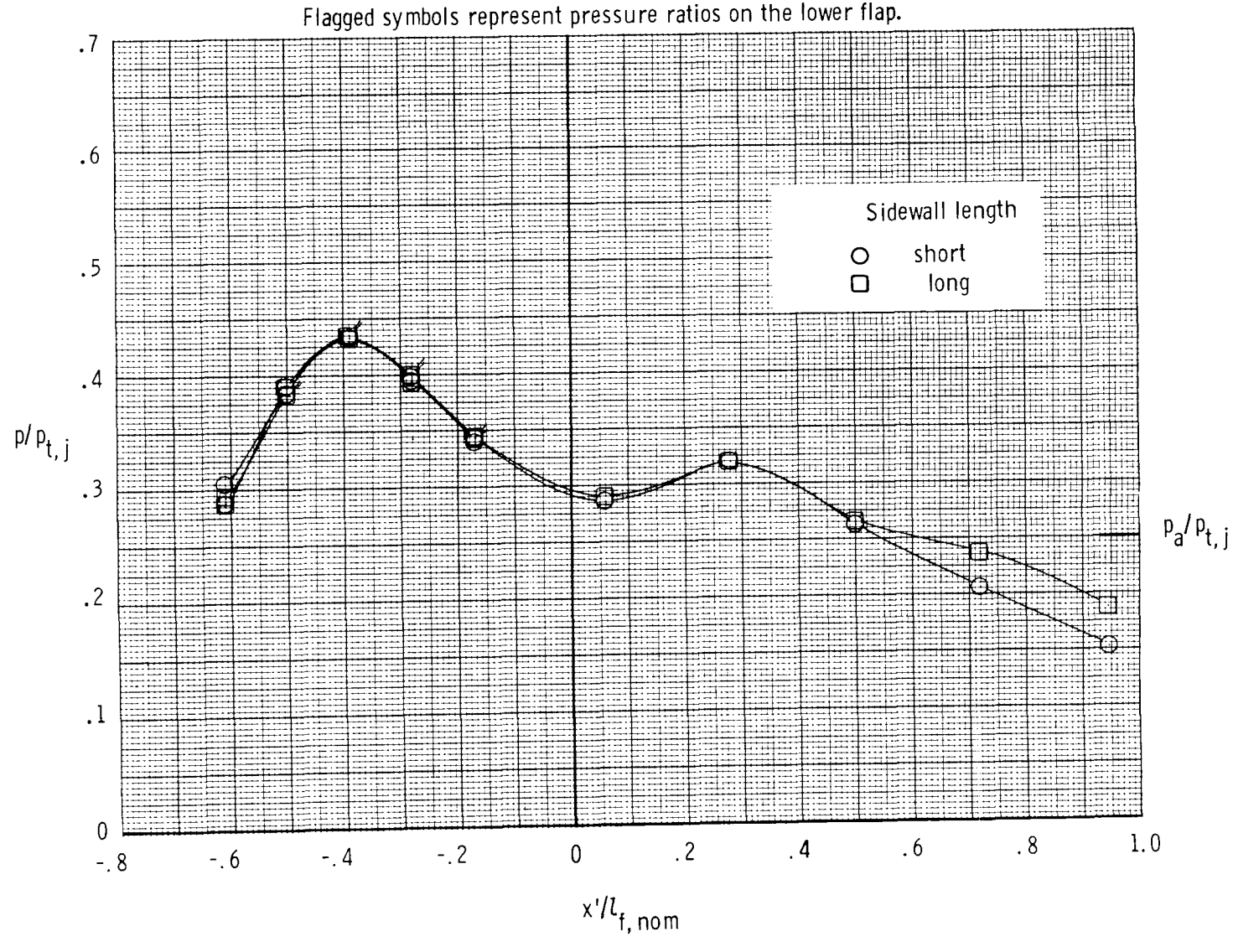

(b) NPR = 4.0.

Figure 34.- Continued.

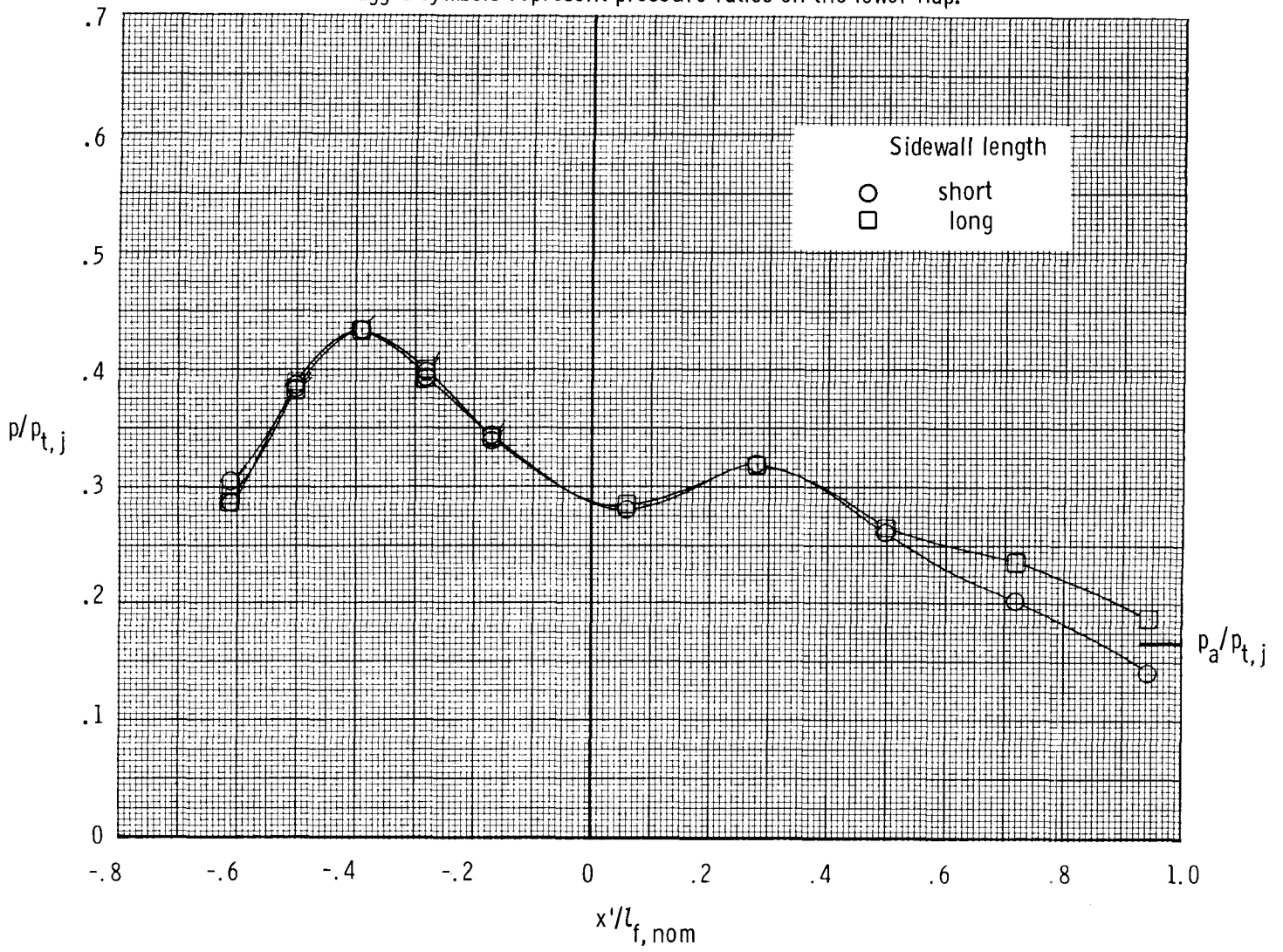

(c) NPR = 6.0.

Figure 34.- Concluded.

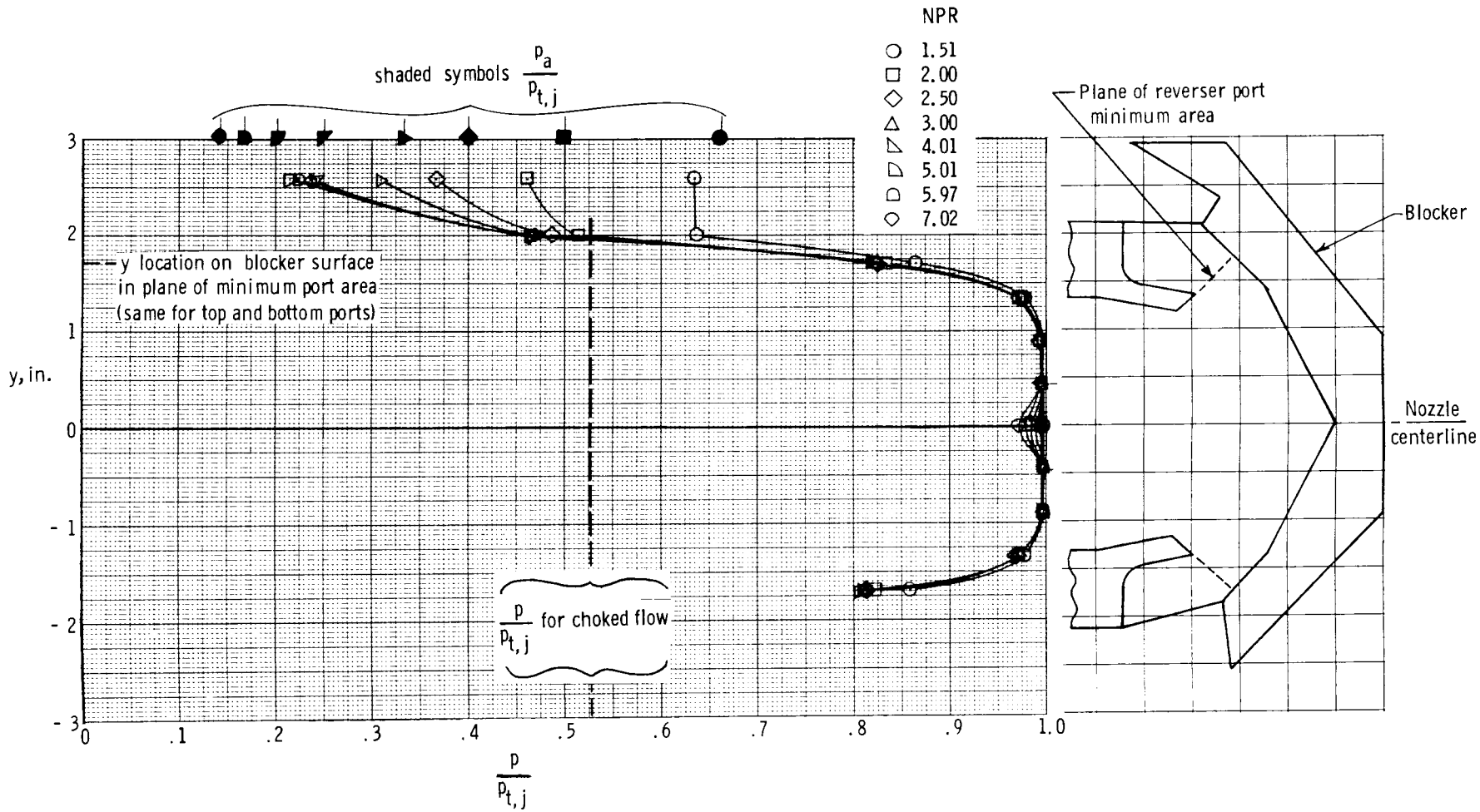

Figure 35.- Effect of nozzle pressure ratio on local static pressure measured on surface of thrust-reverser blocker.

1. Report No.	2. Government Accession No.	3. Recipient's Catalog No.
NASA TP-2549		

4. Title and Subtitle	5. Report Date
Static Internal Performance of a Thrust Vectoring and Reversing Two-Dimensional Convergent-Divergent Nozzle With an Aft Flap	April 1986
	6. Performing Organization Code 505-43-90-07
7. Author(s)	8. Performing Organization Report No.
Richard J. Re and Laurence D. Leavitt	L-16025
	10. Work Unit No.
9. Performing Organization Name and Address	
NASA Langley Research Center Hampton, VA 23665-5225	11. Contract or Grant No.
	13. Type of Report and Period Covered
12. Sponsoring Agency Name and Address	Technical Paper
National Aeronautics and Space Administration Washington, DC 20546-0001	14. Sponsoring Agency Code

15. Supplementary Notes

16. Abstract

The static internal performance of a multifunction nozzle having some of the geometric characteristics of both two-dimensional convergent-divergent and single expansio ramp nozzles has been investigated in the static-test facility of the Langley 16-Foo Transonic Tunnel. The internal expansion portion of the nozzle consisted of two sym metrical flat surfaces of equal length, and the external expansion portion of the nozzle consisted of a single aft flap. The aft flap could be varied in angle independently of the upper internal expansion surface to which it was attached. The effects of internal expansion ratio, nozzle thrust-vector angle (-30° to 30°), aft flap shape, aft flap angle, and sidewall containment were determined for dry and afterburning power settings. In addition, a partial afterburning power setting nozzle, a fully deployed thrust reverser, and four vertical takeoff or landing nozzle configurations were investigated. Nozzle pressure ratio was varied up to 10 for the dry power nozzles and 7 for the afterburning power nozzles.

17. Key Words (Suggested by Author(s))	18. Distribution Statement
Nonaxisymmetric nozzles Internal performance Two-dimensional convergent-divergent Thrust vectoring Thrust reversing VTOL nozzles	Unclassified - Unlimited Subject Category 02

19. Security Classif. (of this report)	20. Security Classif. (of this page)	21. No. of Pages	22. Price
Unclassified	Unclassified	111	A06

For sale by the National Technical Information Service, Springfield, Virginia 22161

NASA-Langley, 19